10	Radio 0,2 m	Ángulo 15°	Colchón 0,06 m	Caudal 37,5 l/s

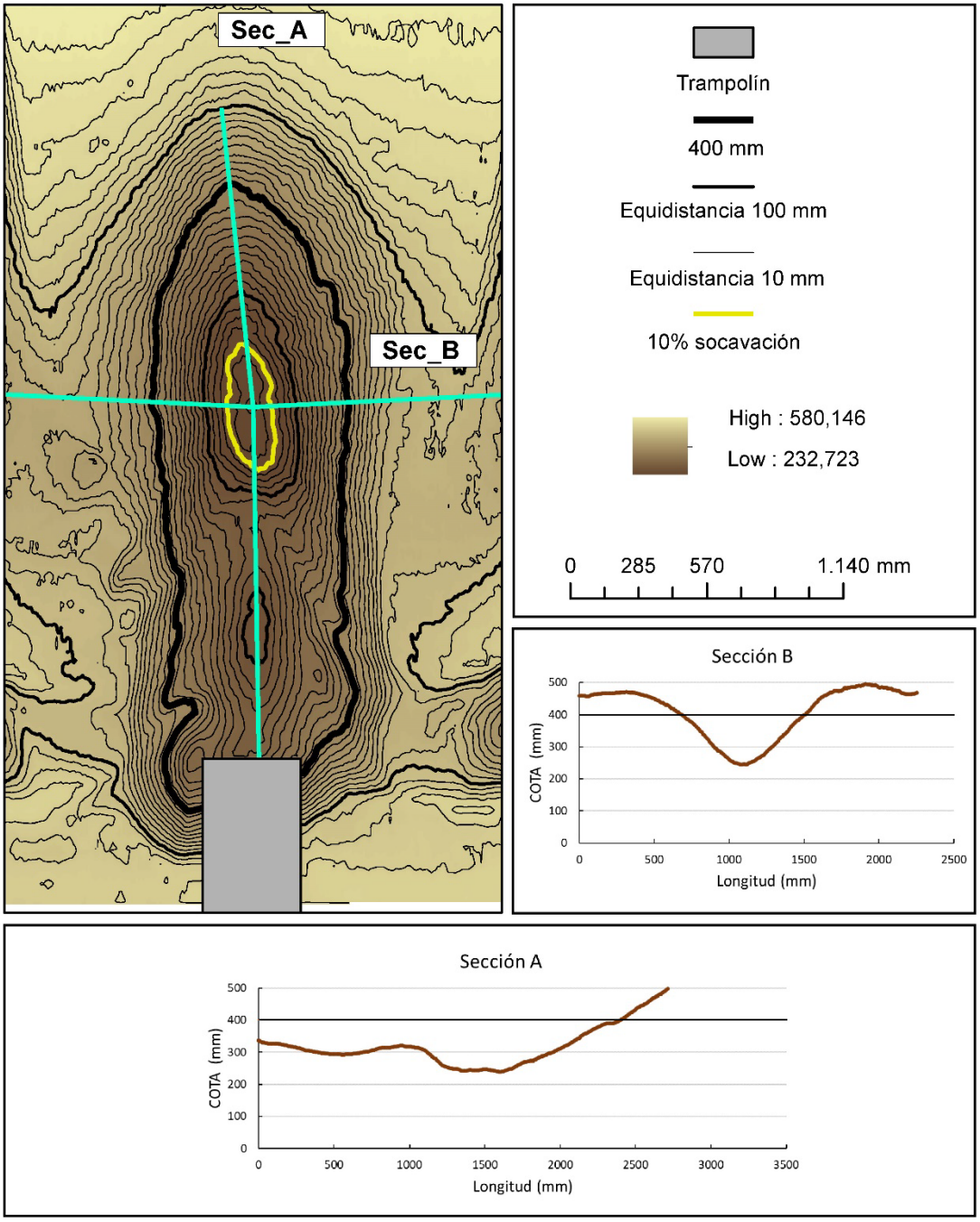

11	Radio 0,2 m	Ángulo 15°	Colchón 0,06 m	Caudal 42 l/s

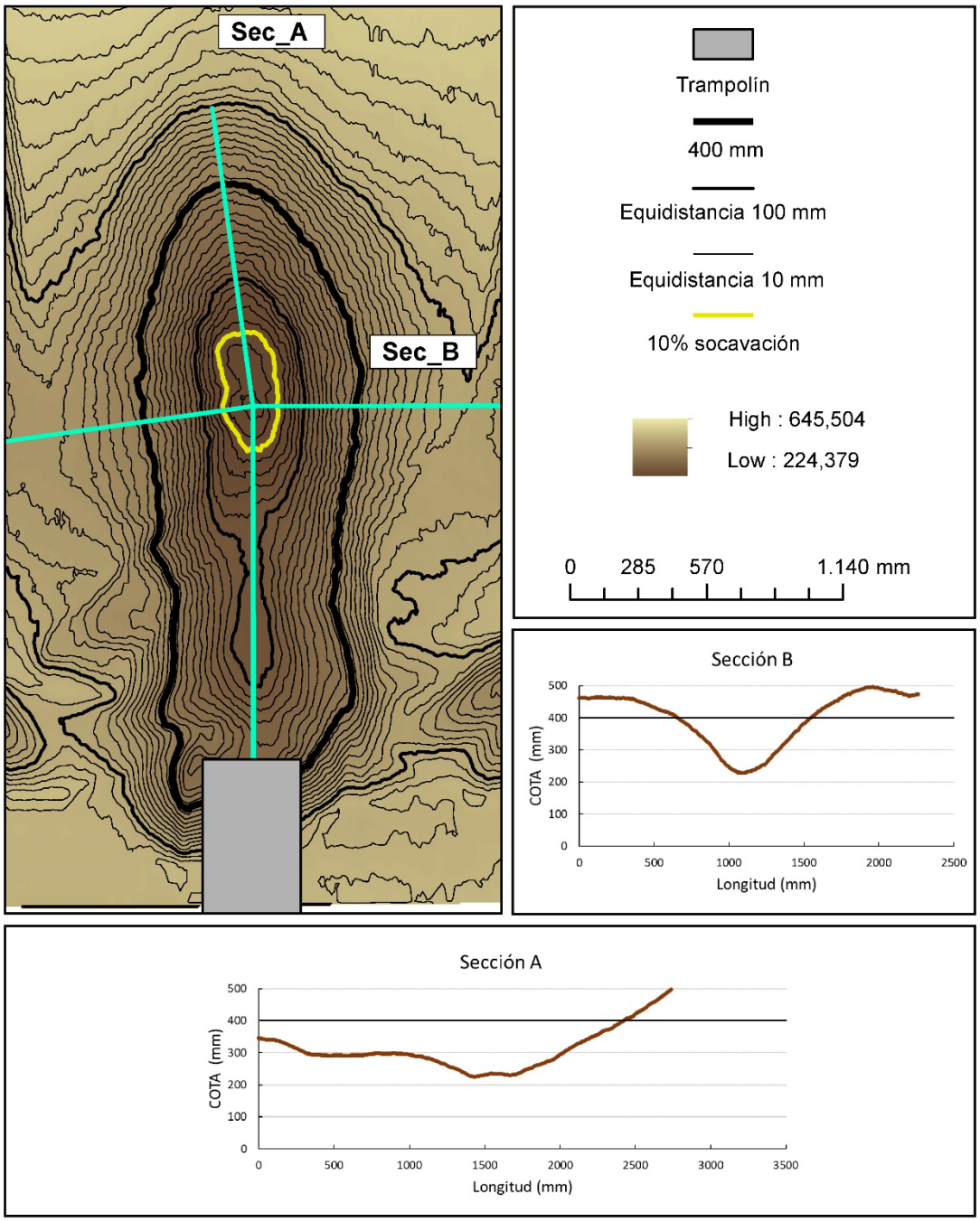

12	Radio 0,2 m	Ángulo 15°	Colchón 0,06 m	Caudal 50 l/s

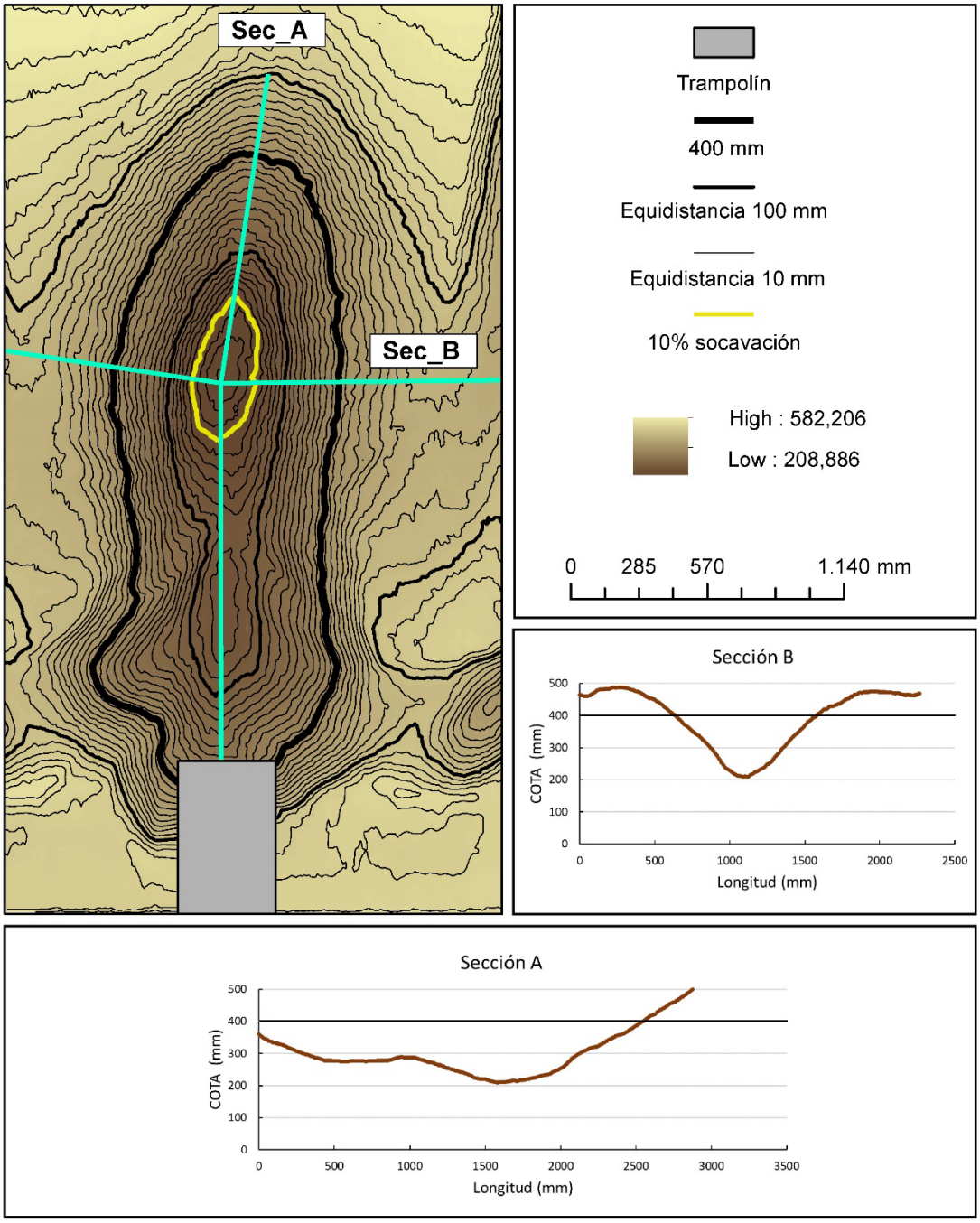

13	Radio 0,2 m	Ángulo 30°	Colchón 0,00 m	Caudal 37,5 l/s

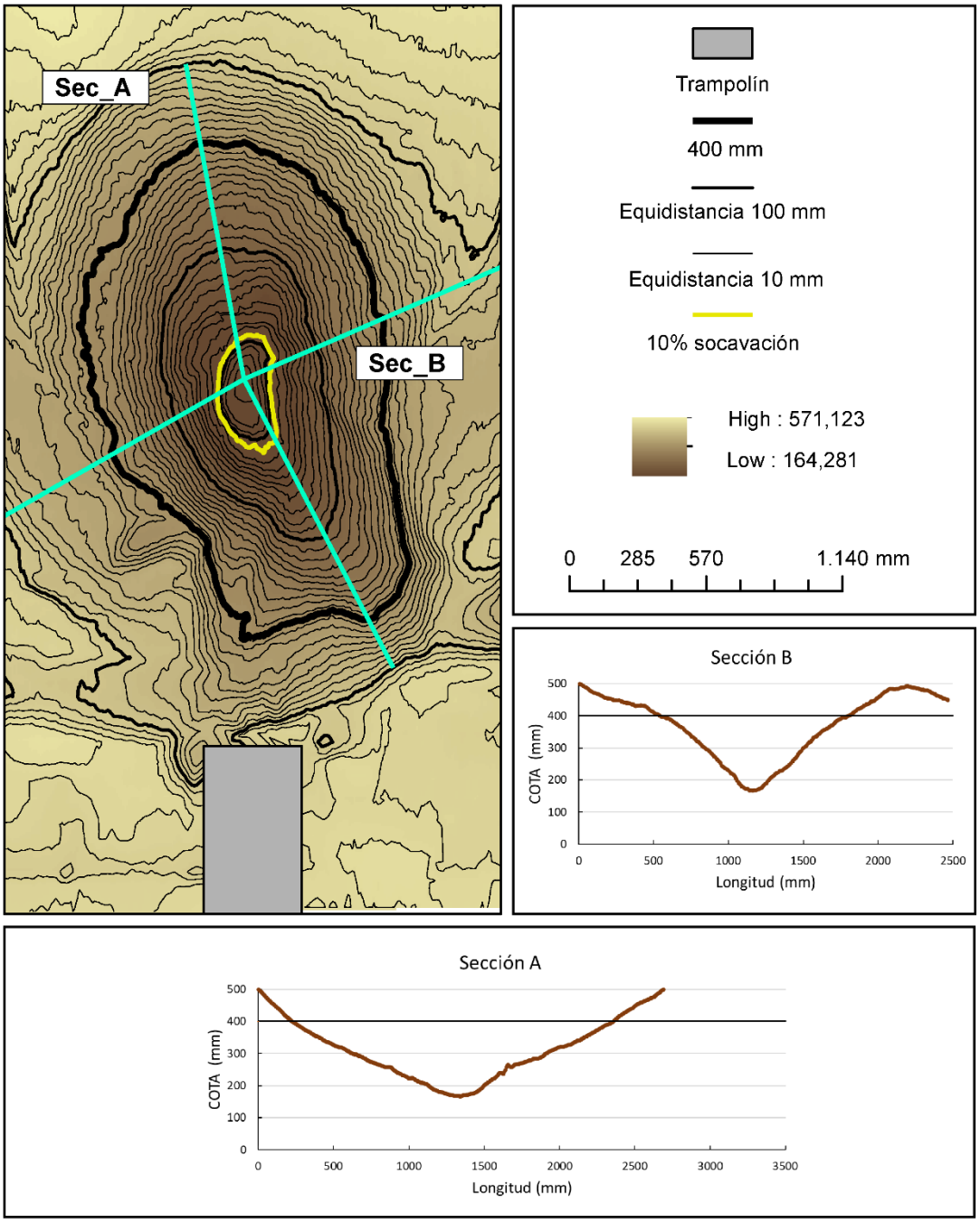

14	Radio 0,2 m	Ángulo 30°	Colchón 0,00 m	Caudal 42 l/s

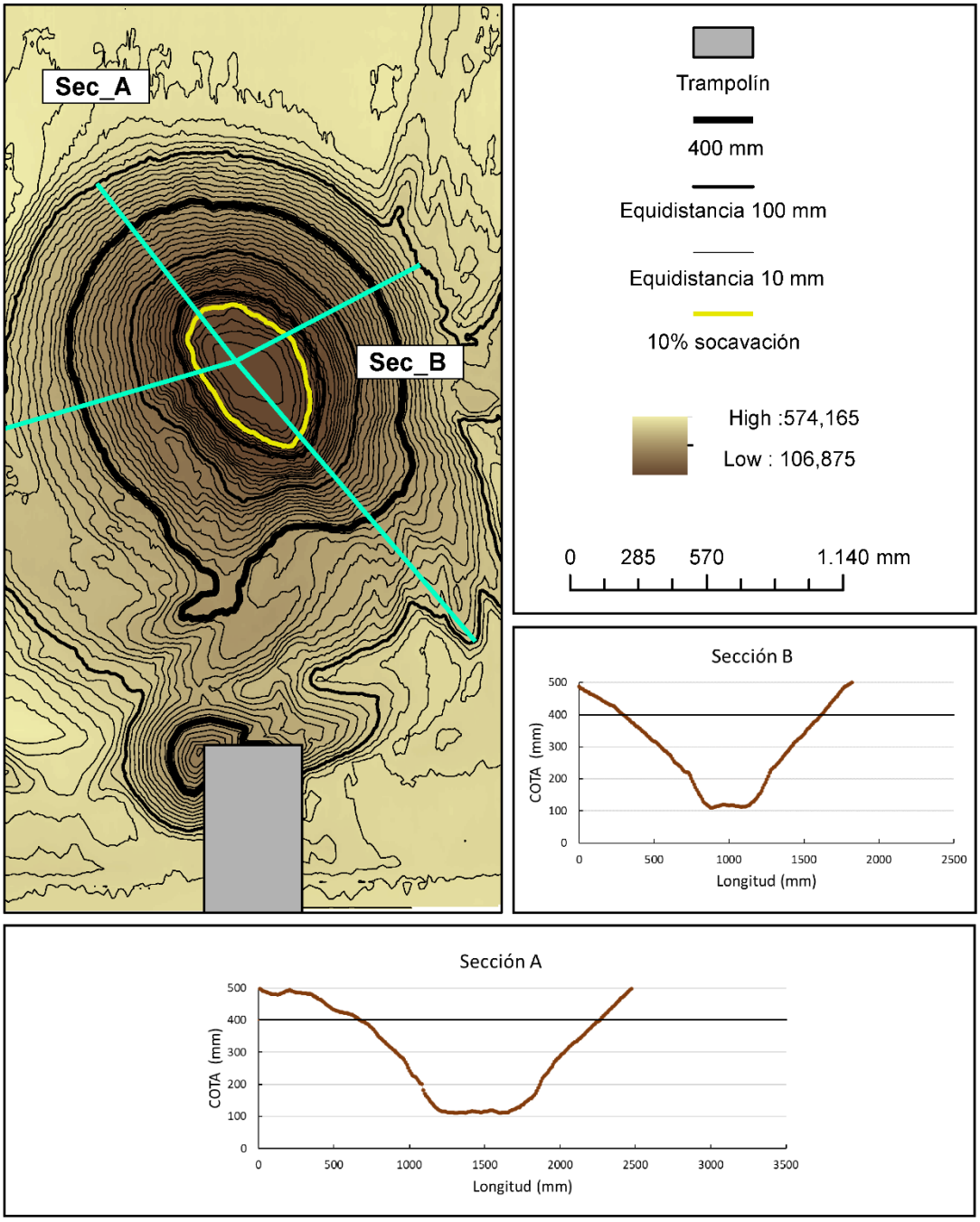

15	Radio 0,2 m	Ángulo 30°	Colchón 0,00 m	Caudal 50 l/s

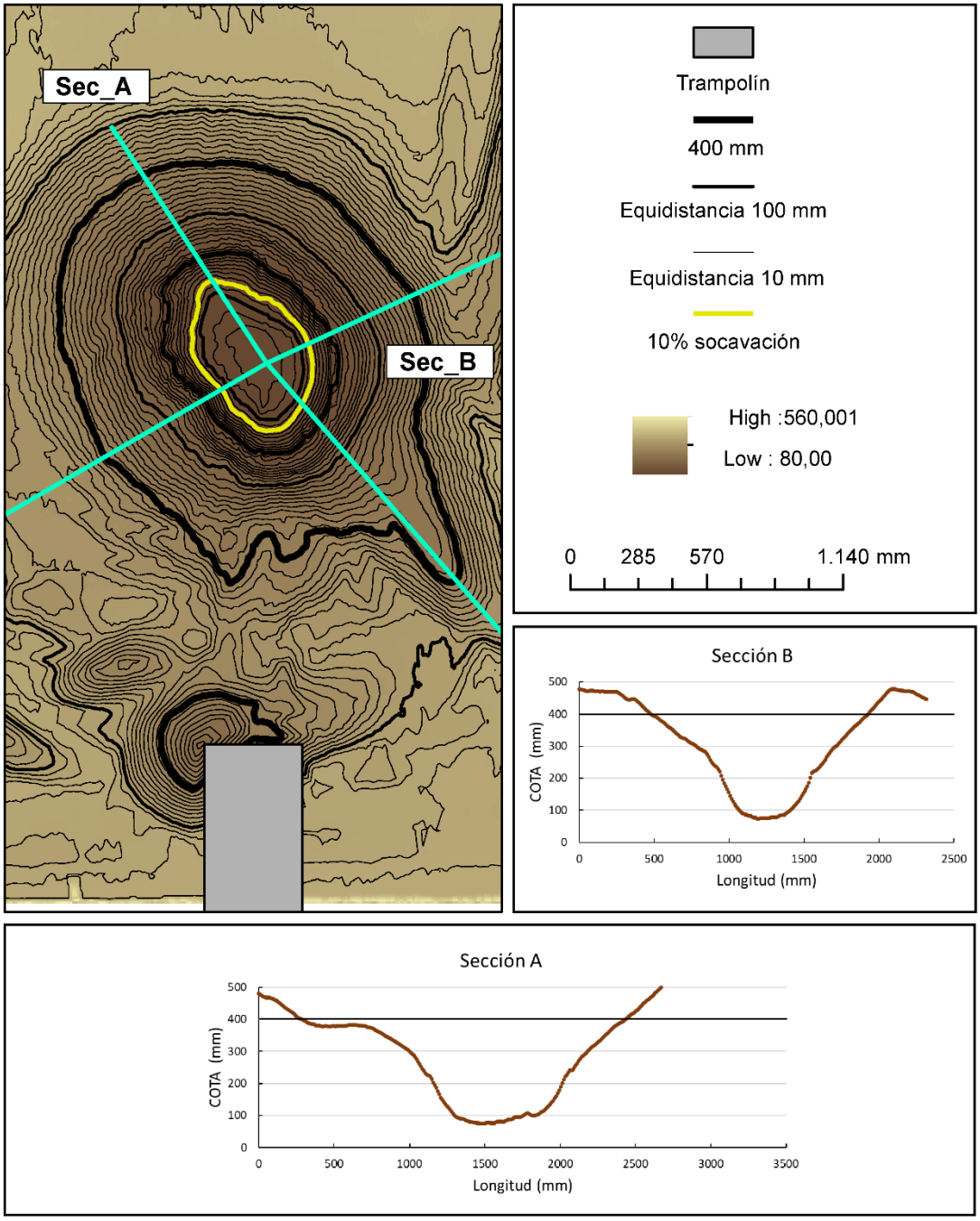

16	Radio 0,2 m	Ángulo 30°	Colchón 0,06 m	Caudal 37,5 l/s

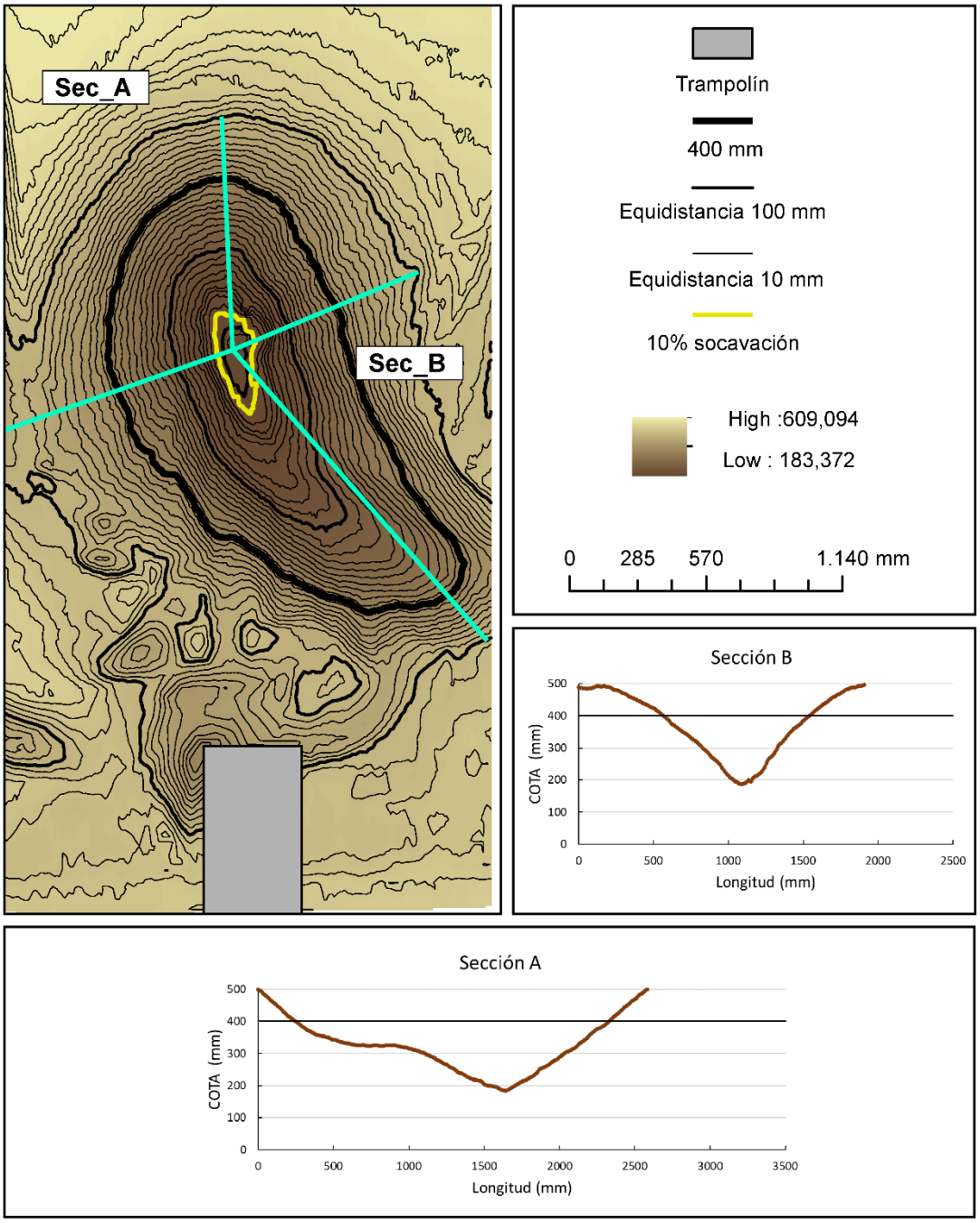

17	Radio 0,2 m	Ángulo 30°	Colchón 0,06 m	Caudal 42 l/s

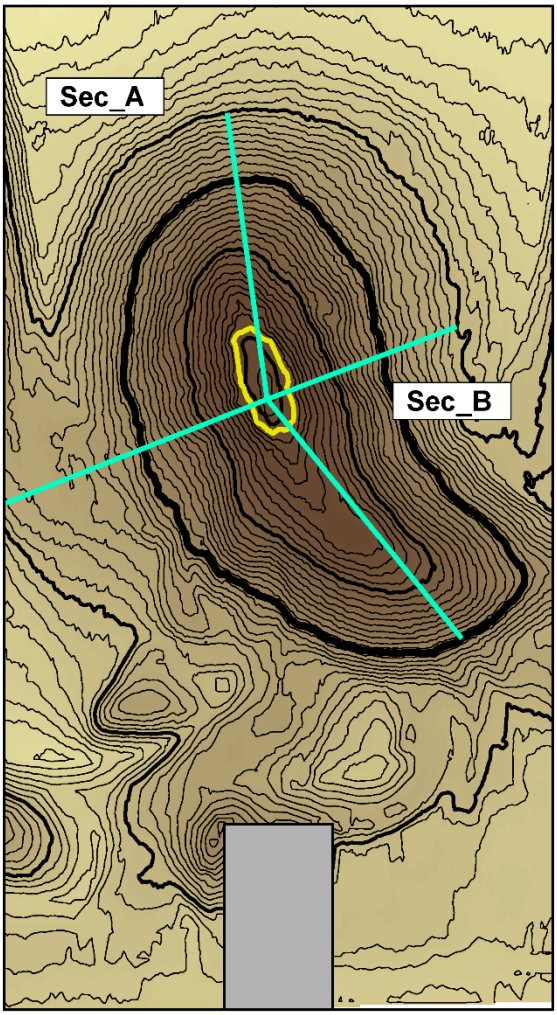

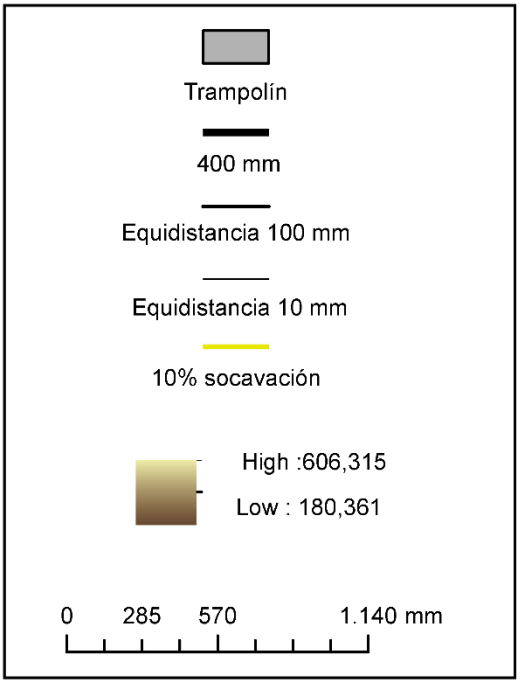

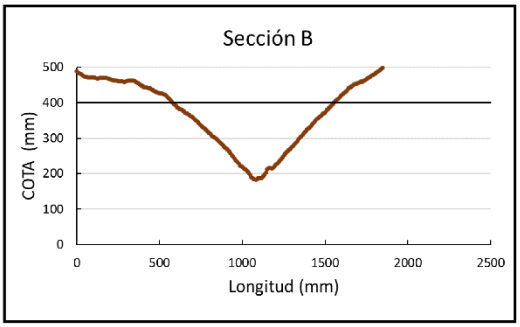

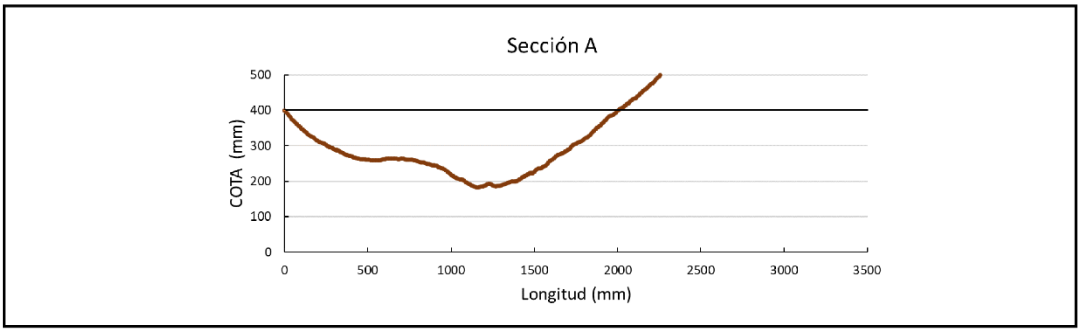

18	Radio 0,2 m	Ángulo 30°	Colchón 0,06 m	Caudal 50 l/s

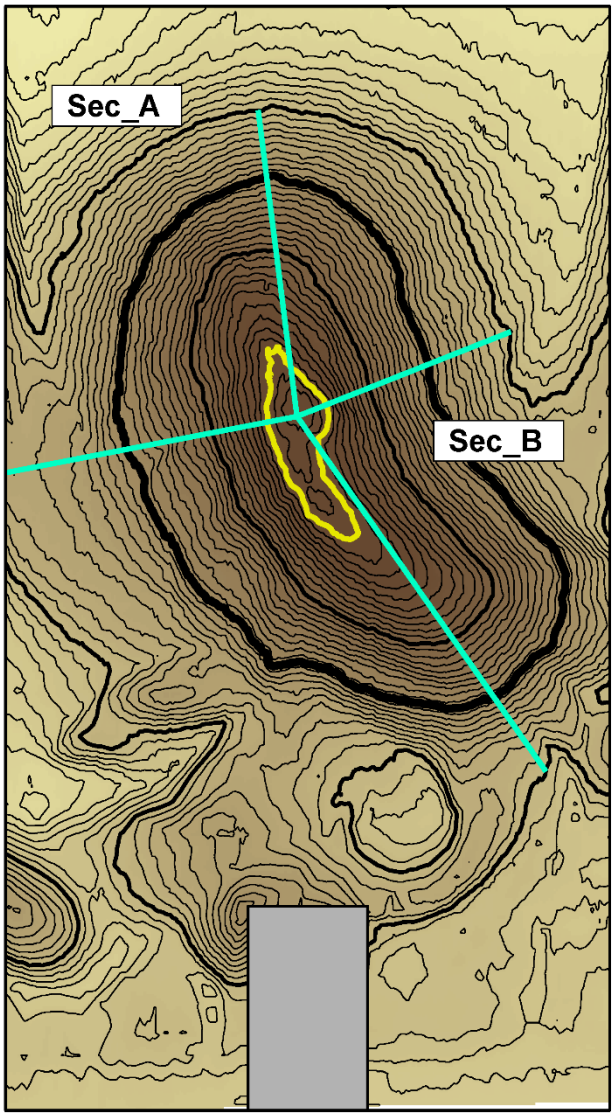

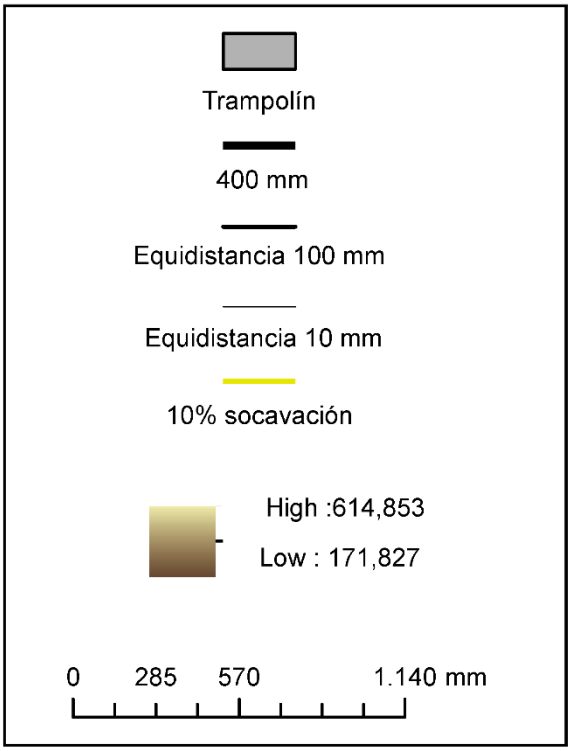

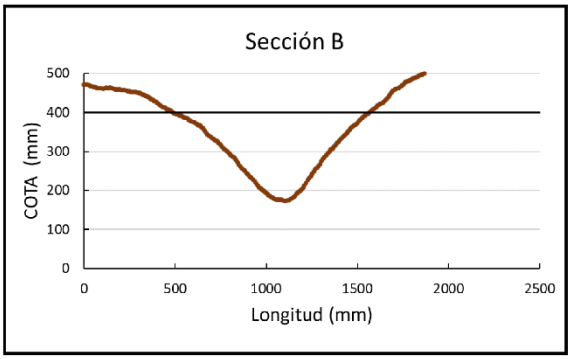

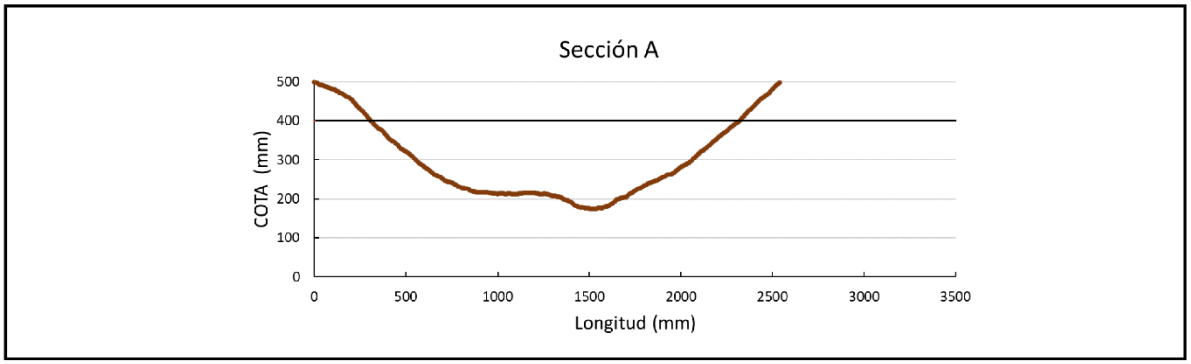

19	Radio 0,2 m	Ángulo 45°	Colchón 0,00 m	Caudal 37,5 l/s

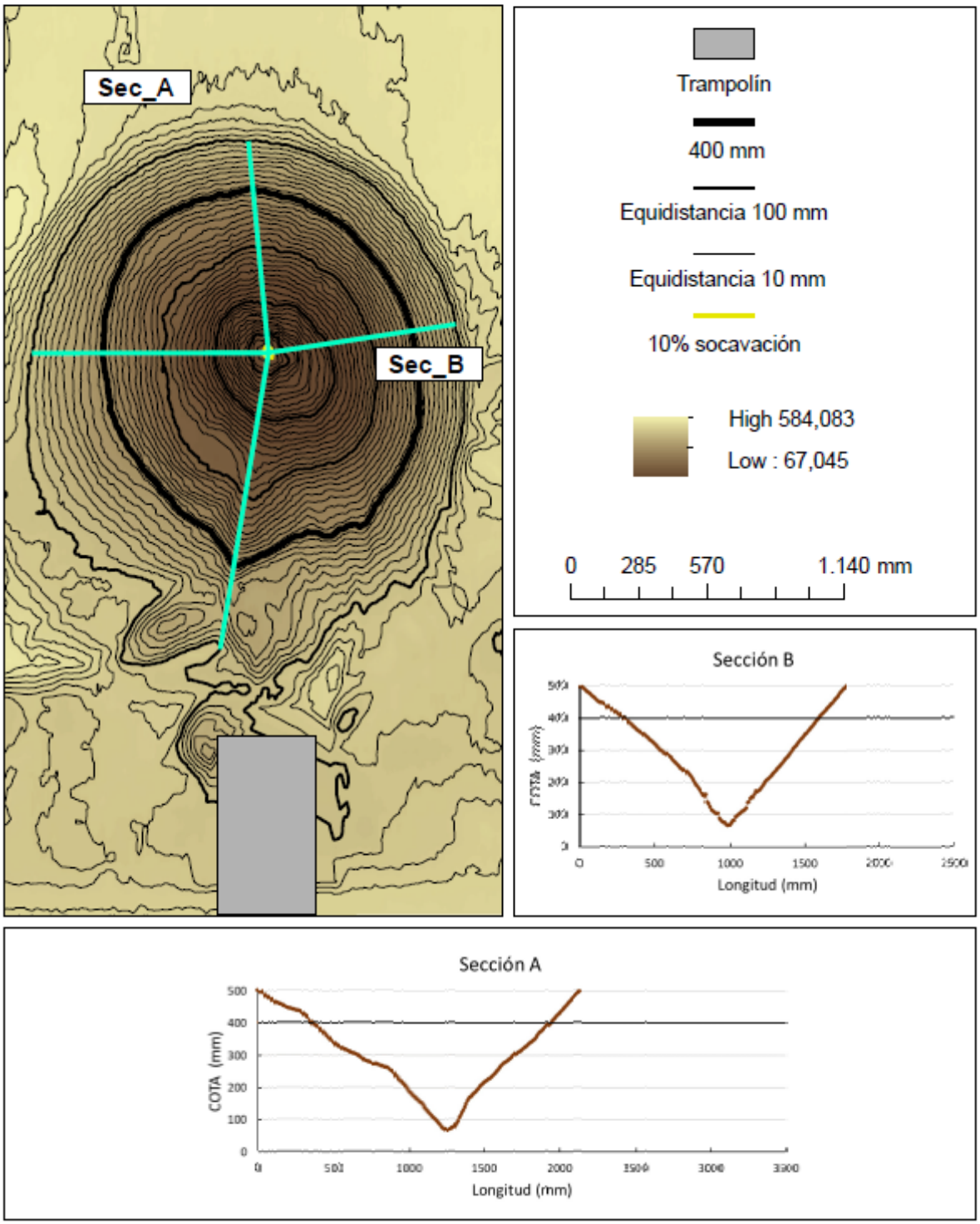

20	Radio 0,2 m	Ángulo 45°	Colchón 0,00 m	Caudal 42 l/s

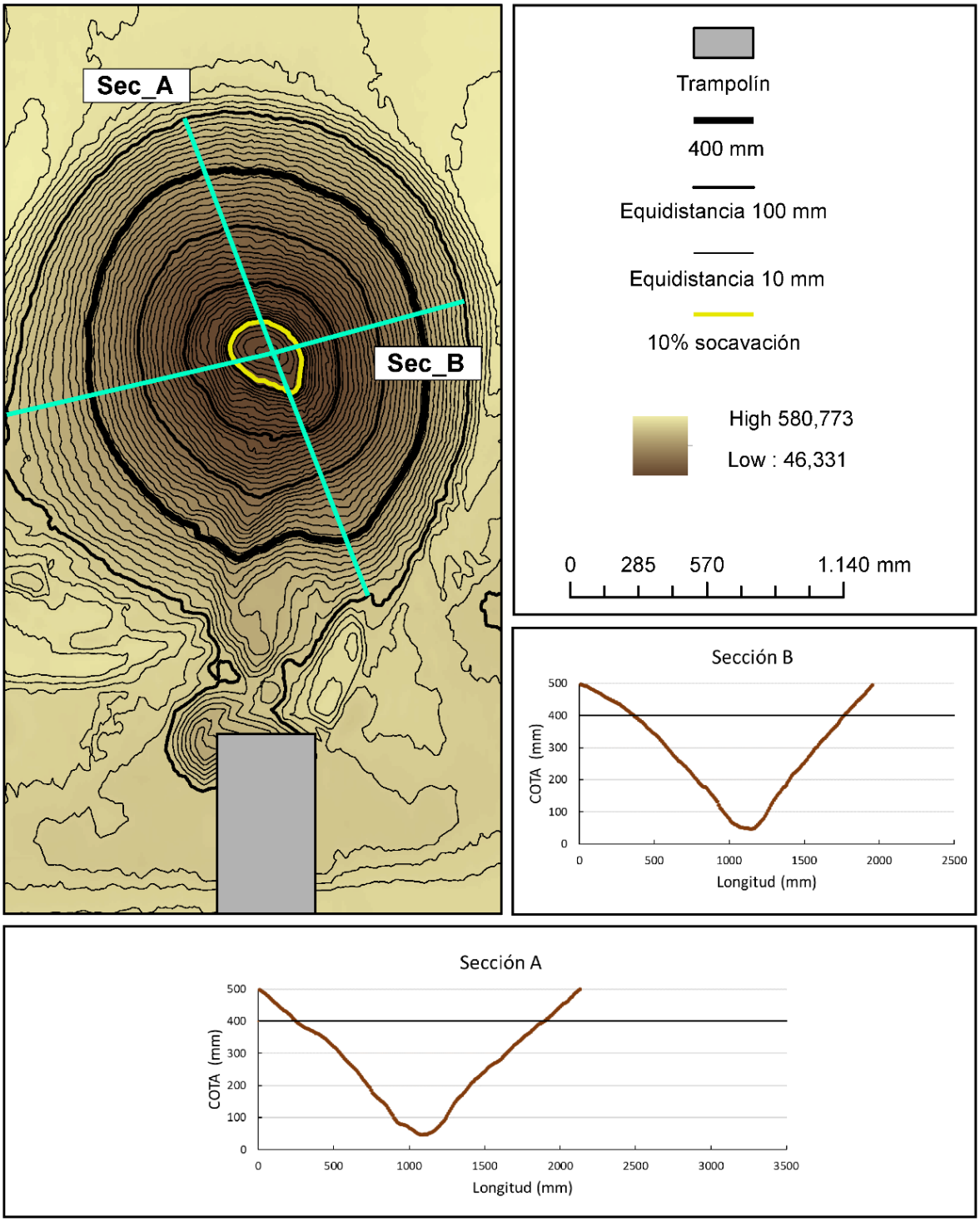

21	Radio 0,2 m	Ángulo 45°	Colchón 0,00 m	Caudal 50 l/s

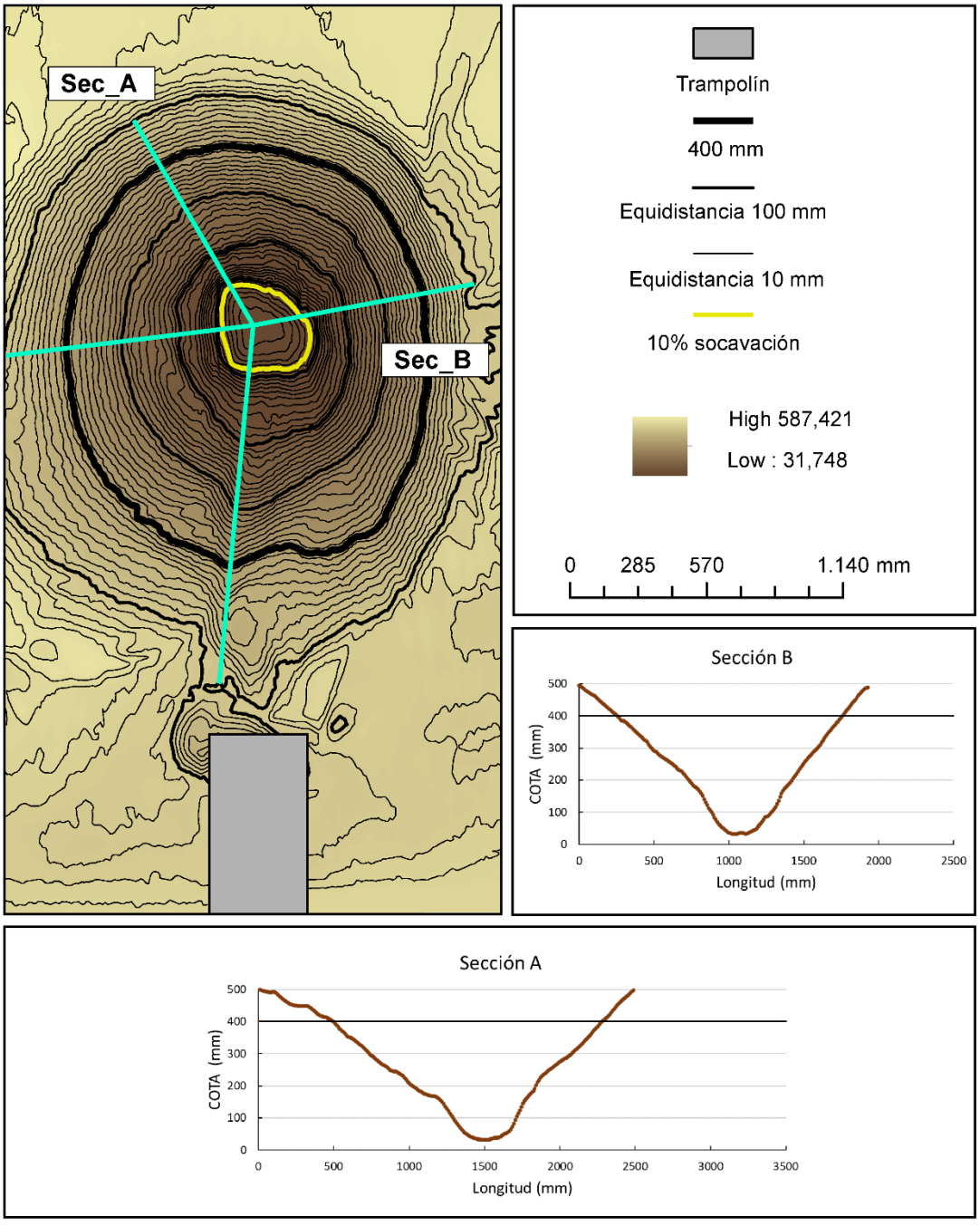

22	Radio 0,2 m	Ángulo 45°	Colchón 0,06 m	Caudal 37,5 l/s

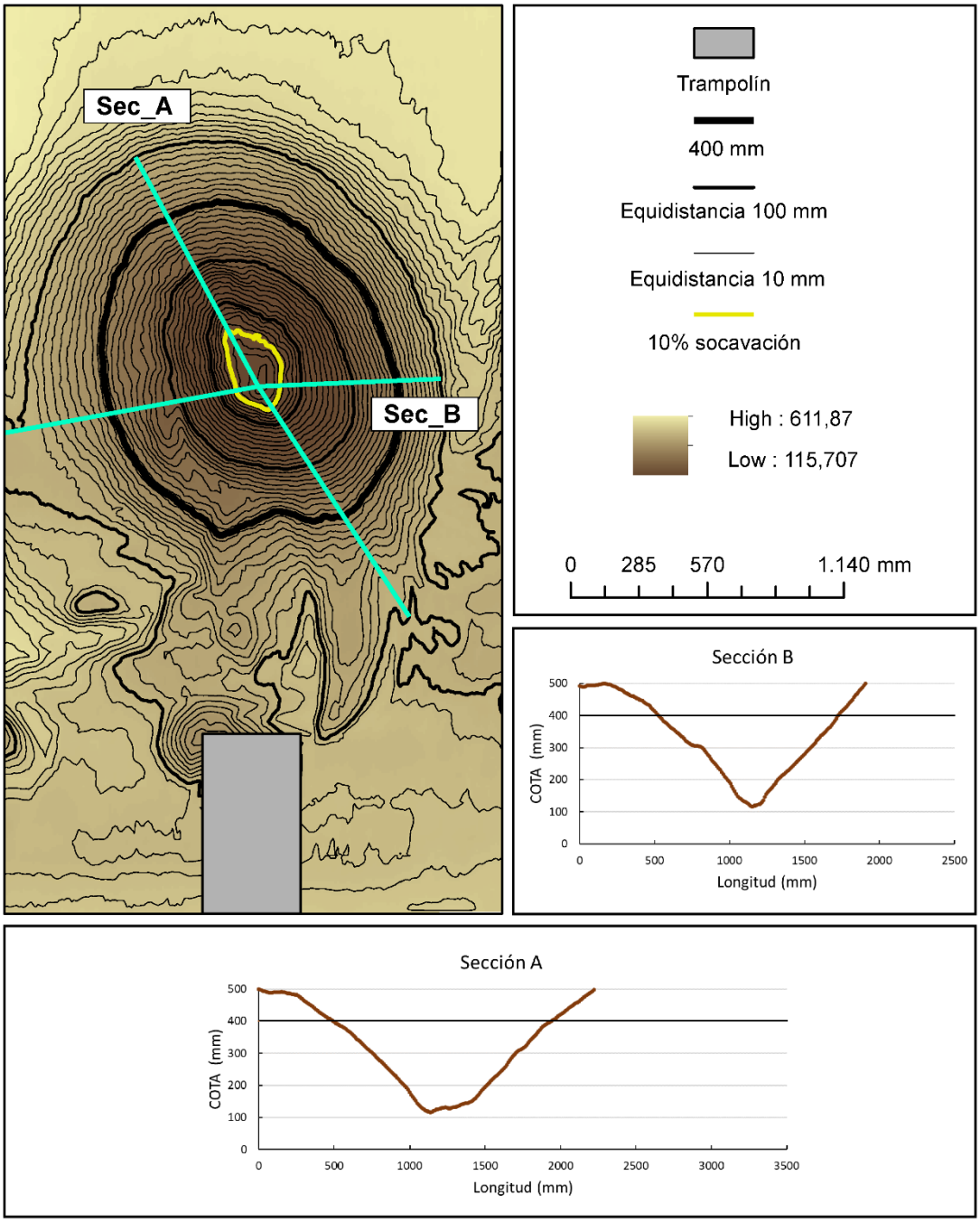

23	Radio 0,2 m	Ángulo 45°	Colchón 0,06 m	Caudal 42 l/s

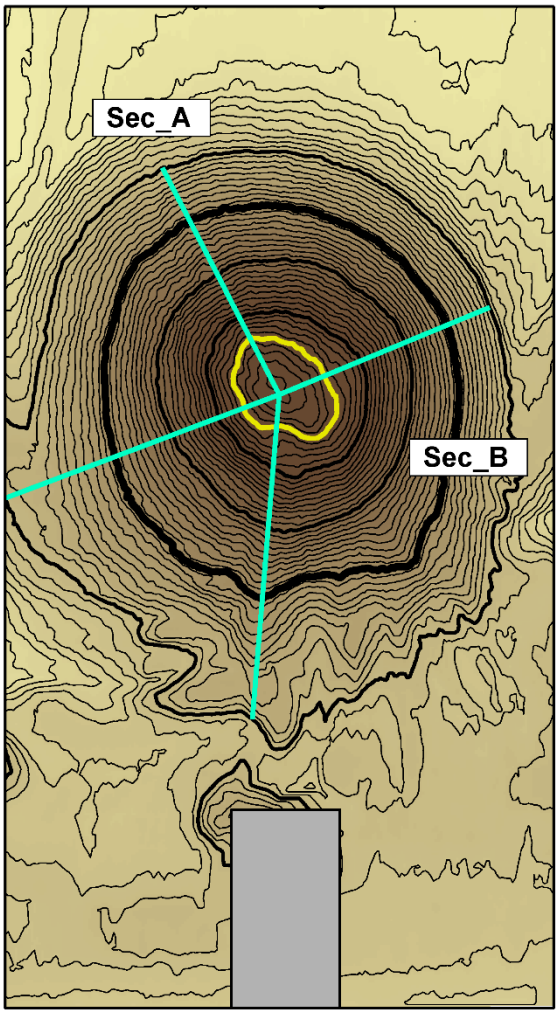

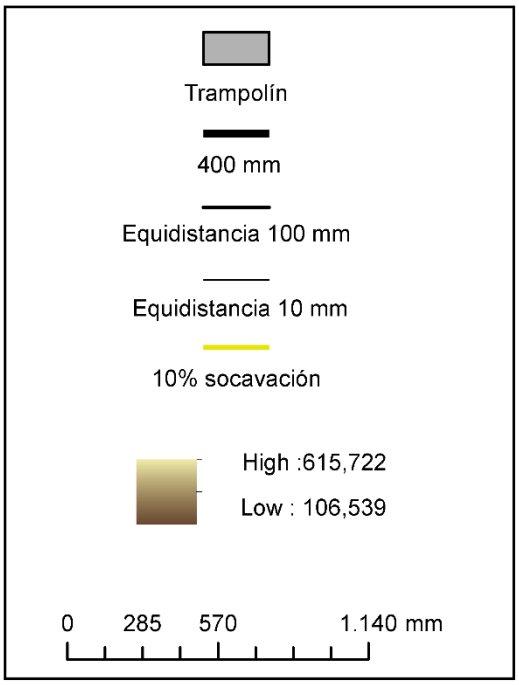

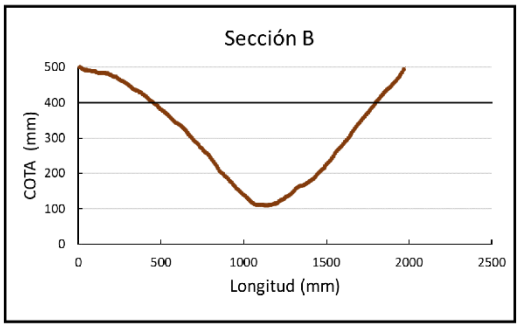

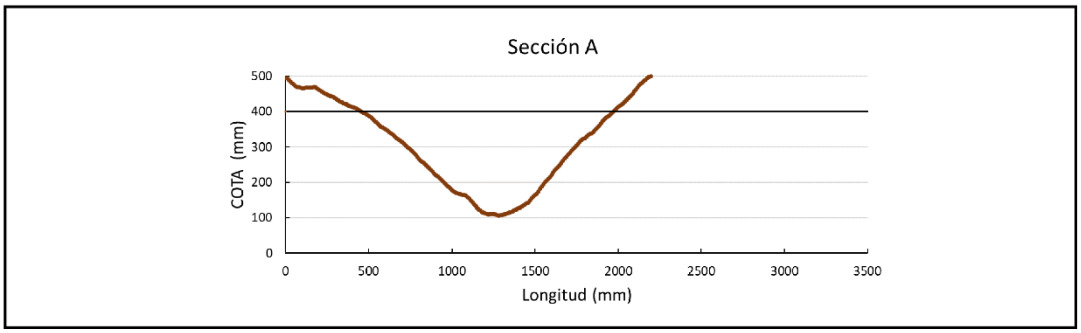

23	Radio 0,2 m	Ángulo 45°	Colchón 0,06 m	Caudal 42 l/s

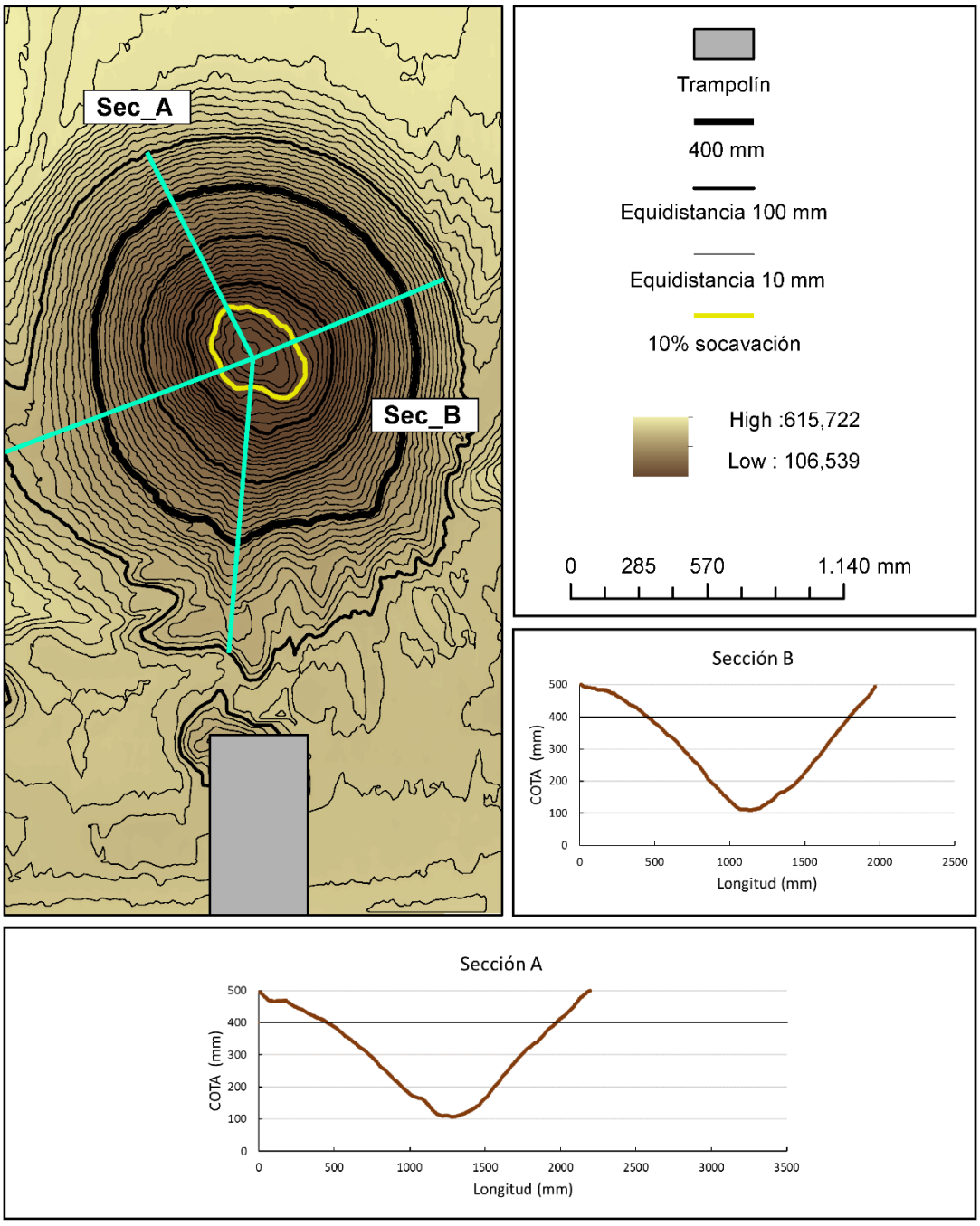

24	Radio 0,2 m	Ángulo 45°	Colchón 0,06 m	Caudal 50 l/s

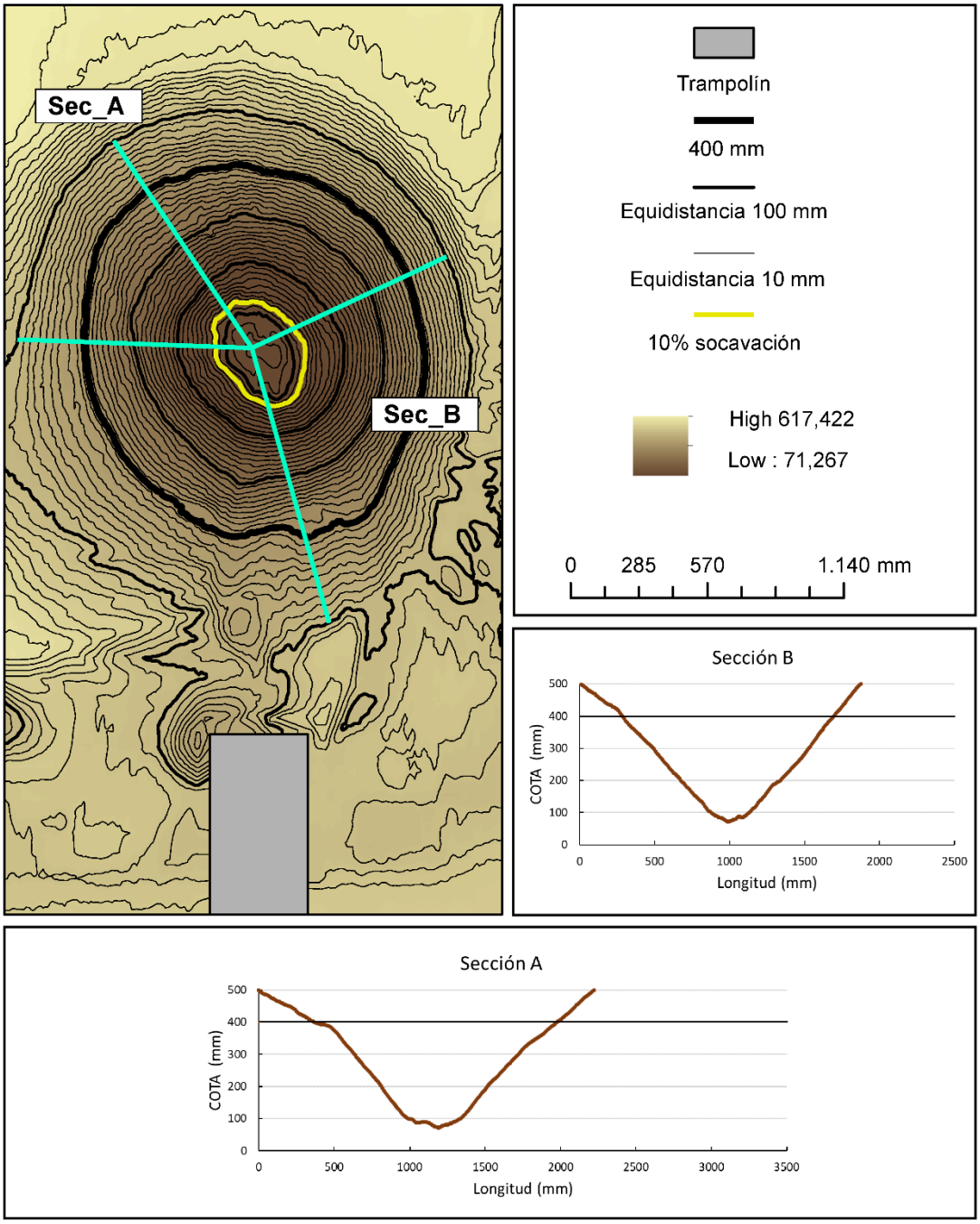

25	Radio 0,3 m	Ángulo 15°	Colchón 0,00 m	Caudal 37,5 l/s

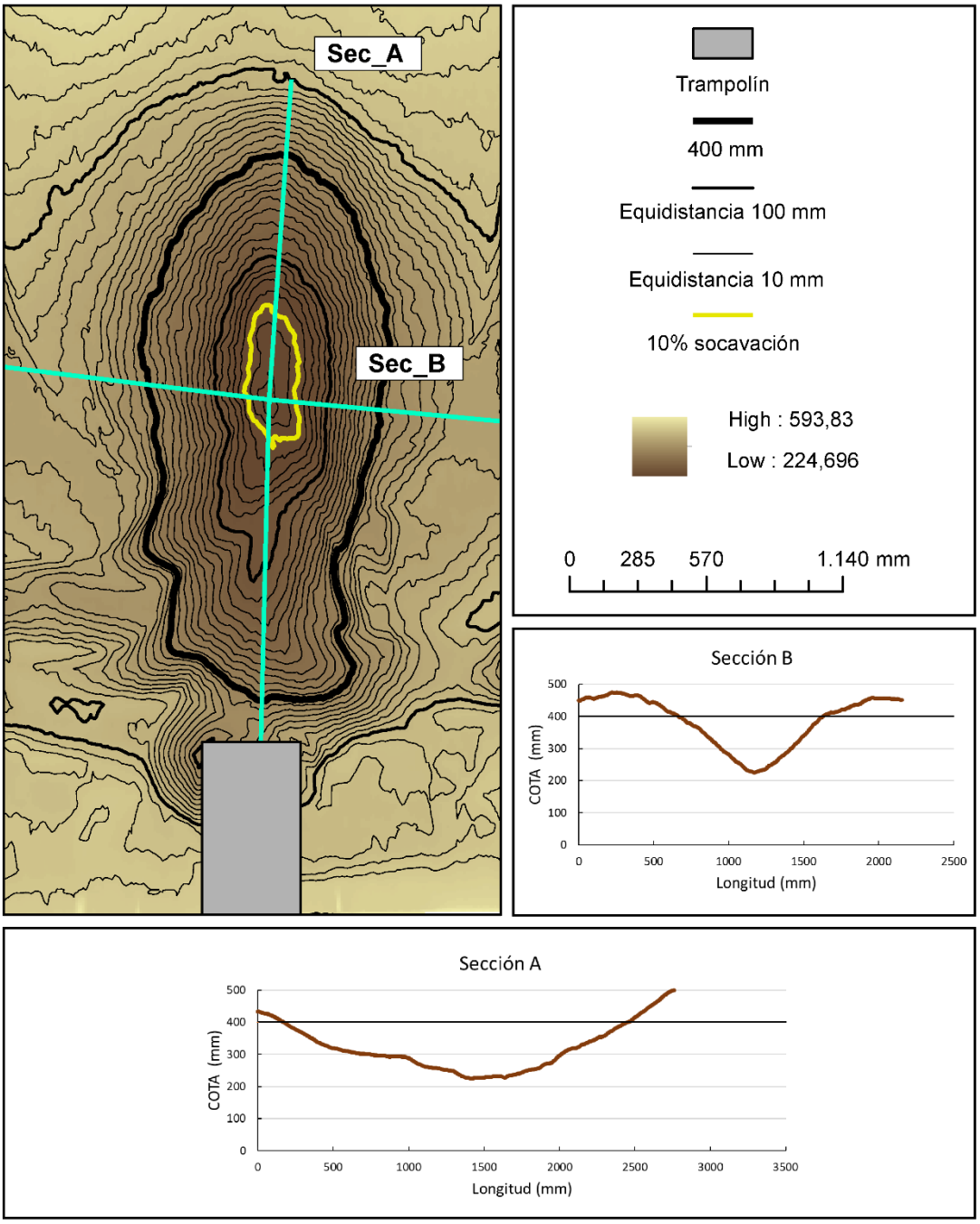

26	Radio 0,3 m	Ángulo 15°	Colchón 0,00 m	Caudal 42 l/s

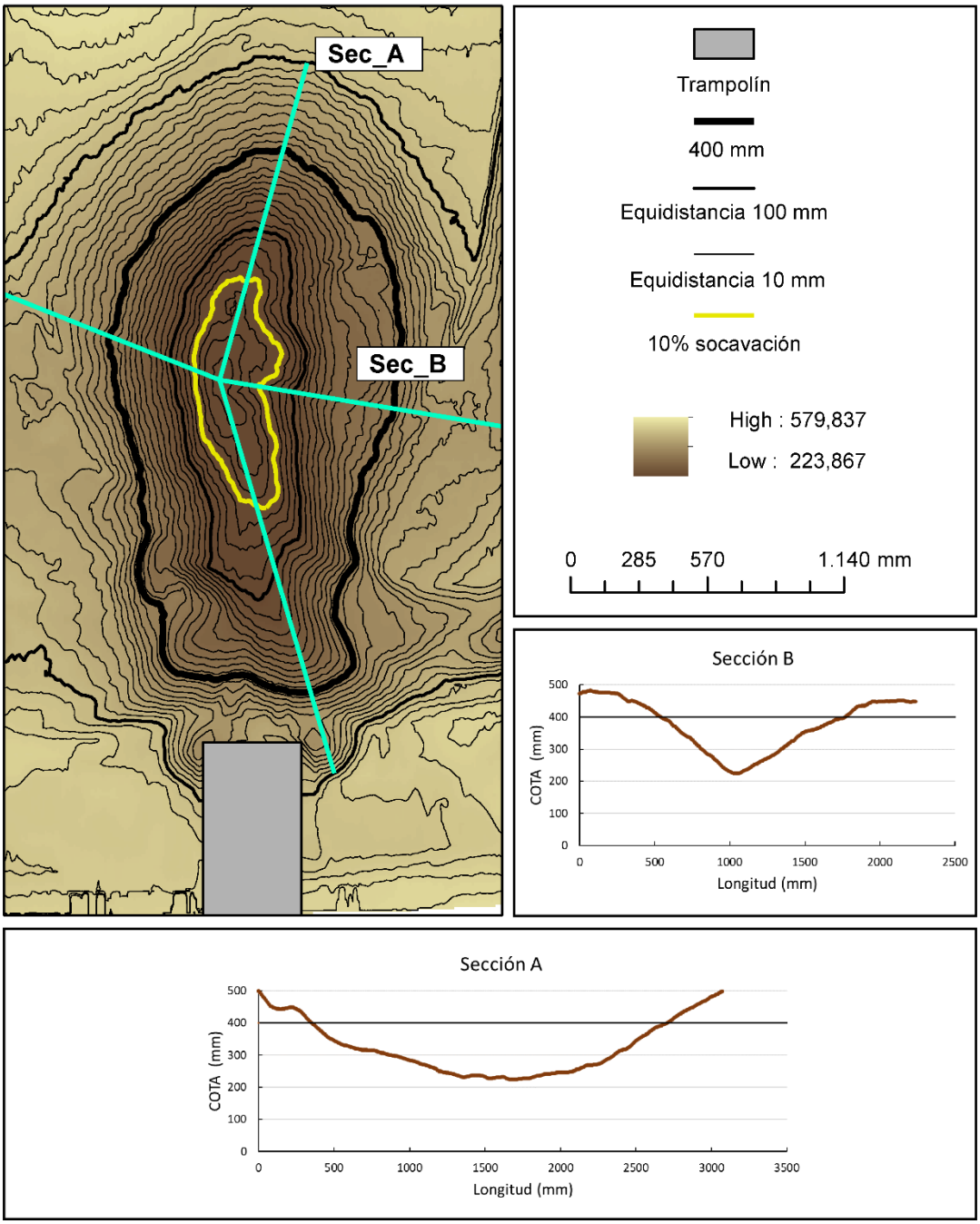

27	Radio 0,3 m	Ángulo 15°	Colchón 0,00 m	Caudal 50 l/s

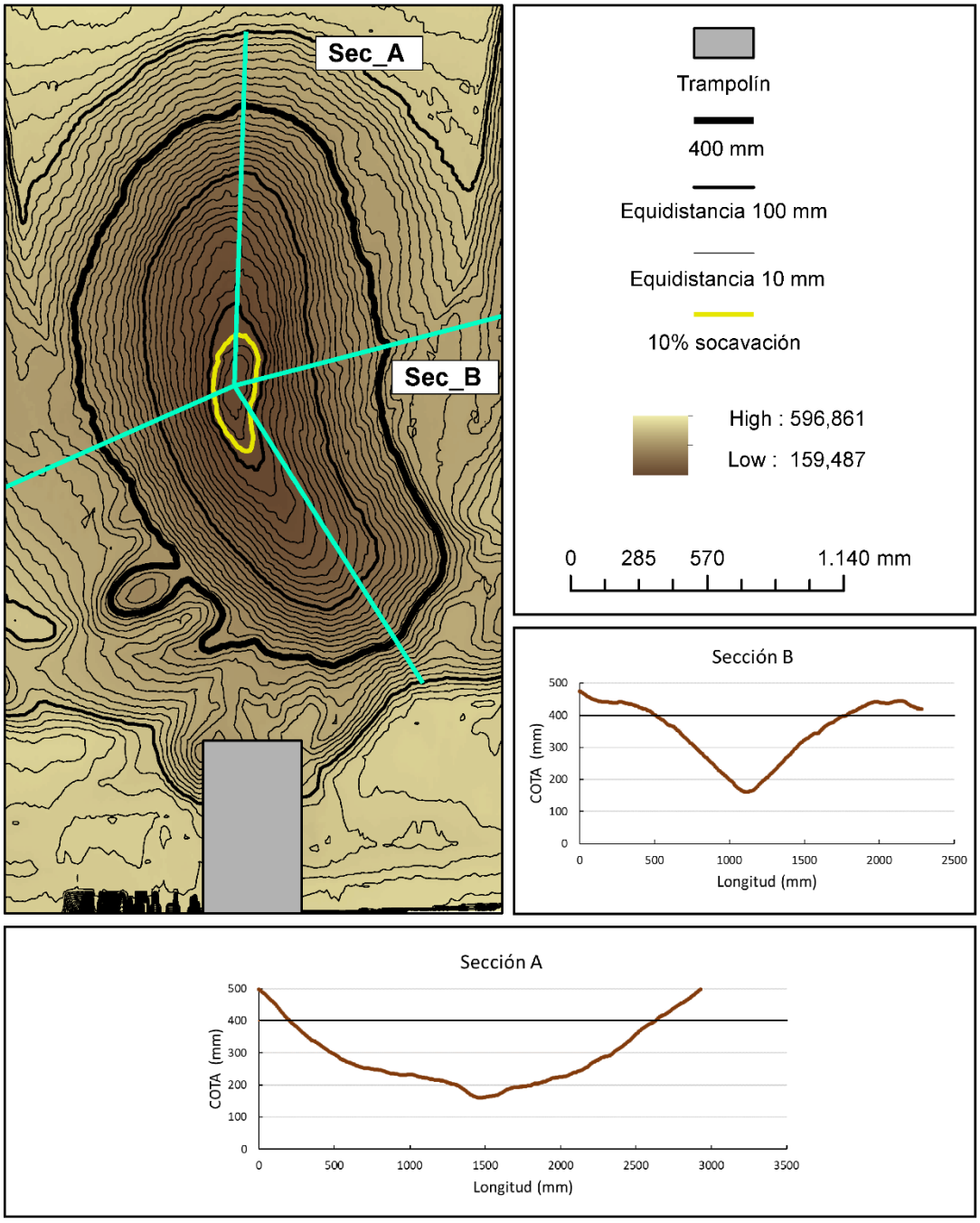

28	Radio 0,3 m	Ángulo 15°	Colchón 0,06 m	Caudal 37,5 l/s

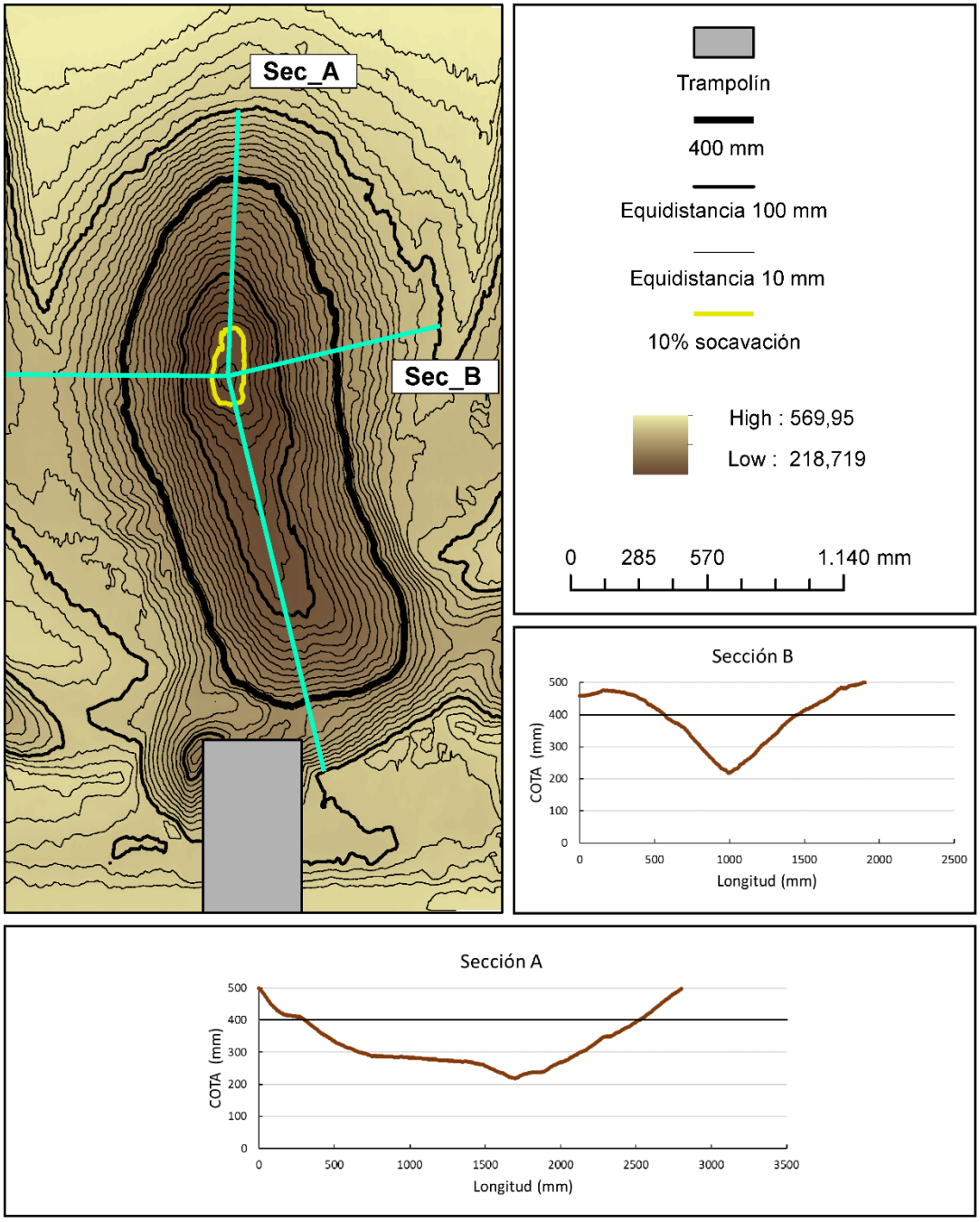

29	Radio 0,3 m	Ángulo 15°	Colchón 0,06 m	Caudal 42 l/s

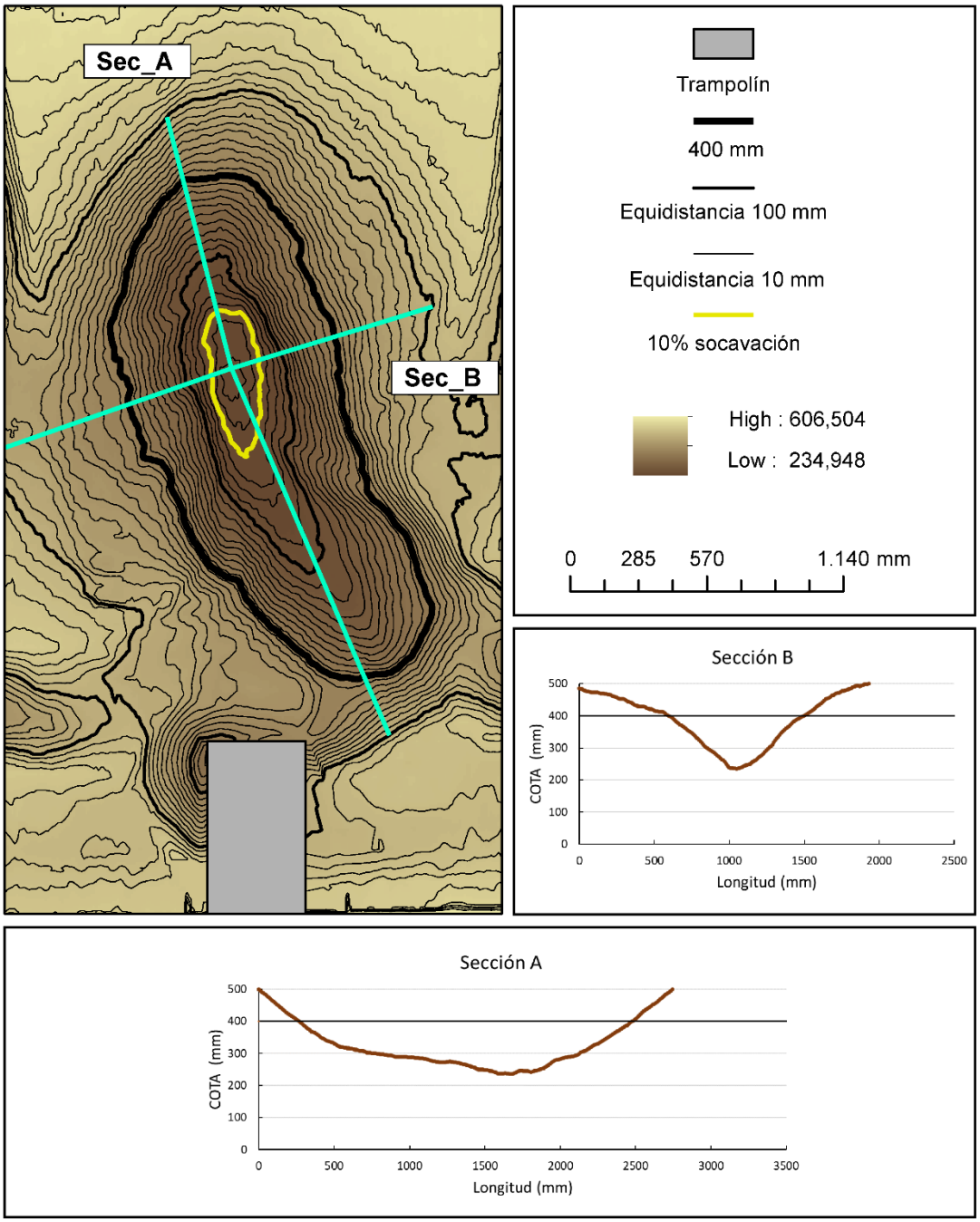

30	Radio 0,3 m	Ángulo 15°	Colchón 0,06 m	Caudal 50 l/s

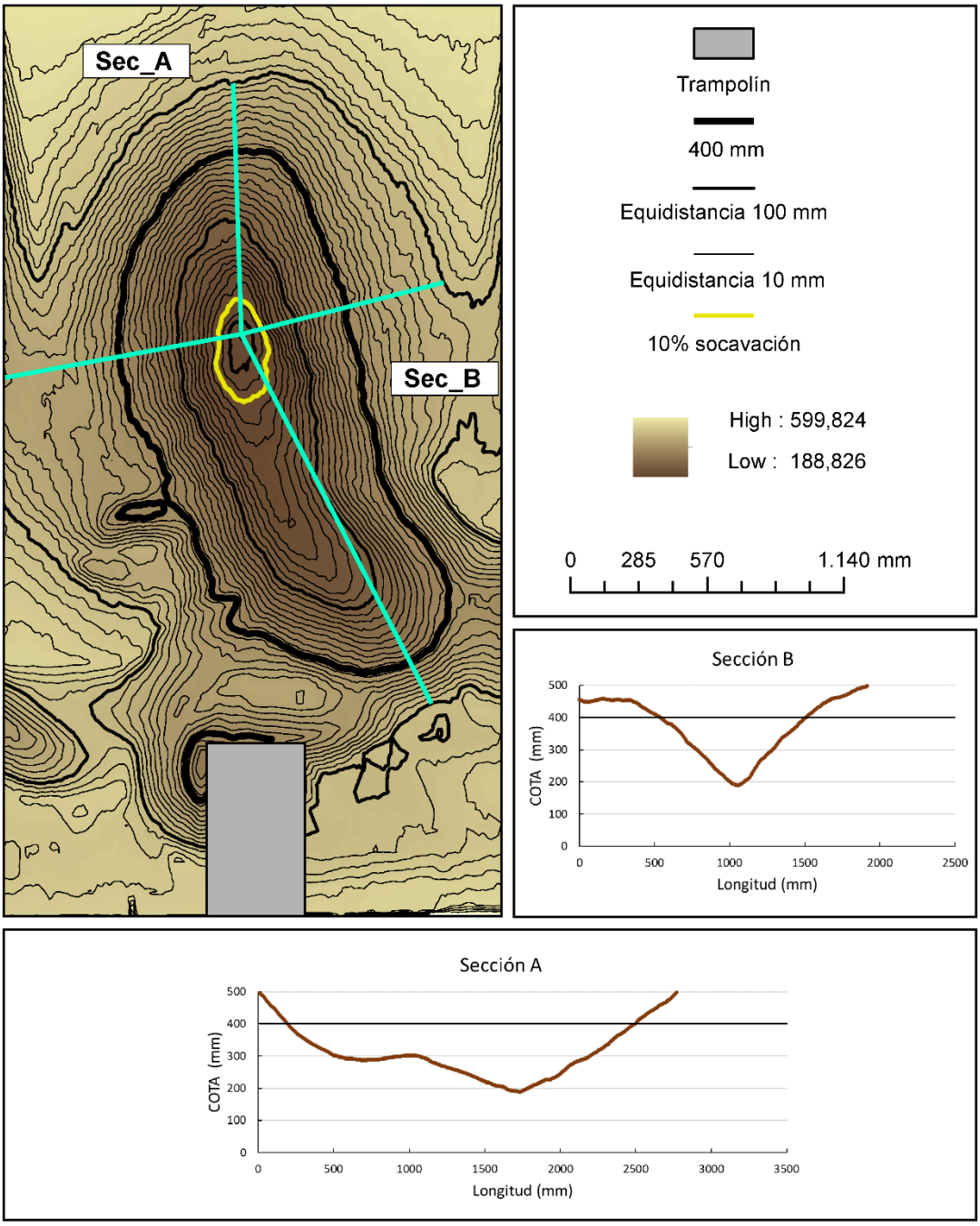

31	Radio 0,3 m	Ángulo 30°	Colchón 0,00 m	Caudal 37,5 l/s

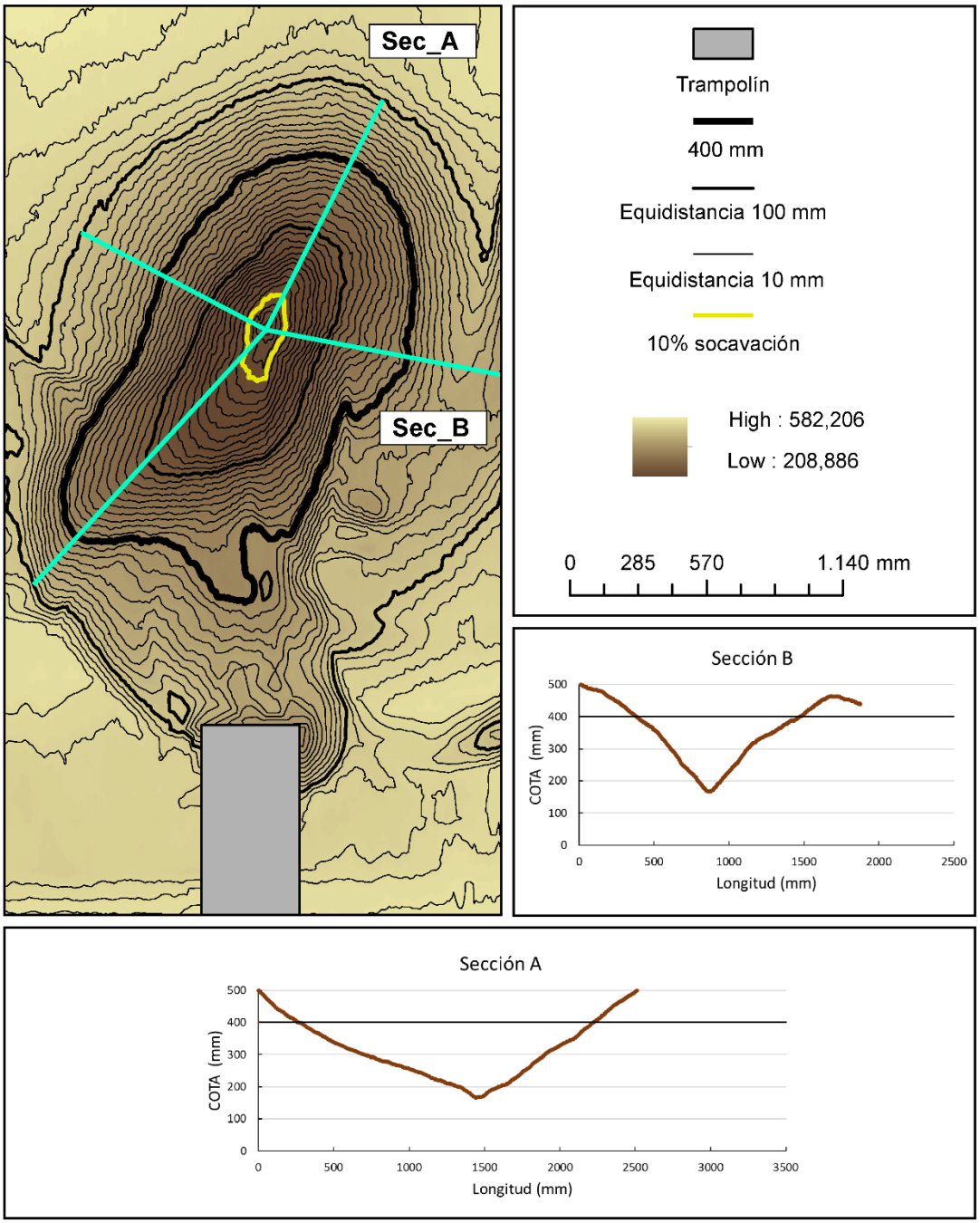

32	Radio 0,3 m	Ángulo 30°	Colchón 0,00 m	Caudal 42 l/s

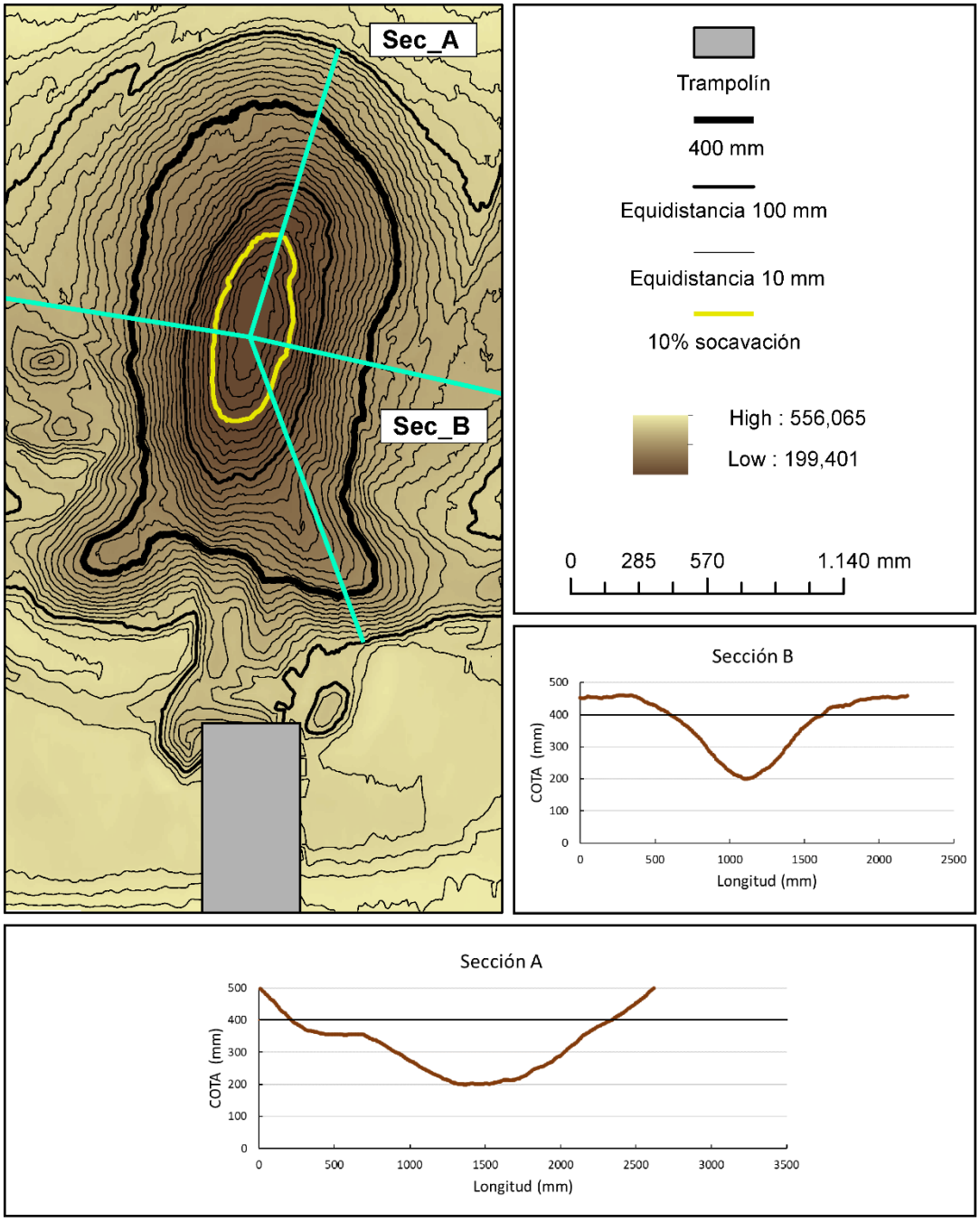

33	Radio 0,3 m	Ángulo 30°	Colchón 0,00 m	Caudal 50 l/s

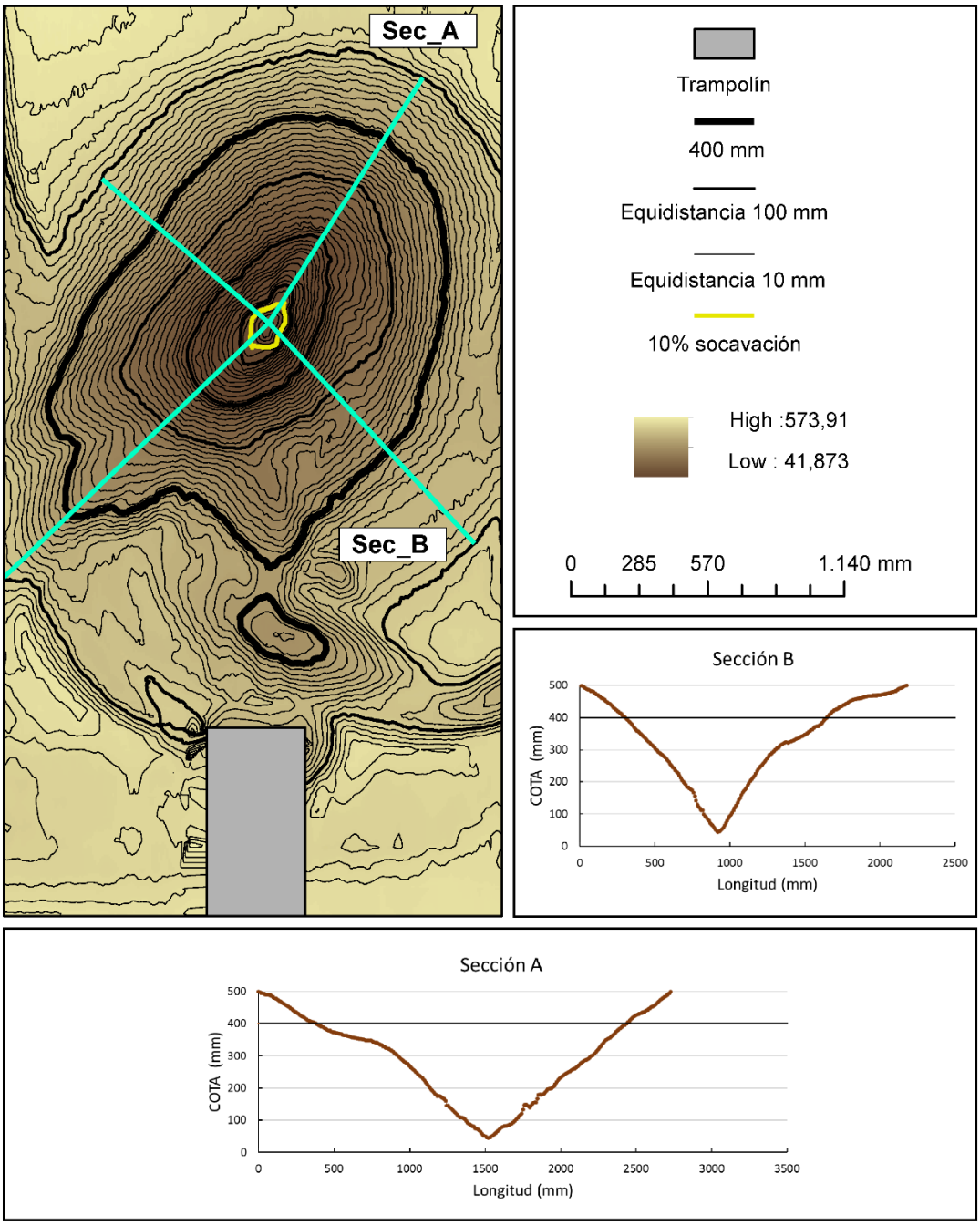

34	Radio 0,3 m	Ángulo 30°	Colchón 0,06 m	Caudal 37,5 l/s

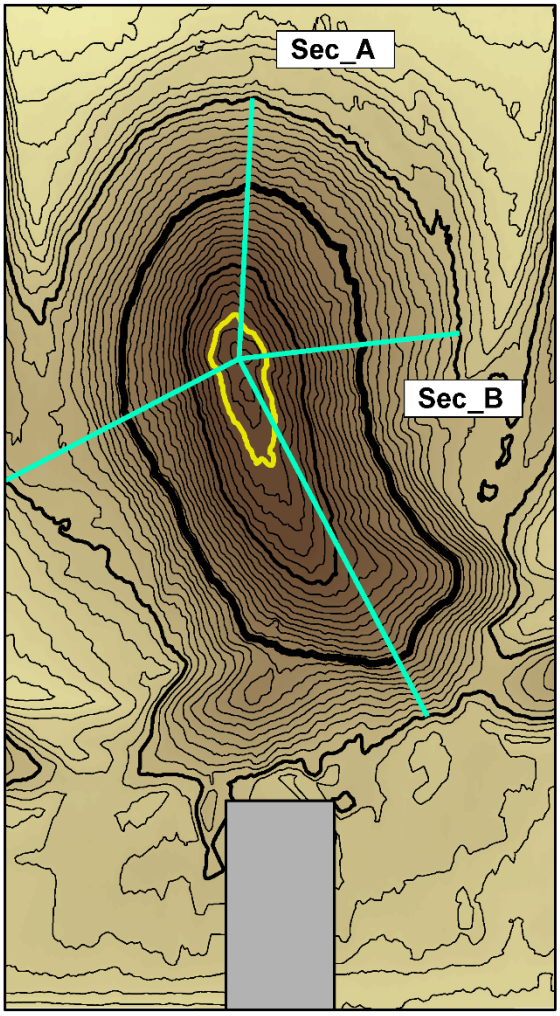

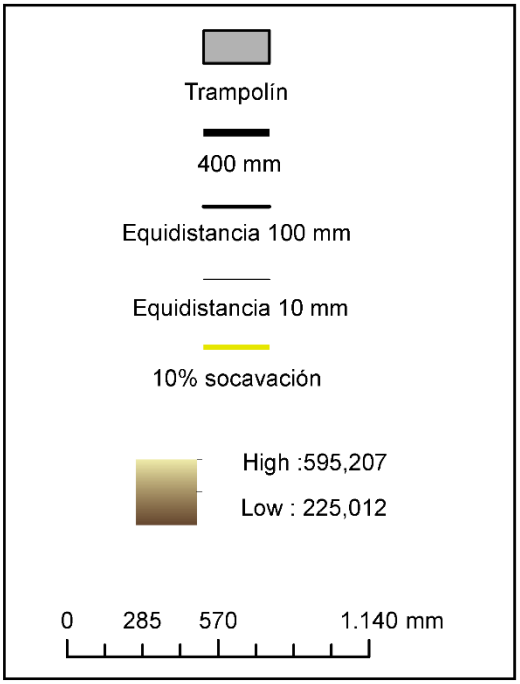

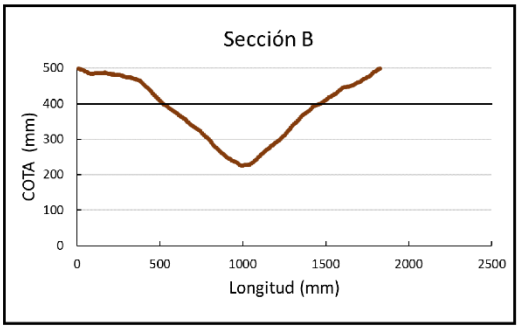

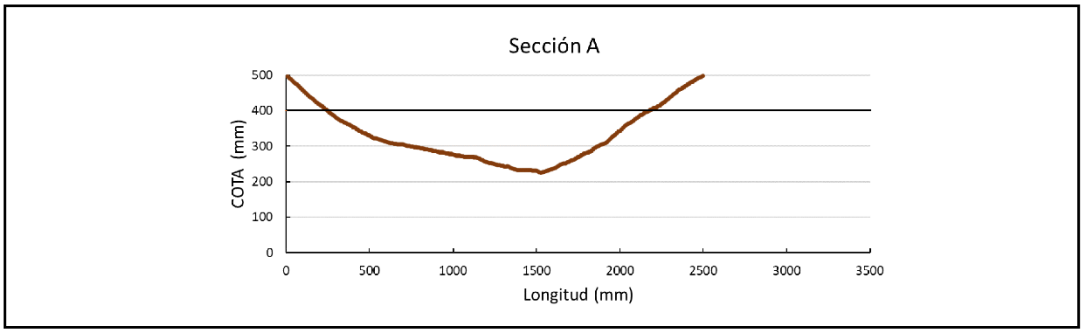

35	Radio 0,3 m	Ángulo 30°	Colchón 0,06 m	Caudal 42 l/s

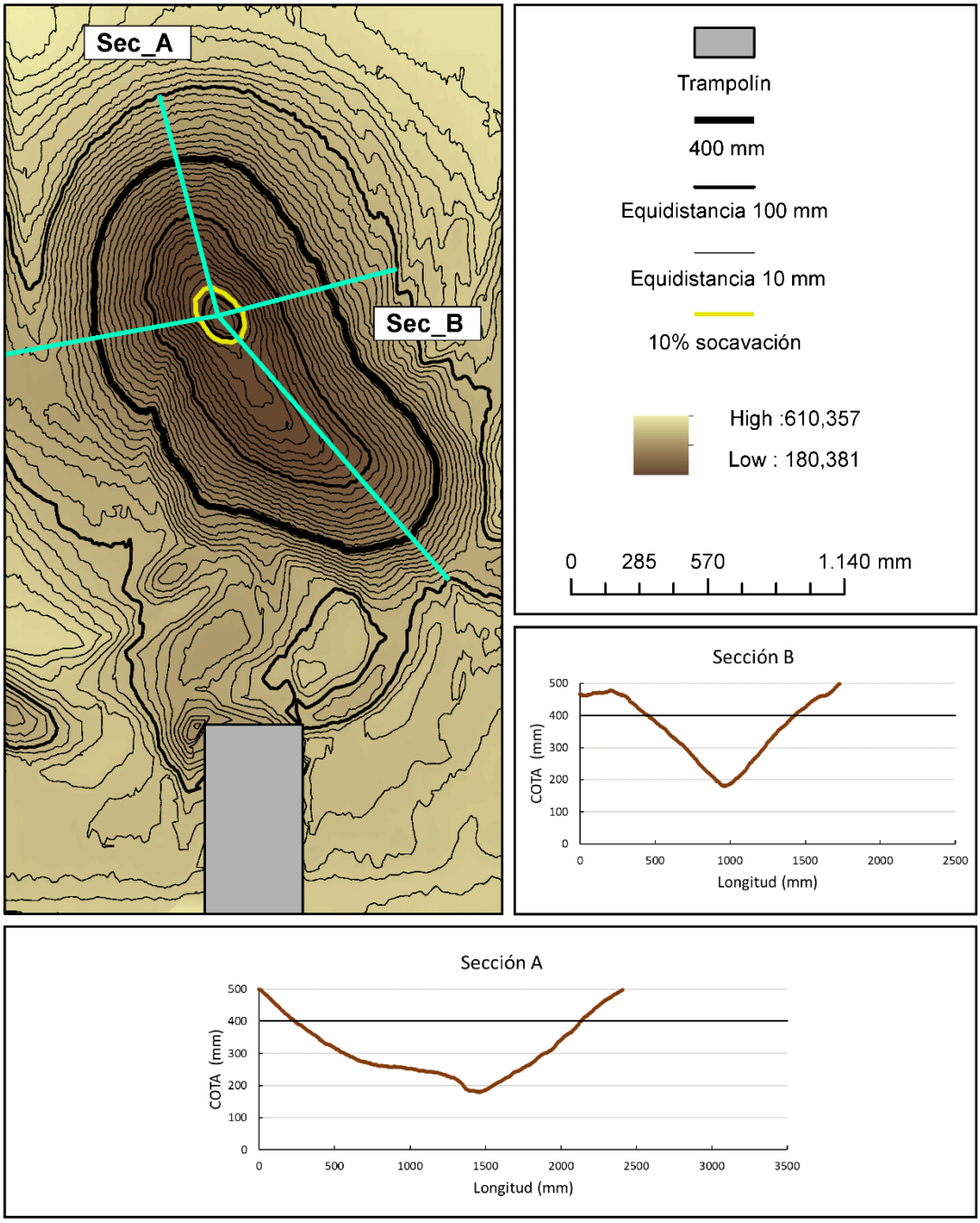

36	Radio 0,3 m	Ángulo 30°	Colchón 0,06 m	Caudal 50 l/s

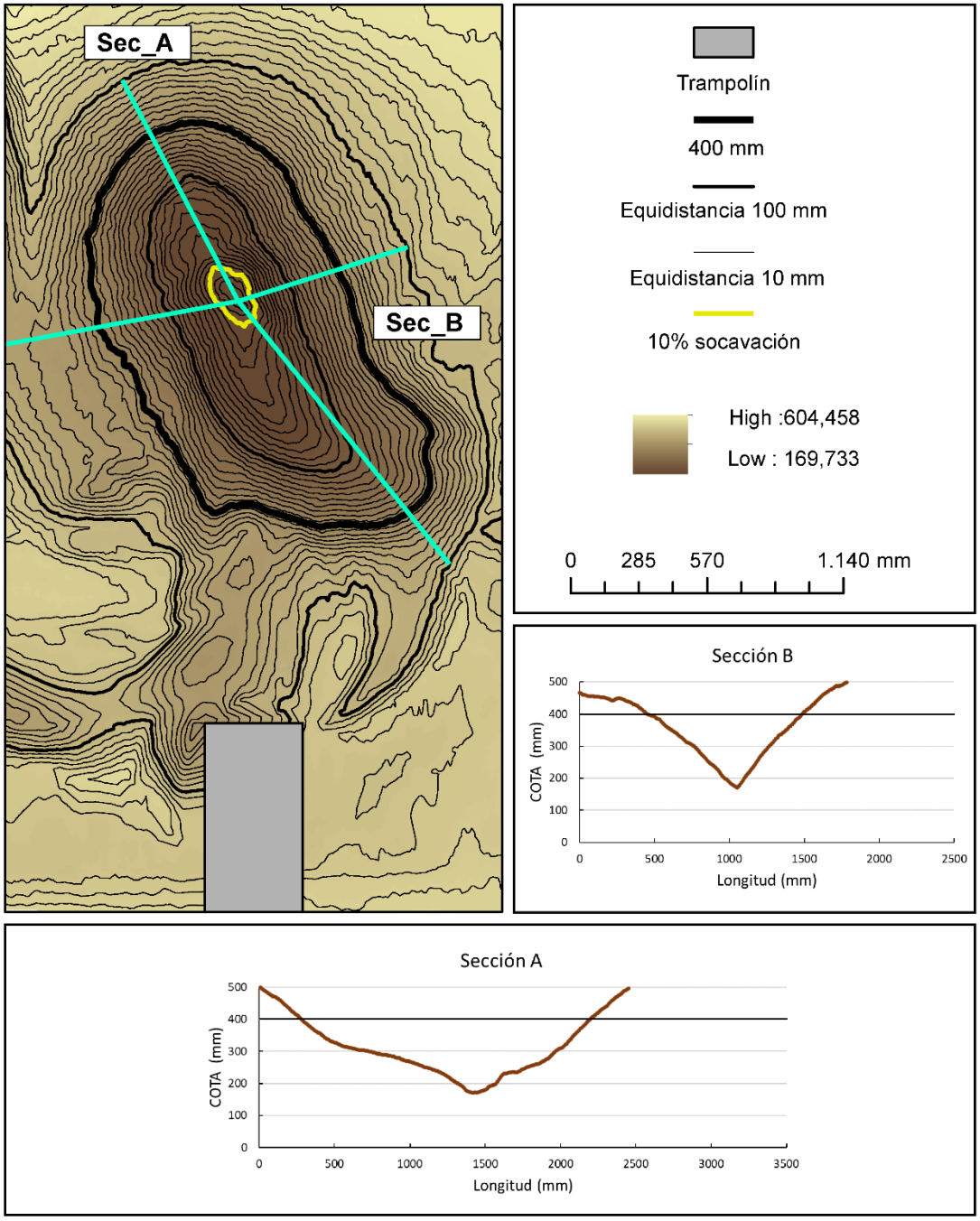

37	Radio 0,3 m	Ángulo 45°	Colchón 0,00 m	Caudal 37,5 l/s

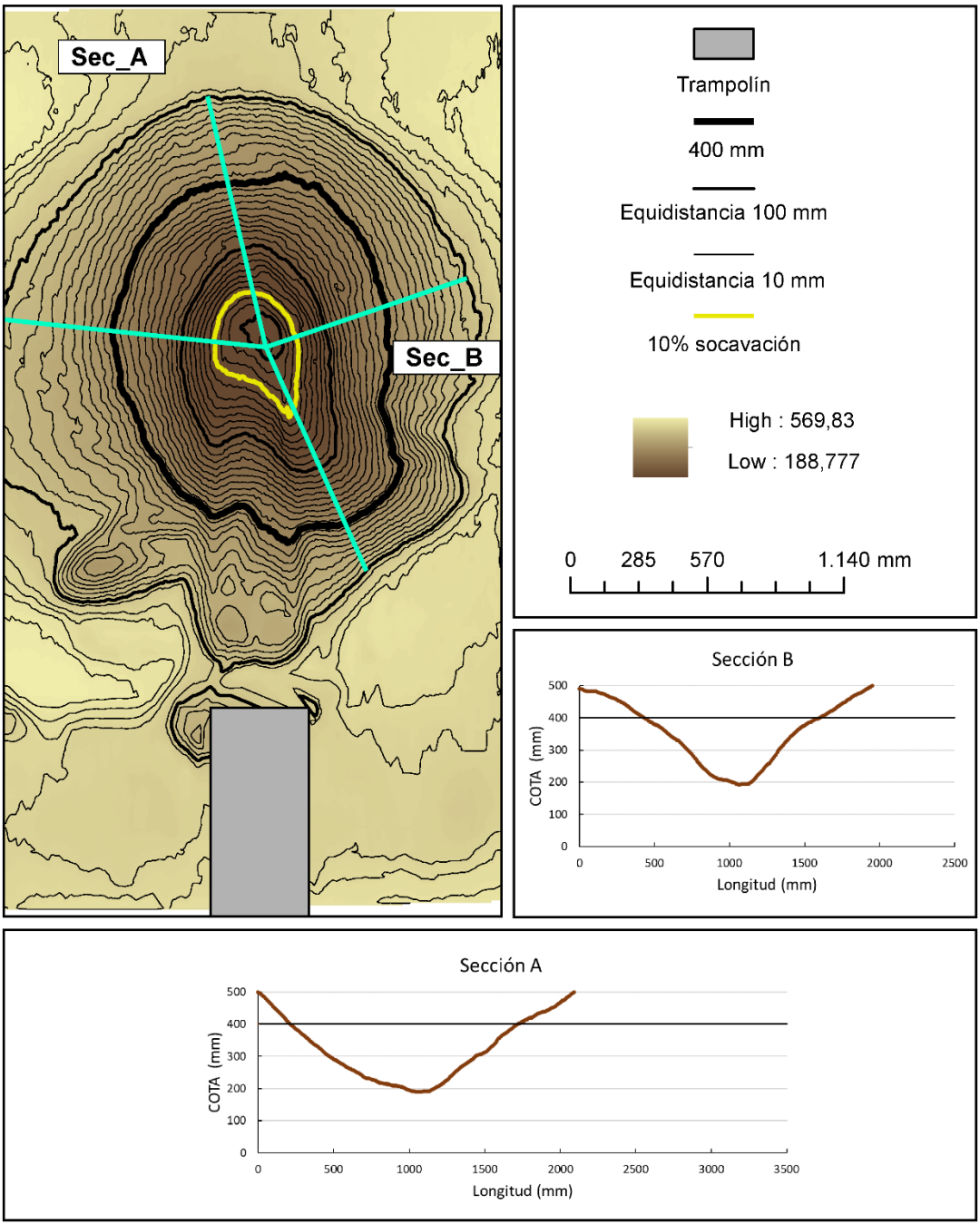

38	Radio 0,3 m	Ángulo 45°	Colchón 0,00 m	Caudal 42 l/s

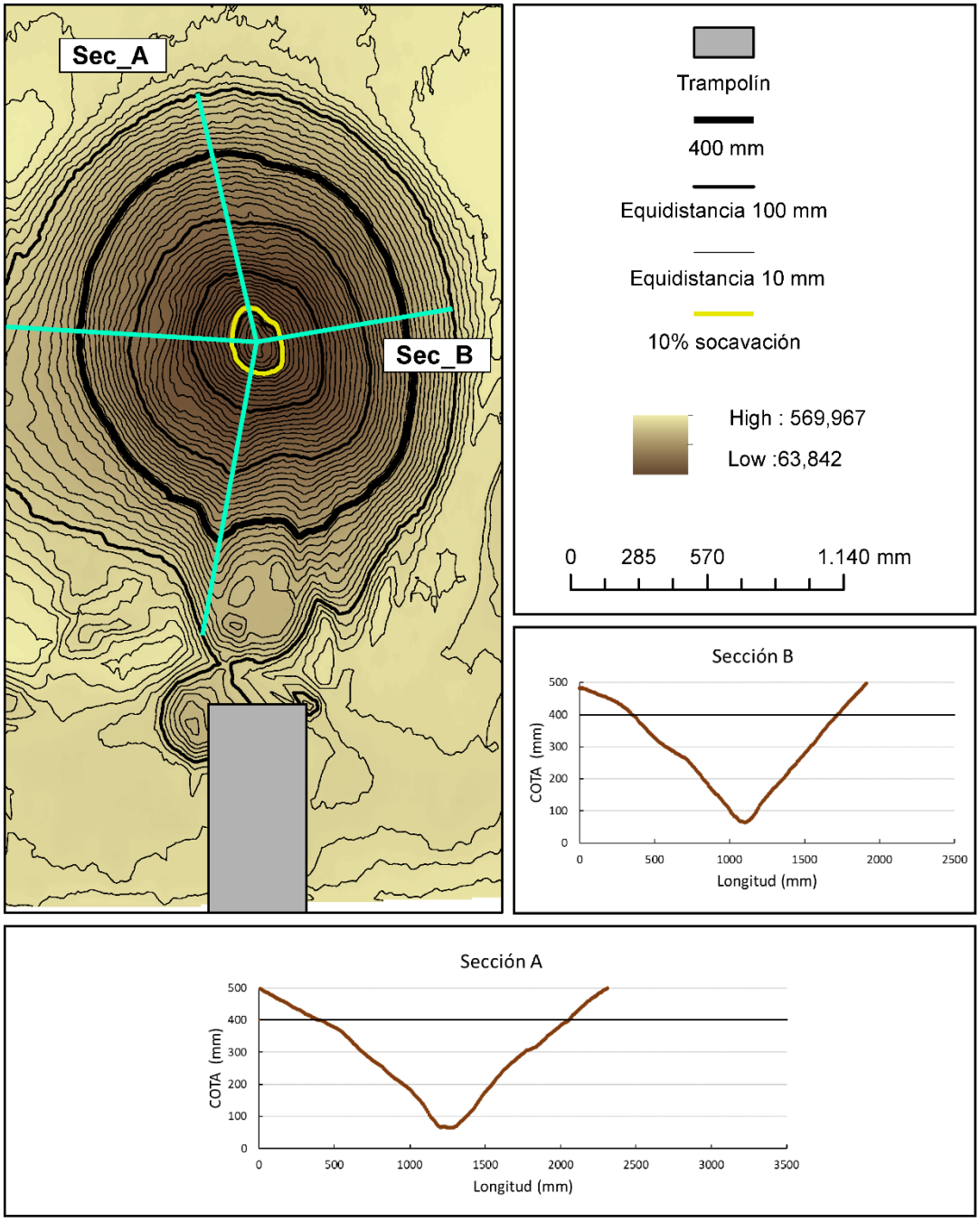

39	Radio 0,3 m	Ángulo 45°	Colchón 0,00 m	Caudal 50 l/s

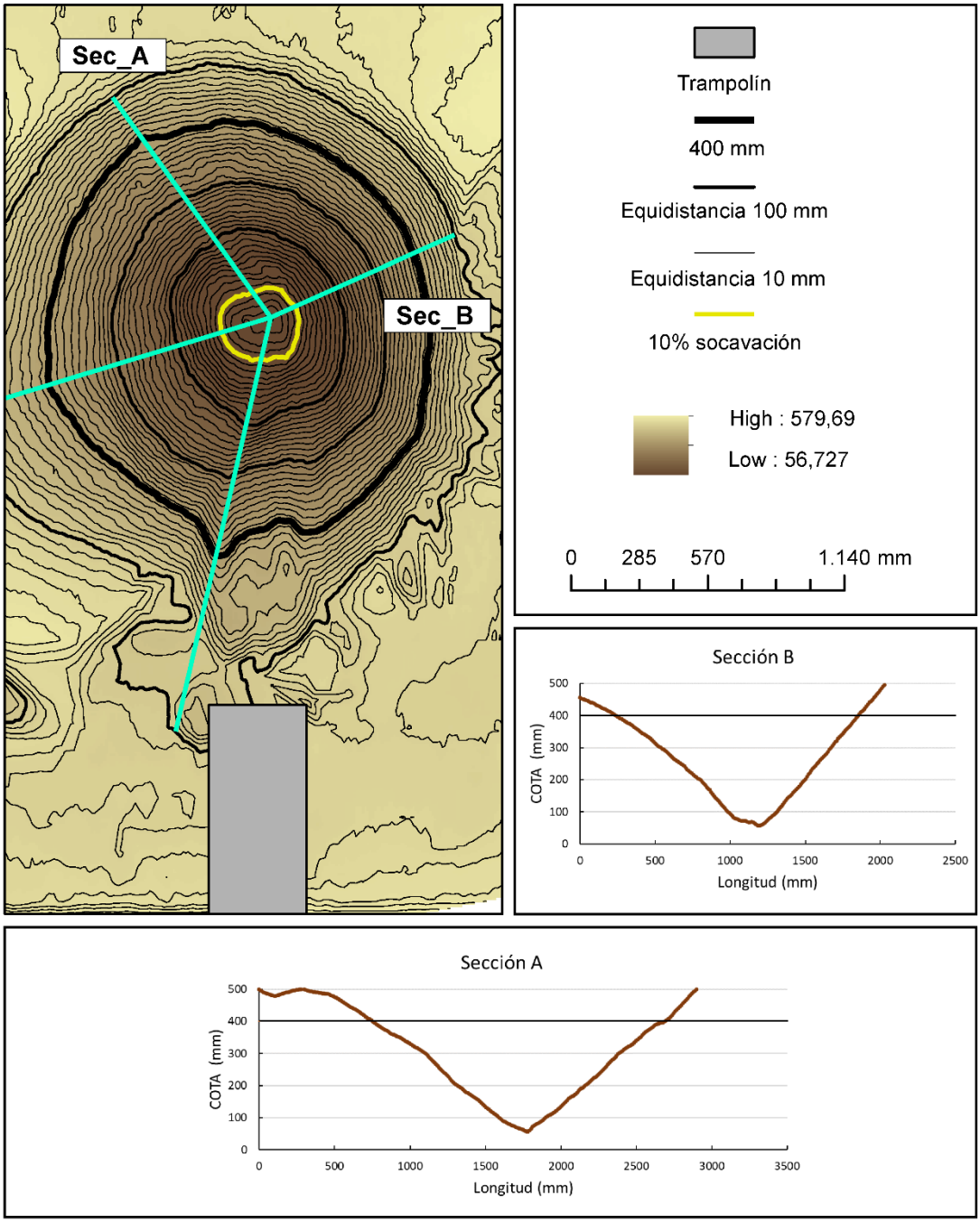

40	Radio 0,3 m	Ángulo 45°	Colchón 0,06 m	Caudal 37,5 l/s

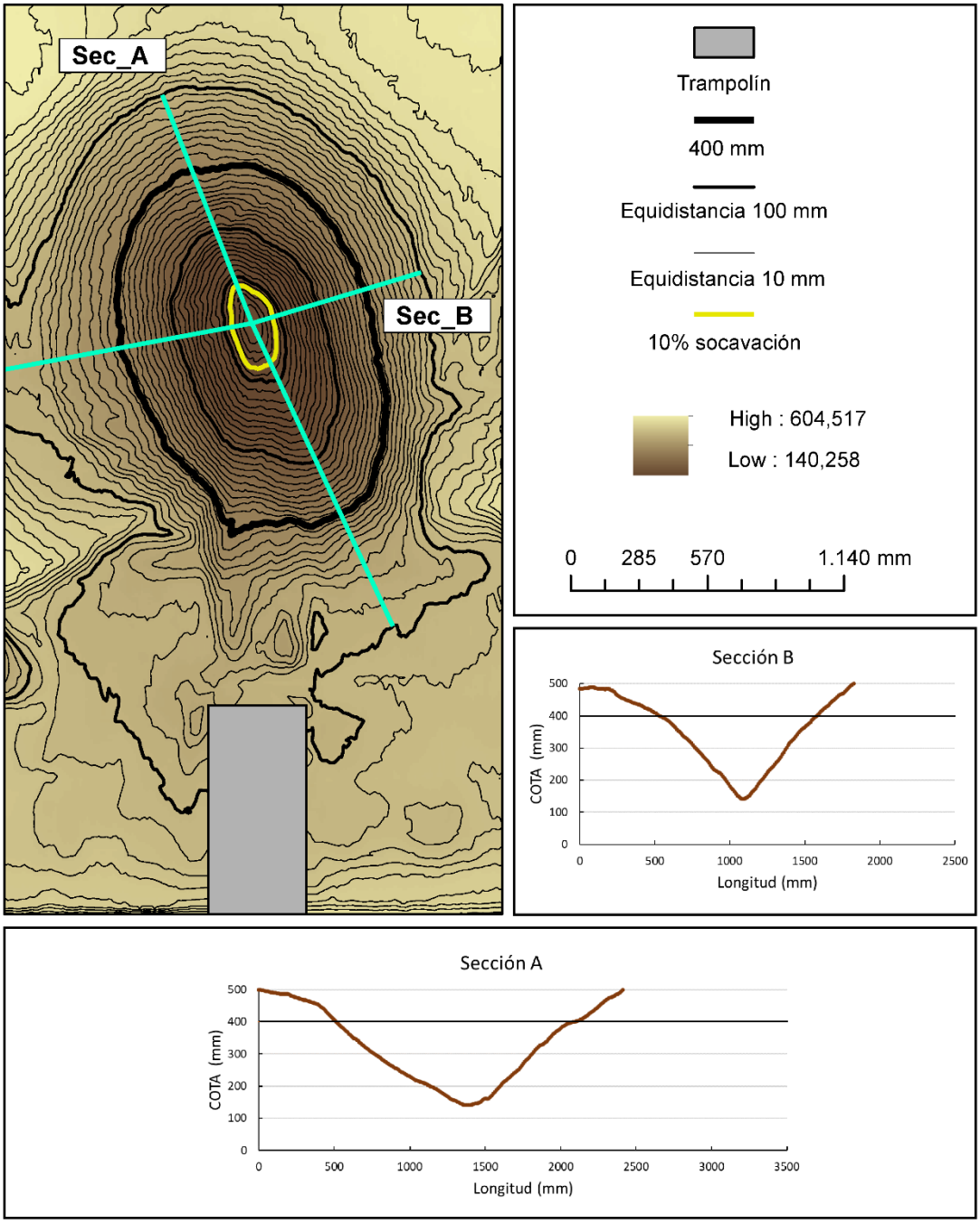

41	Radio 0,3 m	Ángulo 45°	Colchón 0,06 m	Caudal 42 l/s

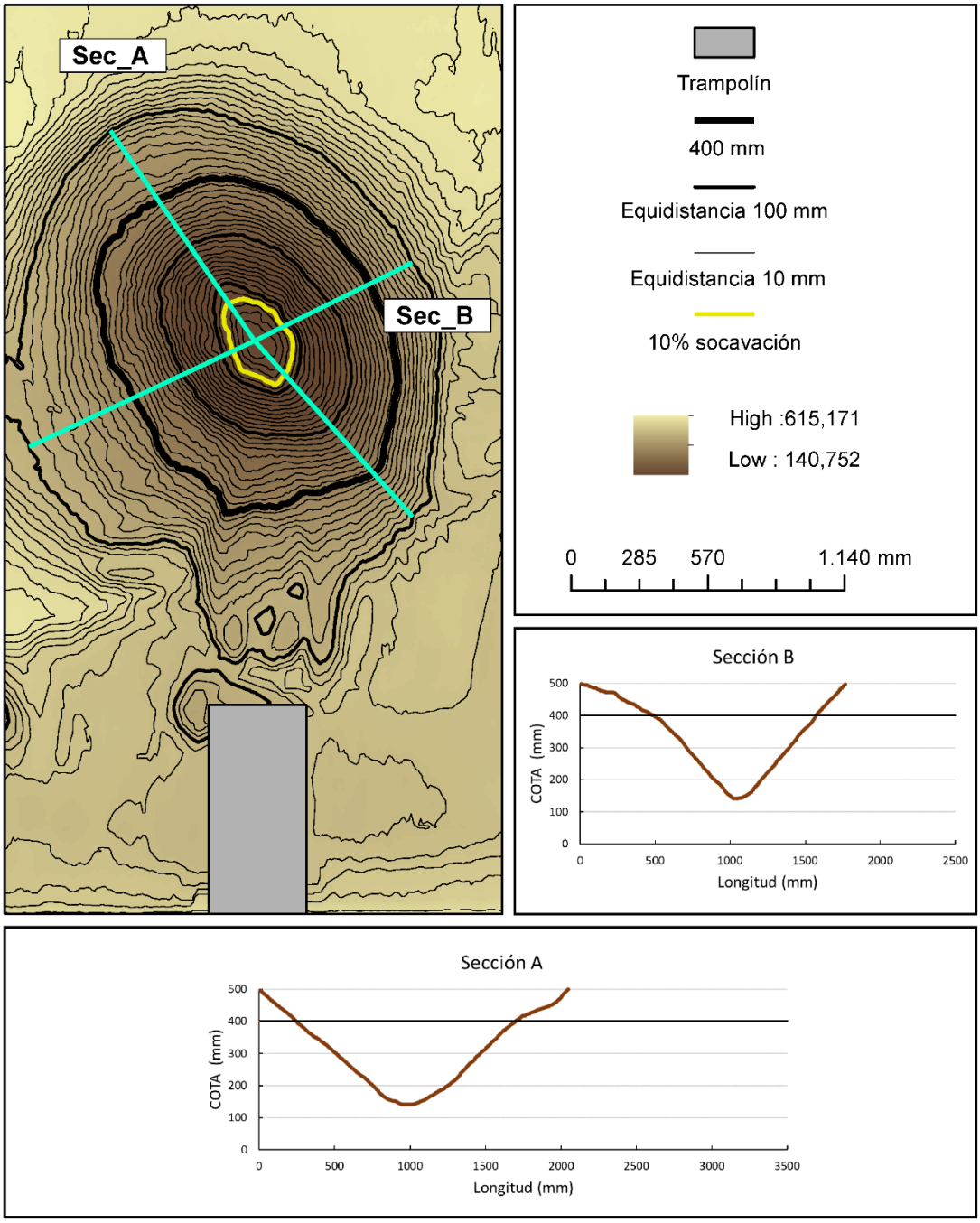

42	Radio 0,3 m	Ángulo 45°	Colchón 0,06 m	Caudal 50 l/s

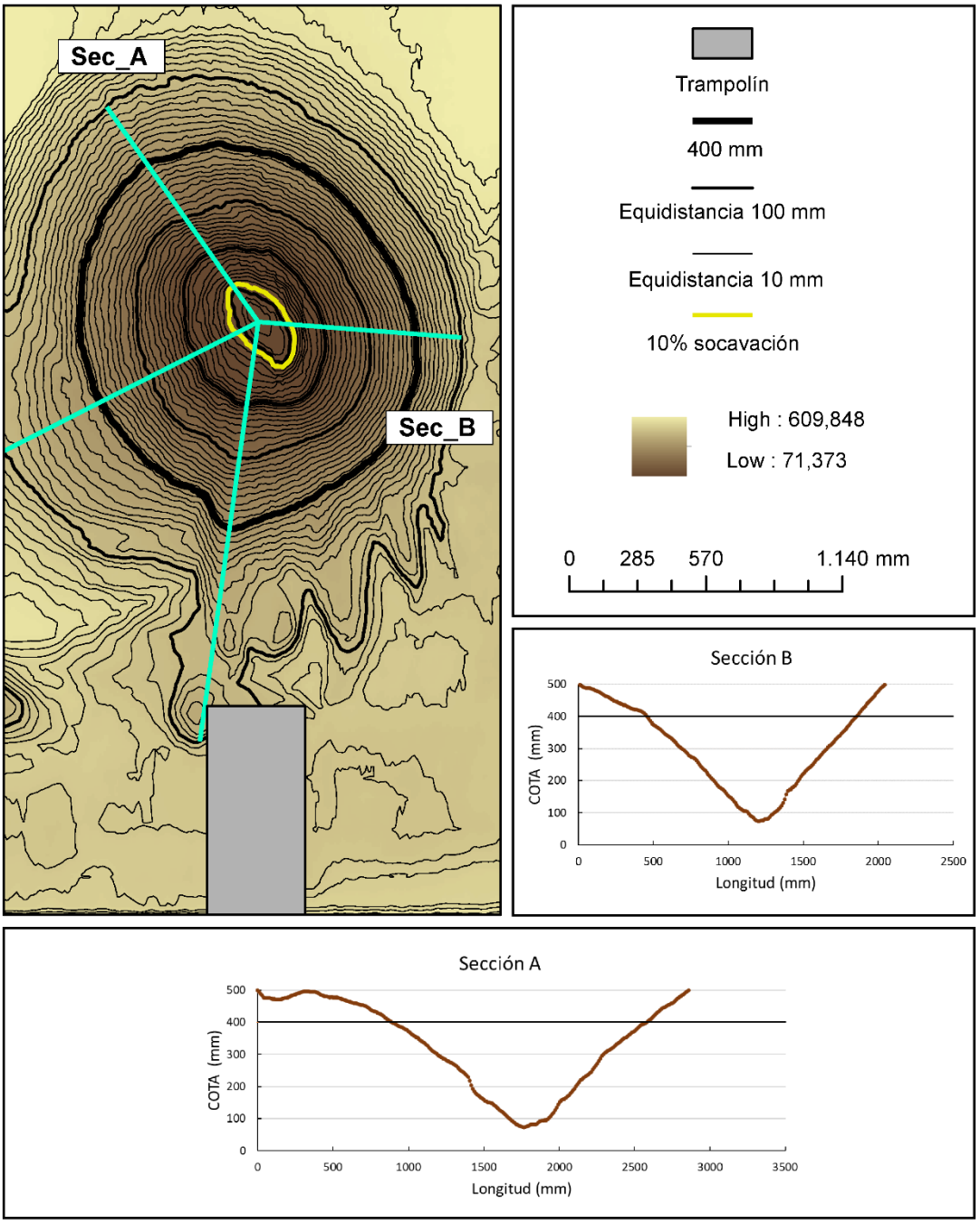

43	Radio 0,4 m	Ángulo 15°	Colchón 0,00 m	Caudal 37,5 l/s

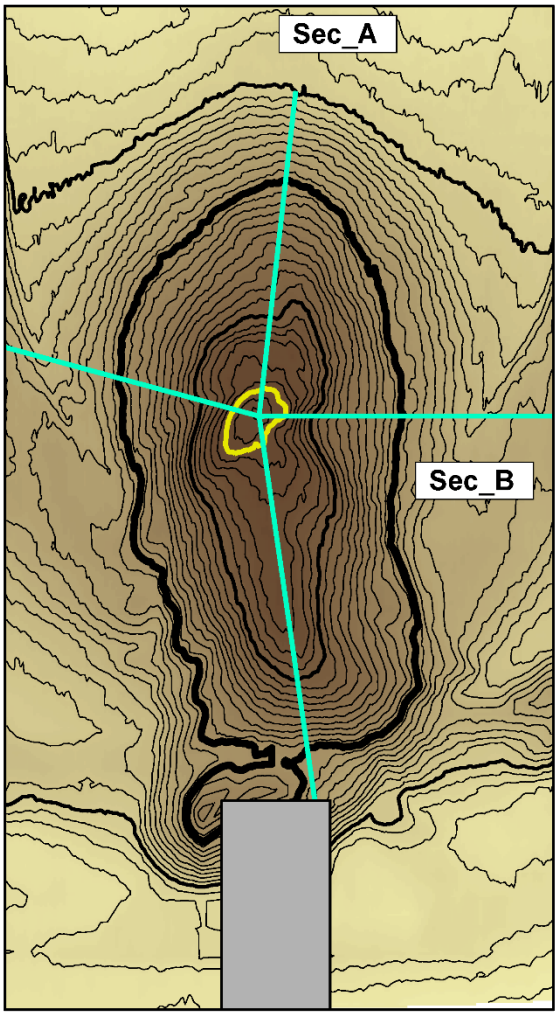

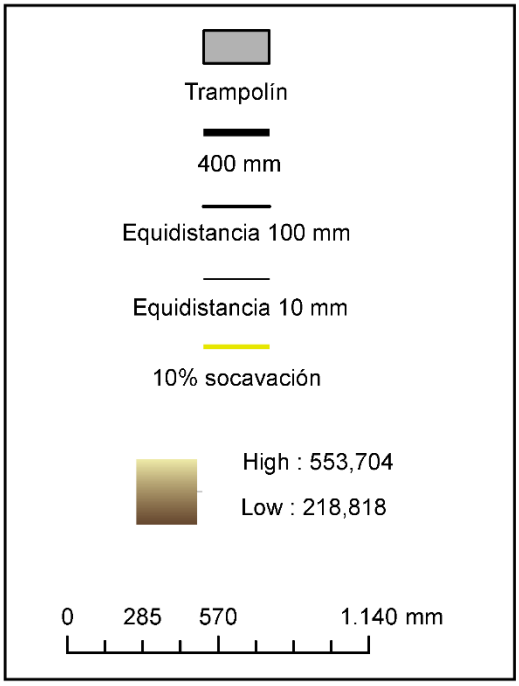

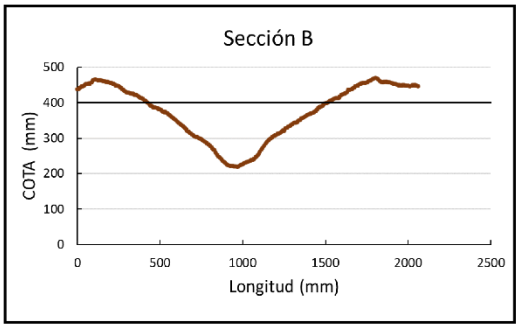

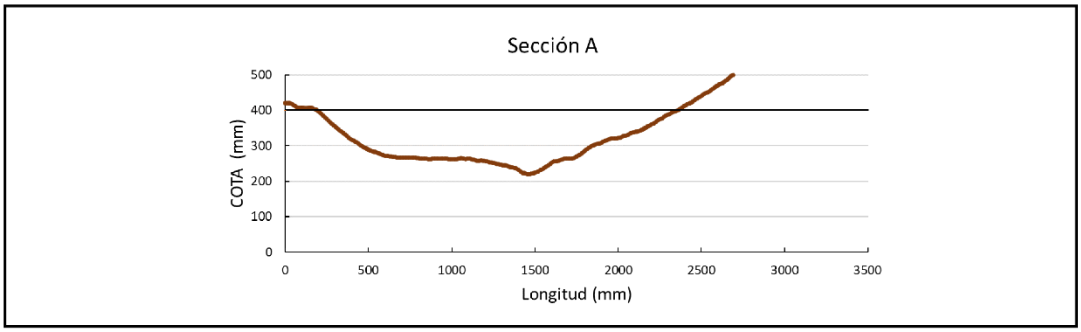

44	Radio 0,4 m	Ángulo 15°	Colchón 0,00 m	Caudal 42 l/s

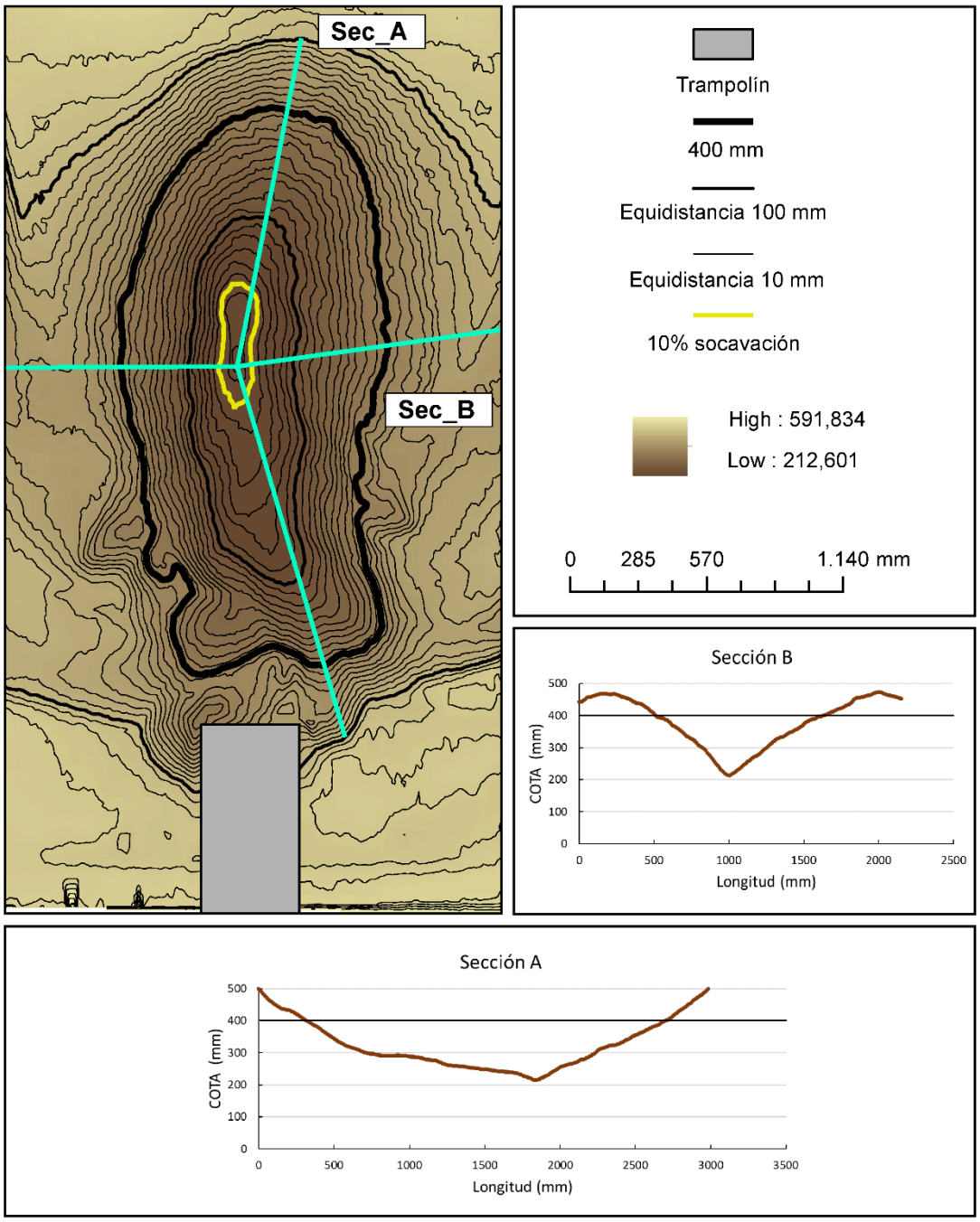

45	Radio 0,4 m	Ángulo 15°	Colchón 0,00 m	Caudal 50 l/s

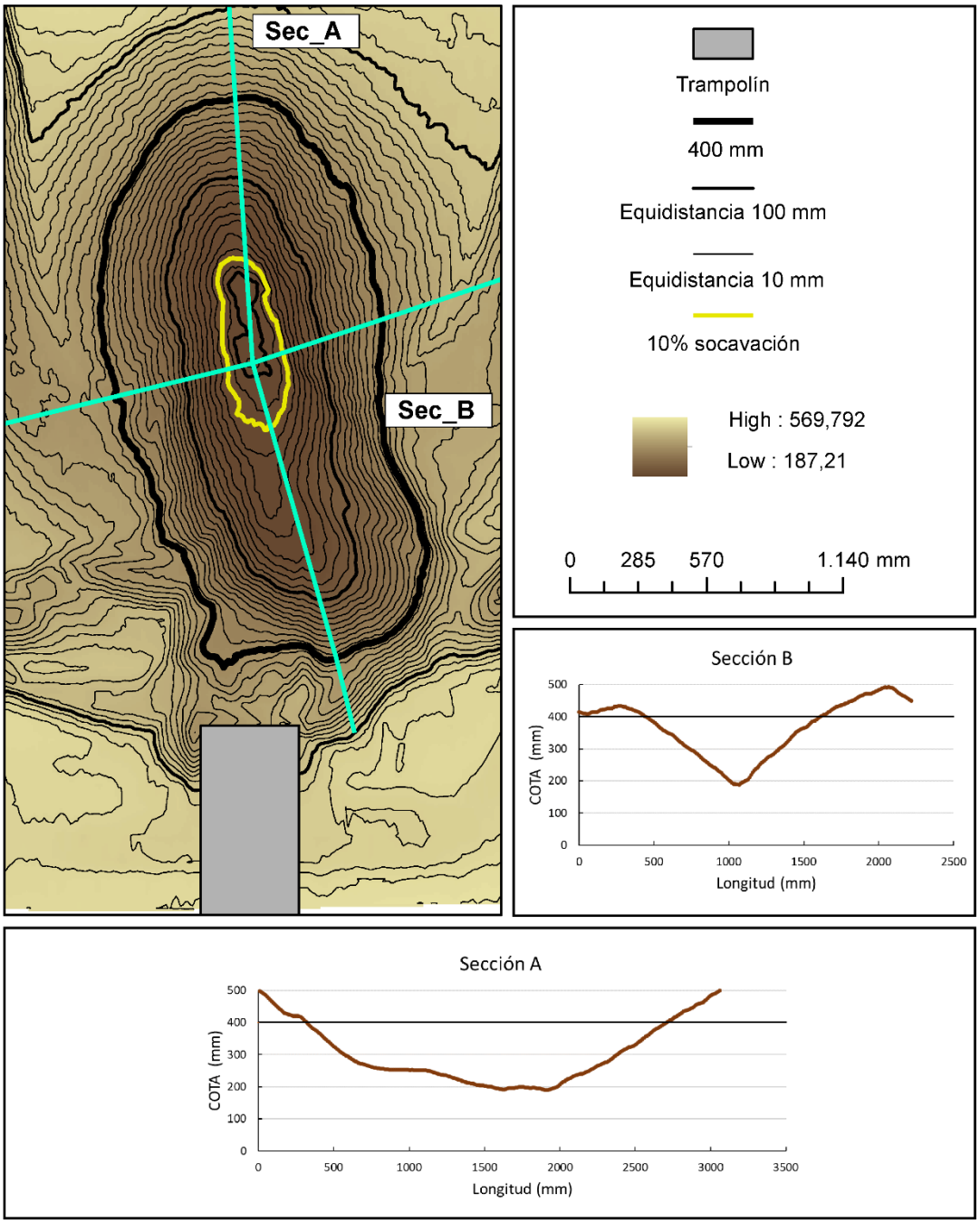

46	Radio 0,4 m	Ángulo 15°	Colchón 0,06 m	Caudal 37,5 l/s

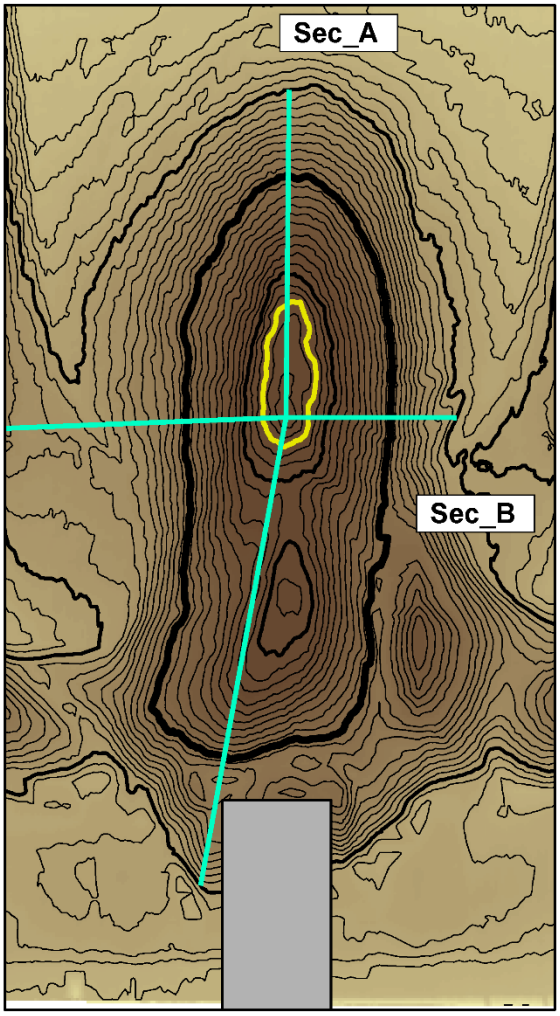

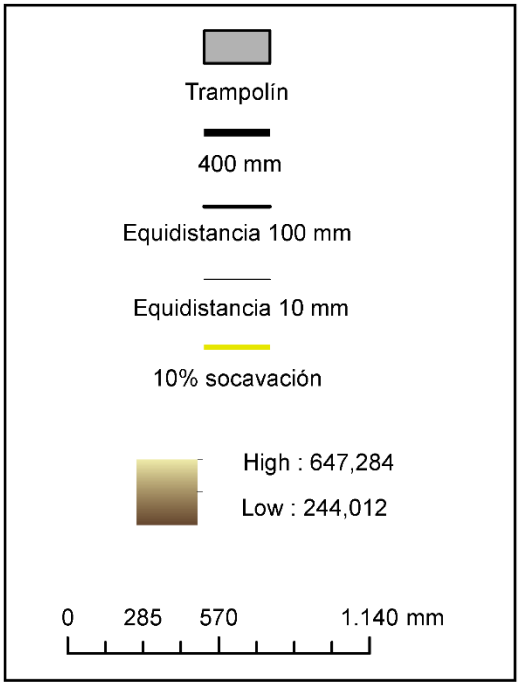

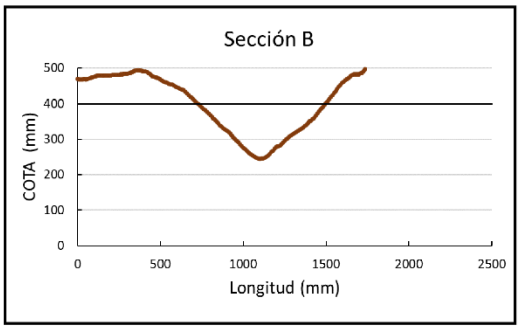

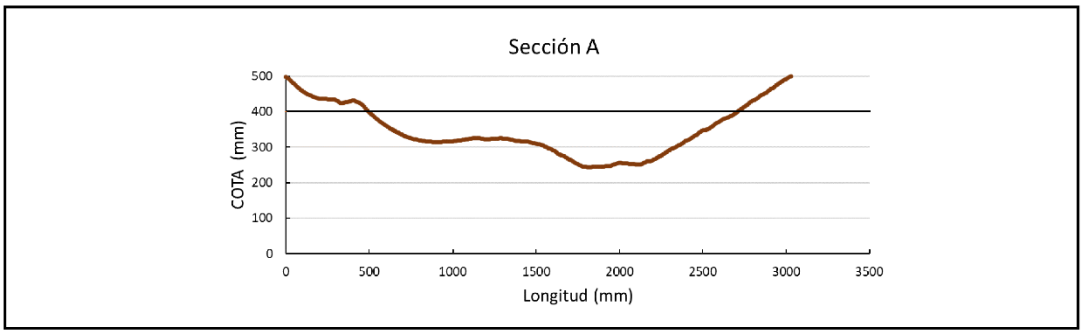

47	Radio 0,4 m	Ángulo 15°	Colchón 0,06 m	Caudal 42 l/s

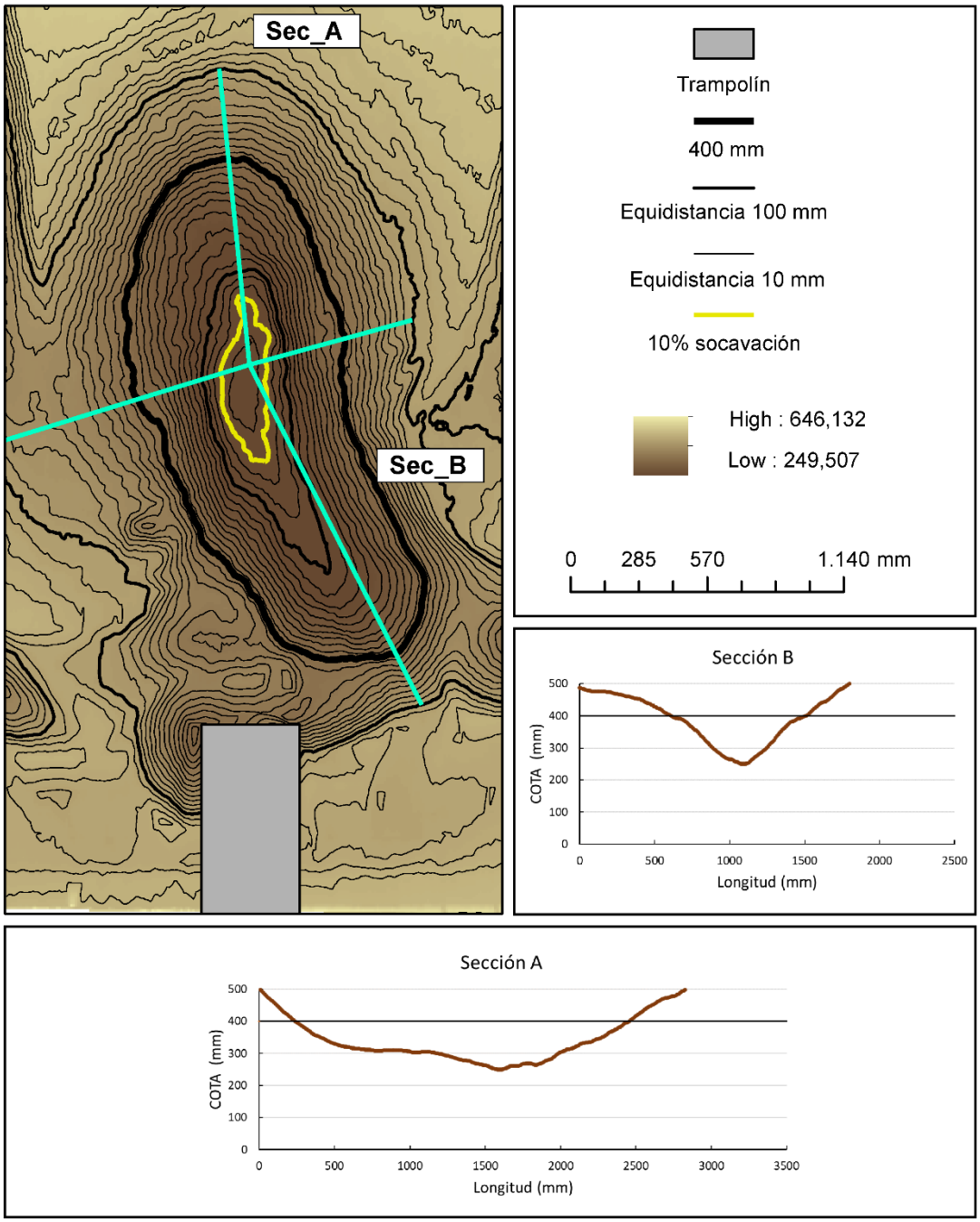

48	Radio 0,4 m	Ángulo 15°	Colchón 0,06 m	Caudal 50 l/s

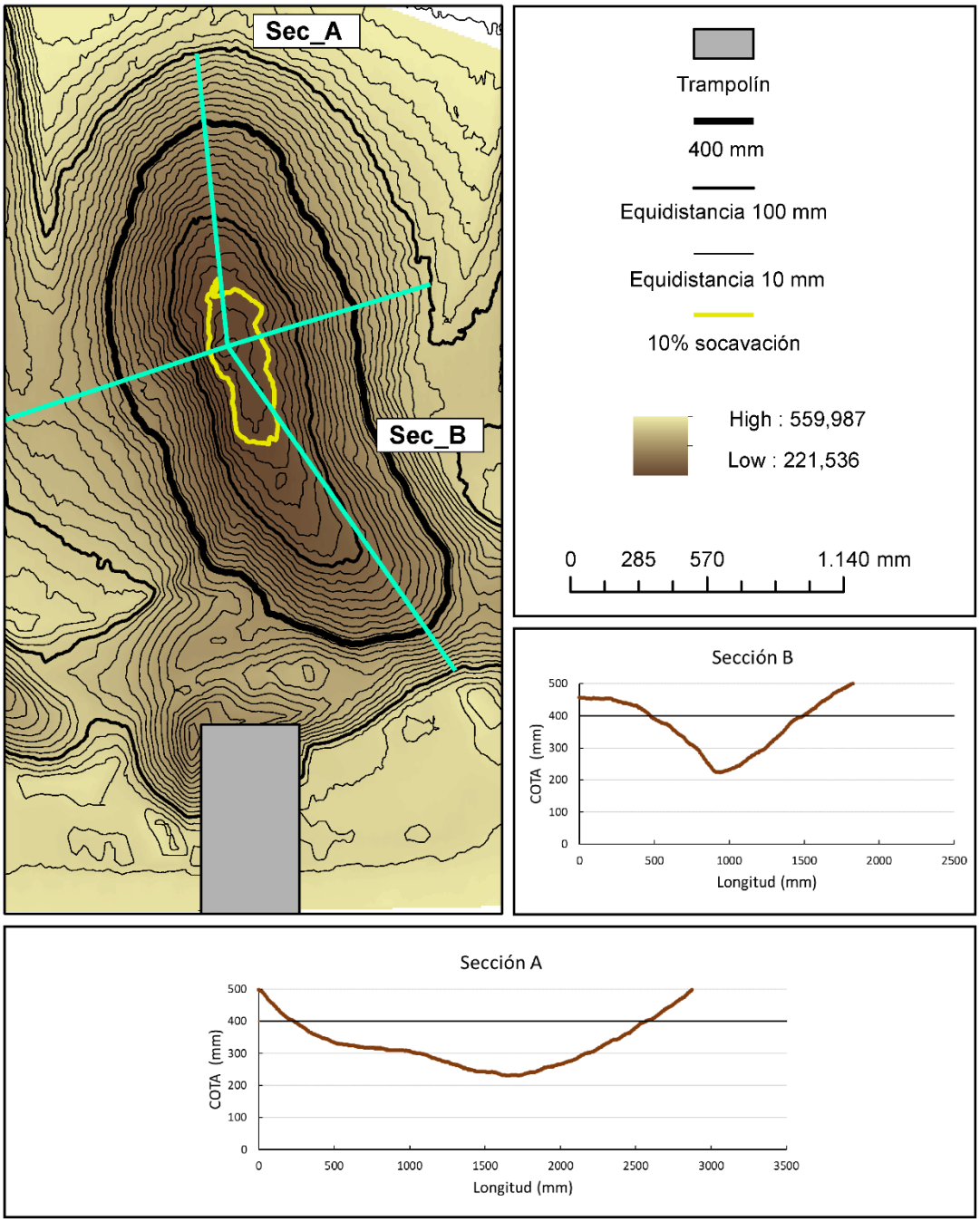

49	Radio 0,4 m	Ángulo 45°	Colchón 0,00 m	Caudal 37,5 l/s

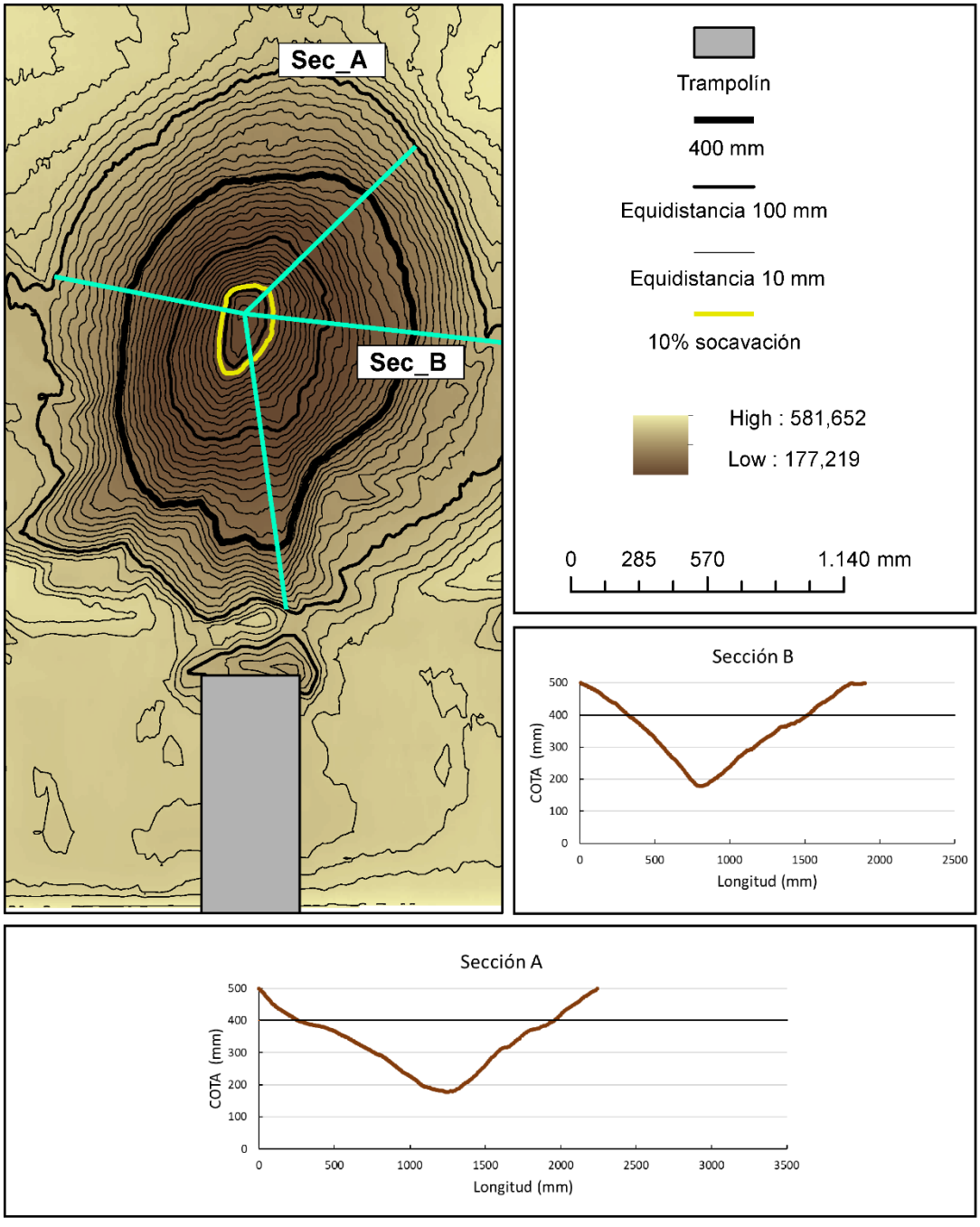

50	Radio 0,4 m	Ángulo 45°	Colchón 0,00 m	Caudal 42 l/s

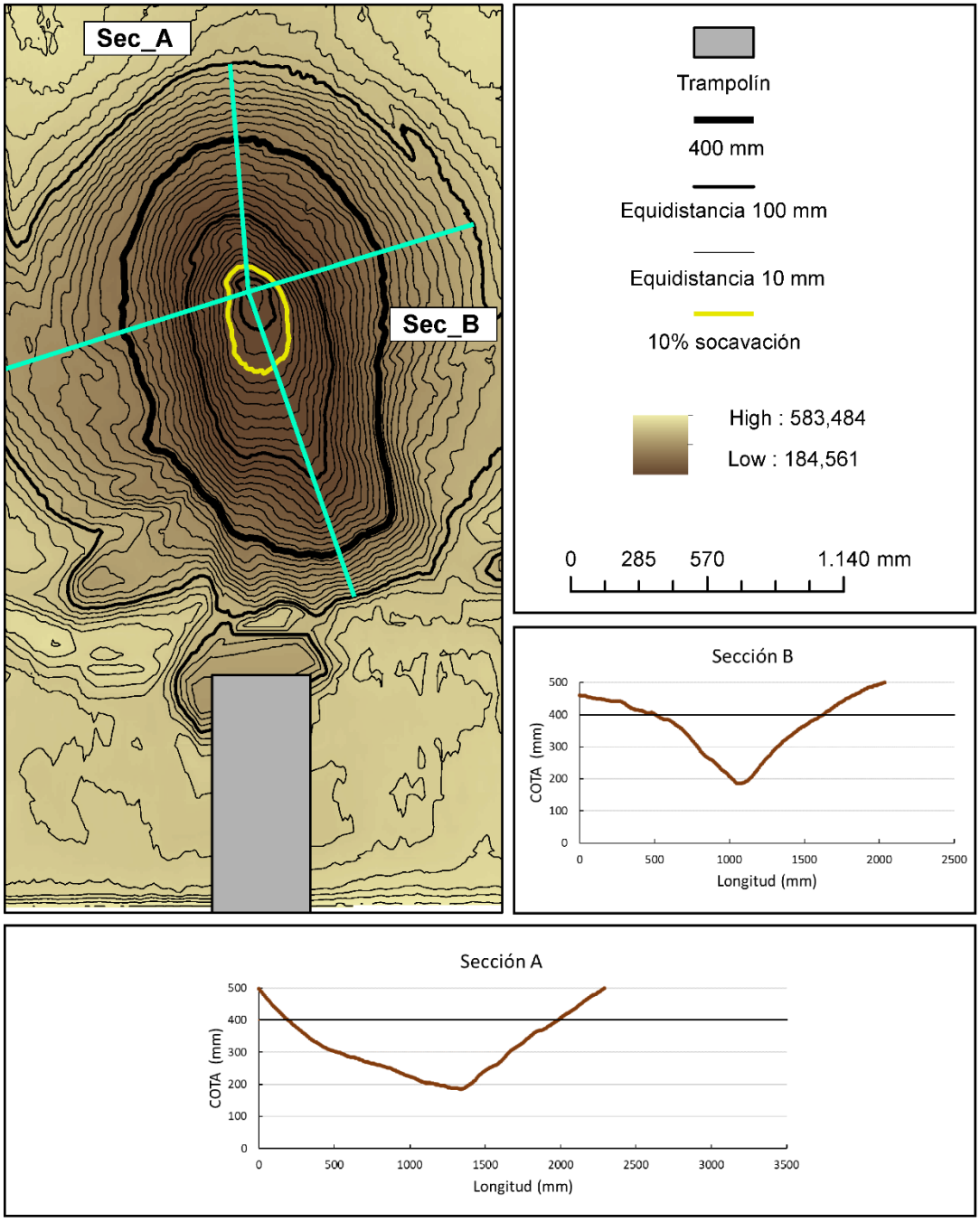

51	Radio 0,4 m	Ángulo 45°	Colchón 0,00 m	Caudal 50 l/s

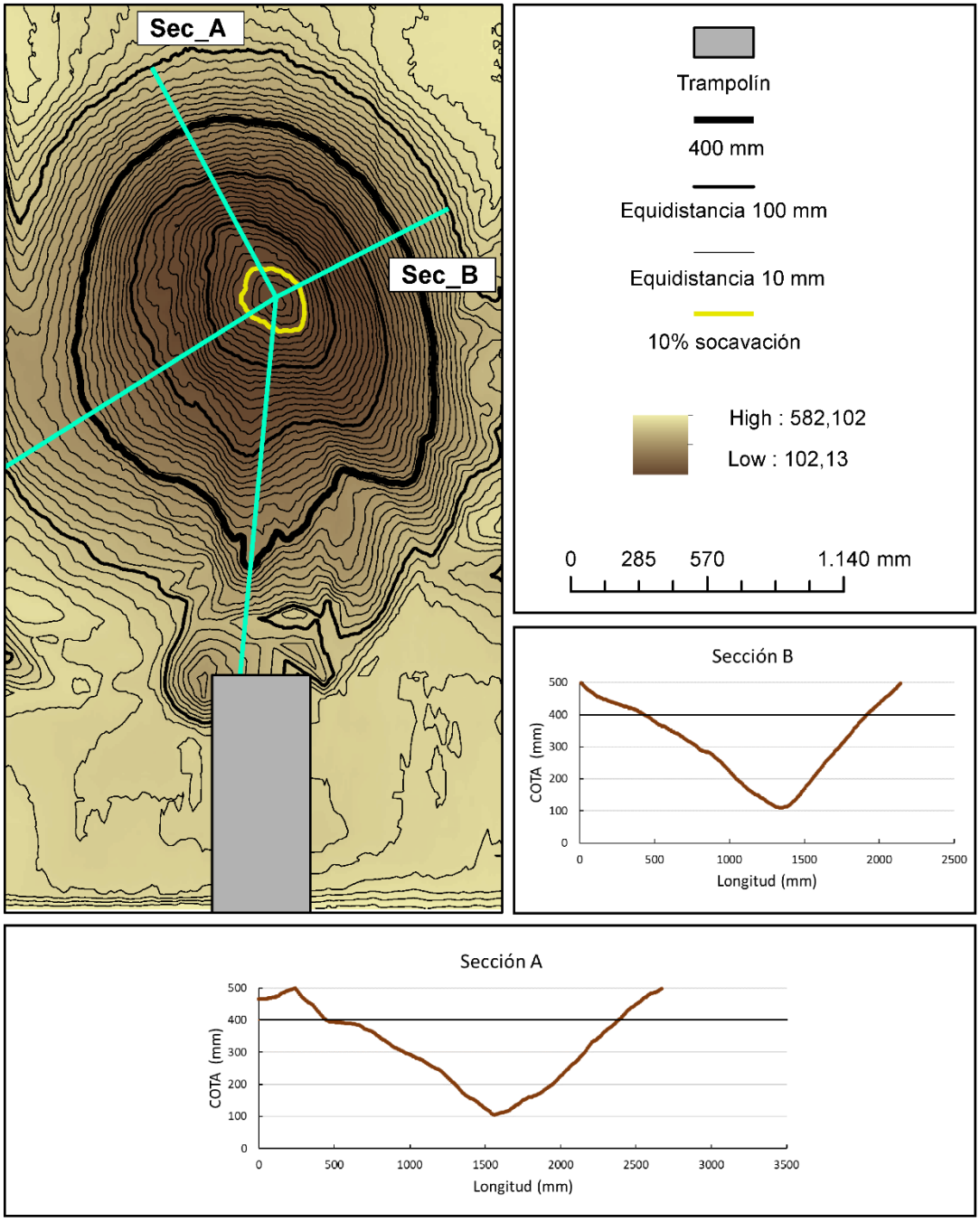

52	Radio 0,4 m	Ángulo 45°	Colchón 0,06 m	Caudal 37,5 l/s

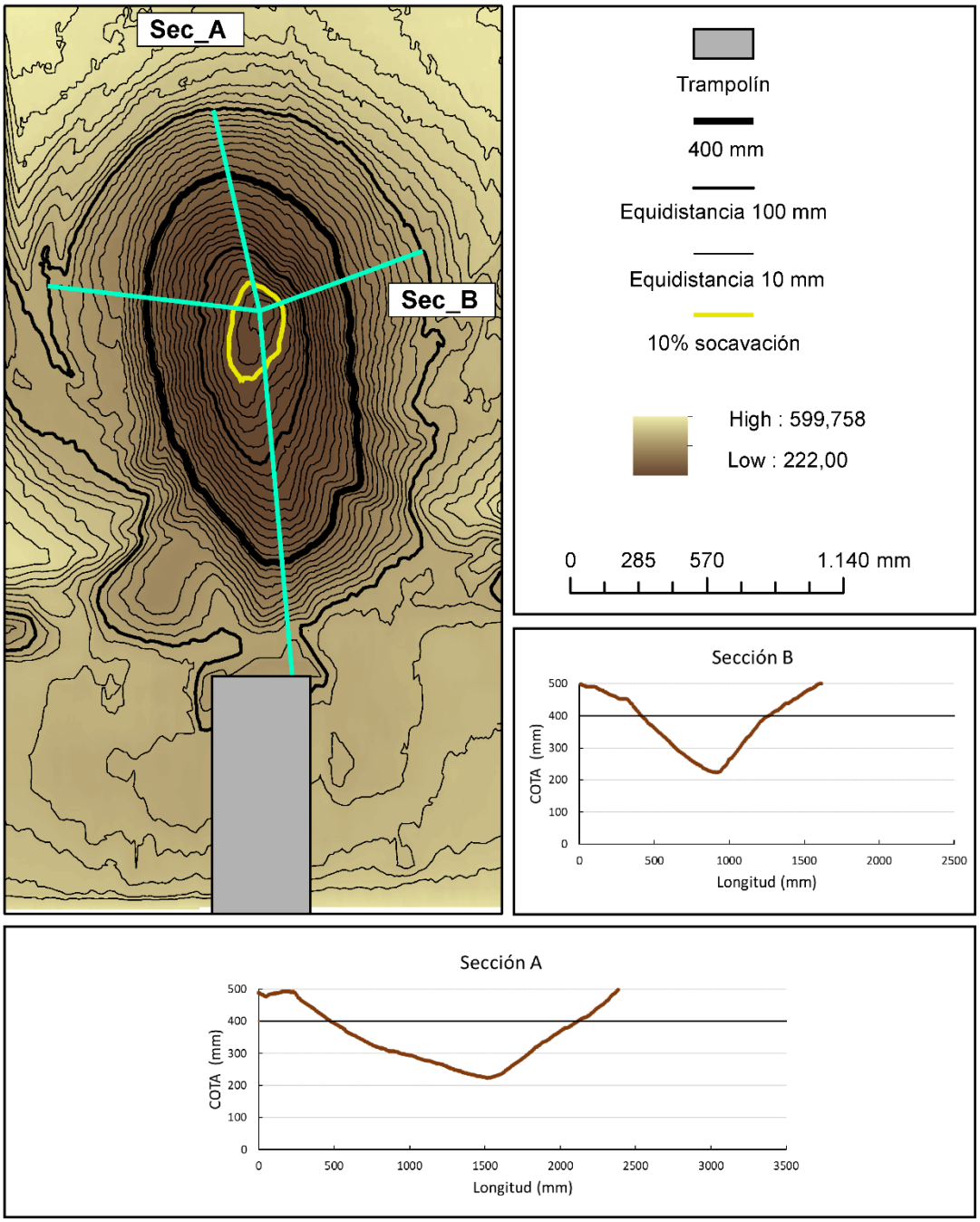

53	Radio 0,4 m	Ángulo 45°	Colchón 0,06 m	Caudal 42 l/s

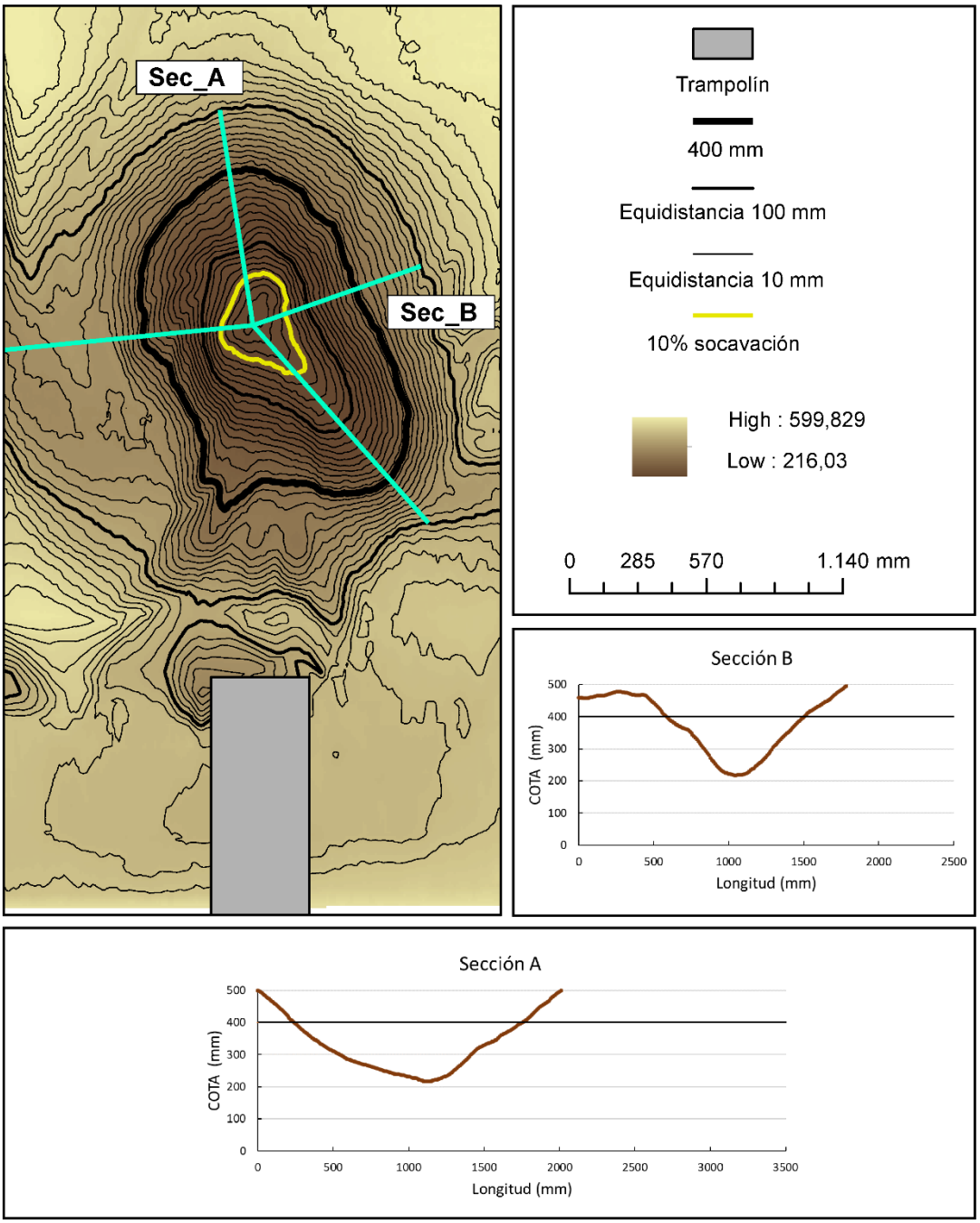

54	Radio 0,4 m	Ángulo 45°	Colchón 0,06 m	Caudal 50 l/s

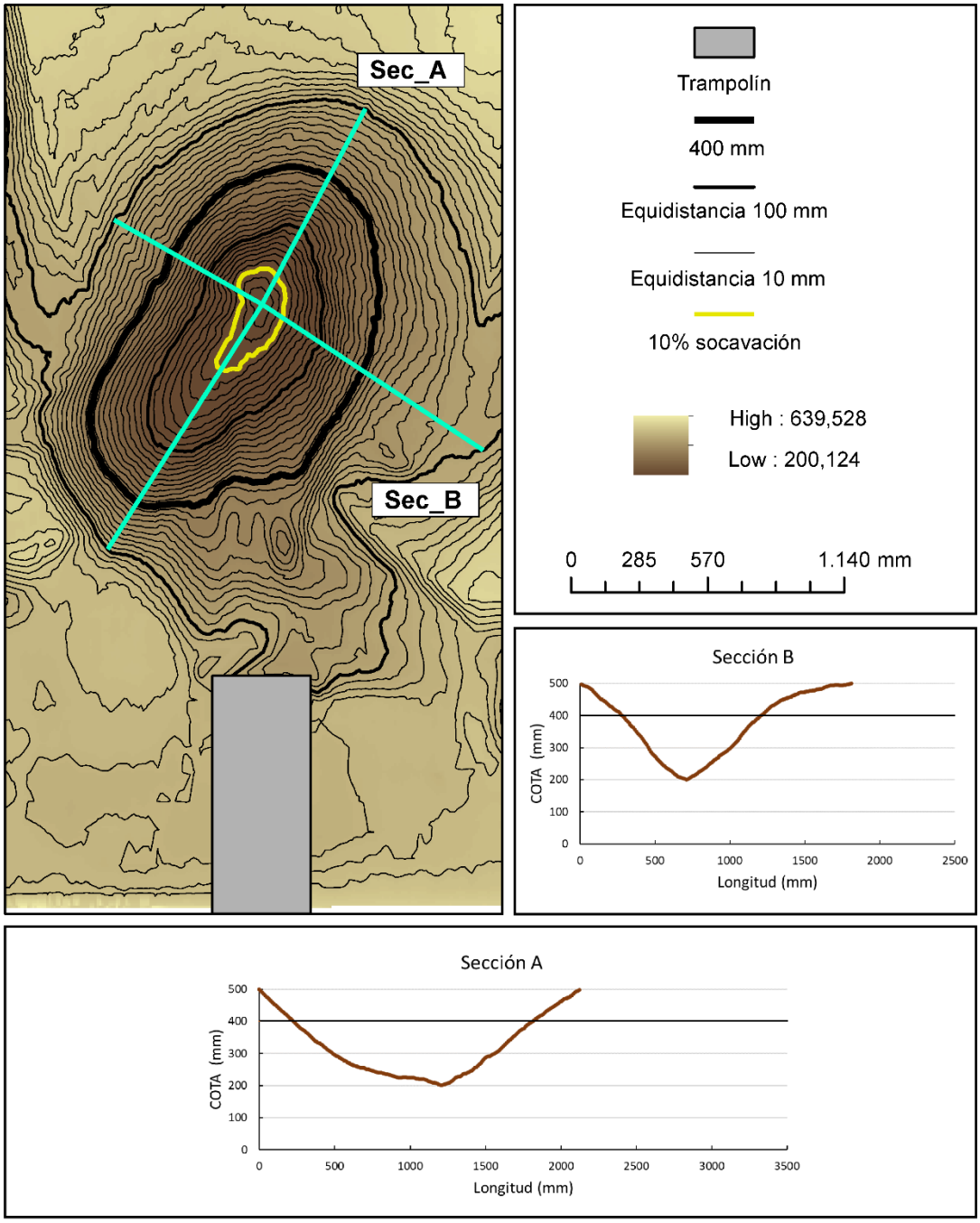

Apéndice 3: Producción Científica

water

MDPI

Article

Discharge Flow Rate for the Initiation of Jet Flow in Sky-Jump Spillways

Raffaella Pellegrino [1,*], Miguel Ángel Toledo [1] and Víctor Aragoncillo [2]

[1] Departamento de Ingeniería Civil: Hidráulica, Energía y Medio Ambiente, Universidad Politécnica de Madrid, 28040 Madrid, Spain; miguelangel.toledo@upm.es
[2] Ingeniero de Caminos, Canales y Puertos; varagonc@gmail.com
* Correspondence: r.pellegrino@upm.es

Received: 25 May 2020; Accepted: 22 June 2020; Published: 24 June 2020

Abstract: The sky-jump spillway is an economical and effective solution to return water to a river, eventually complemented by a pre-excavated basin. However, an inappropriate design could endanger spillways and even the dam itself. For the design of a sky-jump it is necessary to evaluate the position and dimensions of the potential pre-excavated basin based on the characteristics of the water flow to be evacuated and the geometric configuration of the sky-jump. The jump of the water jet occurs when a certain flow rate is reached. This flow rate for the initiation of the jet flow determines the position of the impact area closest to the spillway. We propose a new formula for the determination of the flow rate for the initiation of the jet flow, which incorporates as a novelty the influence of the curvature of the flip bucket. A methodology for the direct determination of the flow rate for the initiation of the jet flow is also presented. The new formula and methodology, based on experimental laboratory work and numerical modeling, will support the designer to choose the energy dissipation way, in the riverbed or inside the flip bucket, for low and frequent discharge flows.

Keywords: hydraulic structure; sky-jump; spillway; flip bucket; chute; basin; erosion; flow rate; jet flow

1. Introduction and Background

The sky-jump spillway was built for the first time in France in 1930 on the Dordogne's hydraulic scheme [1]. Rhone and Peterka [2] studied and improved the design of this type of spillway, which today is commonly used in dams when the speed of the water, in the final stretch of the chute if adequately high [3]. With this type of hydraulic structure, it is possible both to dissipate the energy and direct the jet to a certain area of the riverbed [4]. In fact, the water jet can be directed to the most convenient area and also can be mixed as much as possible with the air along its path to the riverbed. In such a way, the jet loses some of its energy and, if the sky-jump spillway was properly designed, the local scour does not compromise the safety of the dam.

Determining the position of the scour basin during the design stage allows to control the impact zone. The shape and size of the scour basin depend on both the geometrical configuration of the flip bucket and the operating flow rates. Furthermore, the plunge pool water level upstream of impact location is important regarding riverbed scour. The water level range can be from 3 m [5] to 8 m [6].

Three options are available in order to minimize the damage: (a) To completely avoid scour; (b) to design the spillway so that the scour occurs far away from dam foundation and abutments; and (c) to limit the scour extent [7].

Different bucket types are used to achieve an optimal combination with the chute end layout to reach an appropriate impact location of the jet into the plunge pool. When the flow discharge is small, the flip bucket works as a stilling basin and a hydraulic jump appears on it. In this condition the flow passing the

sill falls close to bucket foundation might jeopardize the bucket stability. When the spillway is unregulated, the type of bucket with a drainage channel is used to avoid choking at the small discharge which could endanger dam stability. In this type of bucket, the hydraulic jump does not occur for relatively small discharge, so that a free jet emerges [8].

However, it is important to notice that the hydraulic jump might be used to dissipate the energy for small discharges before the jump occurs, and remaining energy would be easy to dissipate as the falling height from the lip is usually low. In this way, the hydraulic jump inside the flip bucket might be useful to dissipate most of the flow energy in the range of low discharges.

An inadequate flip bucket could jeopardize the downstream area of the dam, as well as the dam itself. Hence there is a need to evaluate the geometric characteristics of the scour basin based on the features of both the water flow to be evacuated and the flip bucket. The first thing that is needed to be able to predict the position of the scour basin is to determine the flow rate for the initiation of the jet flow, which allows to establish with sufficient approximation the position of the scour basin at its extreme closest to the spillway.

Rouve [9] concluded that for a low flow rate range, the jet does not form, and the flip bucket works as a stilling basin ended with an overflow weir. The flow of water arrives through the chute to the flip bucket in supercritical regime and produces a hydraulic jump when contacting the water mass on the flip bucket, which is under subcritical regime. As the flow increases, the hydraulic jump moves towards the lip of the bucket, which is working as an overflow weir, until the flow rate for the initiation of the jet flow Qi (with increasing flow) is reached. The hydraulic jump is then dragged out of the flip bucket, the jet flow occurs and the water if thrown out. The jet flow is maintained, with the sky-jump operating in supercritical regime, until reaching the maximum flow rate. Later on, as the flow rate descends, until the flow rate is reduced to the flow rate for the finishing of the jet flow Q_f (with decreasing flow). A hydraulic jump is then re-established on the flip bucket, which works again as a stilling basin. Therefore, a hysteresis phenomenon occurs, since the flow rates for the initiation and finishing of the jet flow, Q_i and Q_f, are different, being Q_i slightly higher than Q_f.

The hysteresis phenomenon has been studied, both experimentally [10,11] and theoretically [12,13], by several authors [14,15]. The formulas obtained by these authors were developed for flat approach channels, setting obstacles or deflectors at their end, but without considering the effect of the curvature of the flip bucket.

Abecasis and Quintela [16,17] obtained formulas for determining Q_i and Q_f. They applied the momentum Equation to the control volume between two sections, the first located upstream of the obstacle, with a flow depth y_0, and the second on the obstacle, where a section with the critical flow depth y_c was assumed. The formula obtained for Q_f, neglecting the horizontal component of the friction resistance, considering uniform velocity, parallel flow, and assuming a linear distribution of the hydrostatic pressure in the initial and final sections of the control volume, was:

$$\frac{z}{y_0} = \frac{1 + 2F_0^2 - 3F_0^{4/3}}{1 + F_0^{2/3}} \quad (1)$$

where, y_0 is the flow depth and F_0 the Froude number both in the initial section, upstream of the obstacle, and z is the vertical height of the obstacle, equivalent to the depth of the flip bucket.

Applying the momentum Equation again, but assuming a pressure on the upstream face of the obstacle, exerted by a critical flow depth y_c, they obtained the formula for the initiation of the jet flow:

$$\frac{z}{y_0} = \frac{1 + 2F_0^2 - 3F_0^{4/3}}{2F_0^{2/3}} \quad (2)$$

Muskatirovic and Batinic [18] applied the momentum theorem, assuming a hydrostatic distribution on the upstream face of the obstacle, with flow depth y_0, and a hydrostatic distribution over the obstacle corresponding to the critical flow depth y_c. The formula obtained for the end of the jet flow was:

$$\frac{z}{y_0} = \sqrt{1 + 2F_0^2 - 2F_0^{4/3}} - F_0^{2/3} \quad (3)$$

For the initiation of the jet flow, they combined the Equation of the hydraulic jump with the Bernoulli's Equation, obtaining the following relationship:

$$\frac{z}{y_0} = \frac{1}{2}\left(\sqrt{1 + 8F_0^2} - 1\right) + \frac{1 + 4F_0^2 + \sqrt{1 + F_0^2}}{16F_0^2} - 1.5F_0^{2/3} \quad (4)$$

Heller, Hager, and Minor [19] applied the momentum theorem by considering a baffle with height z at the end of a channel. For the end of the jet flow they proposed:

$$\frac{z}{y_0} = \frac{1}{2}\left(\sqrt{1 + 8F_0^2} - 1\right) - F_0^{2/3} \quad (5)$$

and for the initiation:

$$\frac{z}{y_0} = \sqrt{1 + 2F_0^2 - 2F_0^{4/3}} - F_0^{2/3}. \quad (6)$$

Our research was focused on the development of a new formula that includes the effect of the curvature of the flip bucket on the initiation of the jet flow, and also the proposal of a new conceptual framework that leads to a novel procedure for the direct determination and analysis of the flow rate for the initiation of the jet flow.

2. General Approach

To take into account the effect of the flip bucket's radius of curvature a new formula was deduced, that incorporates this parameter by applying the momentum Equation. This formula establishes a relationship between the flow depth y_0 and the number of Froude F_0 at the lowest point of the flip bucket that must be met for jet flow to initiate, and it is the relationship that allows to determine the flow rate for the initiation of the jet flow.

The spillway is considered a system consisting of two elements: The chute and the flip bucket. For each of these elements, it is possible to define a *characteristic curve* that link the flow depth at the lowest point of the flip bucket y_0 and the flow rate Q. The flow rate for the initiation of the jet flow Qi, and the corresponding flow depth y_{0i} are given by the point of intersection of both *characteristic curves*. The approach is analogous to that of determining a pump operating point, when the system consists of the pump, or group of pumps, and the pipe. The characteristic curves link the pump head or head loss and the pumped flow**.**

The flow rate for the initiation of the jet flow must simultaneously satisfy the *flip bucket characteristic curve,* ratio between y_0 and Q (which can be determined from the relationship between z/y_0 and F_0 obtained by the momentum Equation), and the *chute characteristic curve,* which expresses the ratio between y_0 and the flow rate Q compatible with the energy loss that occurs along the channel, for being physically feasible.

The *chute characteristic curve* $y_0 = f(Q)$ may be constructed point to point by applying the Bernoulli theorem to successive sections of the chute, or by using a Computational Fluid Dynamic numerical model. We followed the second option, using the commercial software Flow3D. Three different tools were used along the workflow: Experimental work at the hydraulic laboratory, numerical Computational Fluid Dynamic modeling, and analytical deduction based on the momentum theorem (Figure 1). An empirical flow rate for the initiation of the jet flow was obtained from the physical models at the laboratory. The results of these laboratory tests were used to calibrate and validate the numerical models performed with Flow3D, regarding the flow characteristics along the chute. Once validated, Flow3D models served to

elaborate the *chute characteristic curves* and to determine the *flow rate for the initiation of the jet flow* in the absence of air within the flow.

Later on, the proposed theoretical formula, obtained by means of the momentum theorem, allowed to elaborate the *flip bucket characteristic curve,* taking into consideration the curvature of the bucket. The flow rate for the initiation of the jet flow was determined at the operating point, intersection of both characteristic curves of the chute and the flip bucket**.**

The work ends up comparing and analyzing the three flow rates for the initiation of the determined jet flow: Experimental or empirical, numerical, and analytical or theoretical, in order to discuss the validity of the proposed methodology and formula.

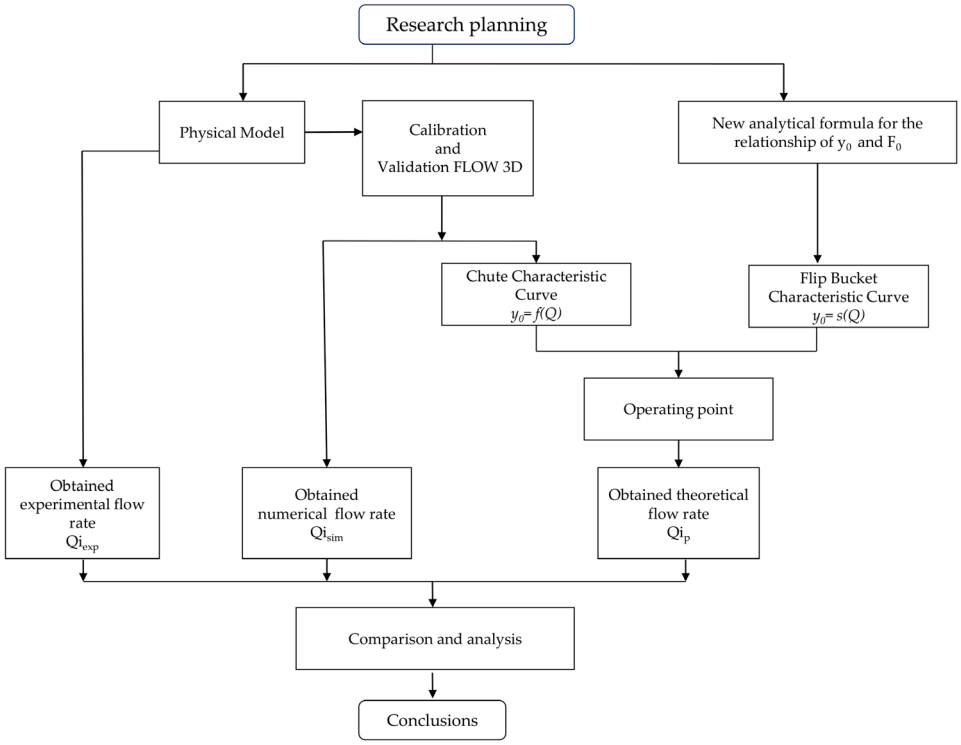

Figure 1. Workflow of the research.

3. New Formula for The Initiation of the Jet Flow

The flip bucket operates like a weir and presents a hydraulic jump for low flow rates, so it is not possible to define a clear flow depth y_0 at the lowest point of the flip bucket (Figure 2). As the supercritical flow from the chute increases, the hydraulic jump moves towards the lip of the flip bucket until the energy of the flow is enough to completely sweep the hydraulic jump out of the flip bucket and the jet flow occurs. When the stream of water jumps, the flow regime is supercritical all along the chute–bucket system. Therefore, the flow depth y_0 at the lowest point of the flip bucket is determined by the upstream conditions, with control section at the ogee crest of the spillway.

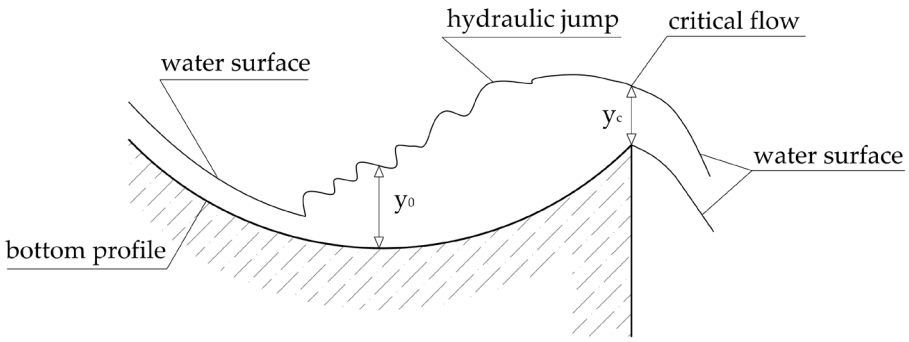

Figure 2. Flip bucket working as a weir for low flow rates.

We apply the momentum theorem in the horizontal direction [20]. The considered control volume is between the two vertical sections: (A) Passing through the lowest point of the flip bucket and (B) containing the lip (Figure 3). We accept, as Heller et al. [19], critical flow on the lip of the flip bucket before the jet flow occurs, since it is working as a weir, with a regimen change from subcritical to supercritical.

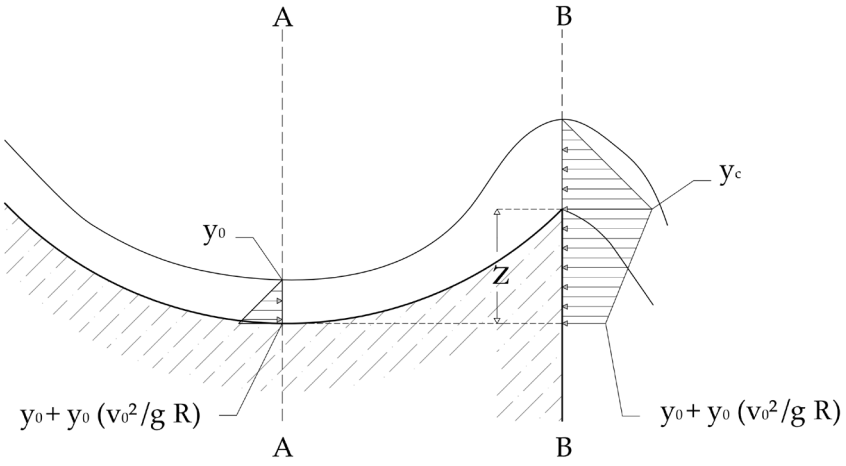

Figure 3. Head of pressure laws on the initial and final sections at the moment of the jet flow initiation.

In section (A), y_0 is the flow depth at the bottom of the flip bucket, where the corresponding speed is v_0. In section (B) the flow is critical (depth y_c) and the corresponding speed v_c. The radius of curvature R and depth of the flip bucket z are also relevant parameters.

In the initial section (A), the hydrostatic pressure was considered plus the increase of the dynamic pressure due to the curvature of the flow in the flip bucket [21]. For simplicity, linear distribution was assumed. The resulting force on section (A) is:

$$S_A = \frac{1}{2} y_0 \left(y_0 + y_0 \frac{v_0^2}{gR} \right). \quad (7)$$

In the final section (B), the hydrostatic pressure corresponding to the critical flow depth on the flip bucket's lip was assumed. The horizontal component of the resulting pressures on the flip bucket was determined considering, for simplicity, a linear distribution of pressure between the lowest point and the

lip of the flip bucket. These pressures are applied to the vertical projection of the flip bucket, resulting the force:

$$S_B = \frac{z}{2}\left(y_c + y_0 + \frac{y_0 v_0^2}{gR}\right). \quad (8)$$

Neglecting the horizontal component of friction resistance, considering uniform velocity and parallel flow, and applying the momentum Equation, we obtained Equation (9):

$$\frac{1}{2}y_0\left(y_0 + y_0\frac{v_0^2}{gR}\right) + \frac{q^2}{y_0 g} = \frac{1}{2}y_c^2 + \frac{z}{2}\left(y_c + y_0 + \frac{y_0 v_0^2}{gR}\right) + \frac{q^2}{y_c g} \quad (9)$$

being q the unit flow rate and g the gravity acceleration. This Equation (9) can be expressed in a different and more compact way using the Froude number at the initial section (A) F_0, and the parameter z/y_0. For that, we divide Equation (9) by y_0 and substitute for:

$$y_0 v_0 = y_c v_c \quad (10)$$

$$F_0 = \frac{v_0}{\sqrt{g y_0}} \quad (11)$$

$$y_c = \sqrt[3]{\frac{y_0^2 v_0^2}{g}} \quad (12)$$

and the resulting formula is:

$$\frac{z}{y_0} = \frac{1 + 2F_0^2 - 3F_0^{\frac{4}{3}}}{1 + F_0^{\frac{2}{3}}} - \frac{F_0^2}{1 + F_0^{\frac{2}{3}}}\left[\frac{(z - y_0)}{R}\right]. \quad (13)$$

Equation (13) includes the effect of the curvature of the flip bucket by means of the parameter R: Flip bucket radius of curvature. It is a novelty related to the previous existing formulas. It can be observed that the obtained formula differs from that of Abecasis and Quintela (Equation (1)) just in the negative term of the second member of the equality, that includes the radius as a parameter. This term approaches zero when increasing the radius and, at the limit, it becomes zero, as befits a straight bucket, without curvature, which is the hypothesis adopted by Abecasis and Quintela.

4. The Method of the Characteristic Curves

The sky-jump spillway can be considered as a system made up of two elements: The chute and the flip bucket. The lowest point of the bucket deflector (Section A; Figure 4) was defined as the limit between them. It is analogous to a pumping system, consisting of a pump, or group of pumps, and the pump piping. In this analogy, the chute and the pump piping might be considered analogous elements, since the frictional force, along with the gravity force, dominates the behavior in both elements. The flip bucket and the pump group might also be considered analogous. In both cases, energy is required for water elevation. In the case of the group of pumps it is provided by the engines; in the case of the flip bucket the energy is provided by the water stream coming from the chute.

Like in the case of a pumping system, there is an operating point for the chute–bucket system. The operating point is the intersection of the characteristic curves of the elements of the system: Chute and flip

bucket. Both characteristic curves express a relationship between the flow depth at the lowest point of the flip bucket y_0 and the flow rate Q. The operating point defines the flow rate for the initiation of the jet flow and the flow depth at the lowest point of the flip bucket at that instant.

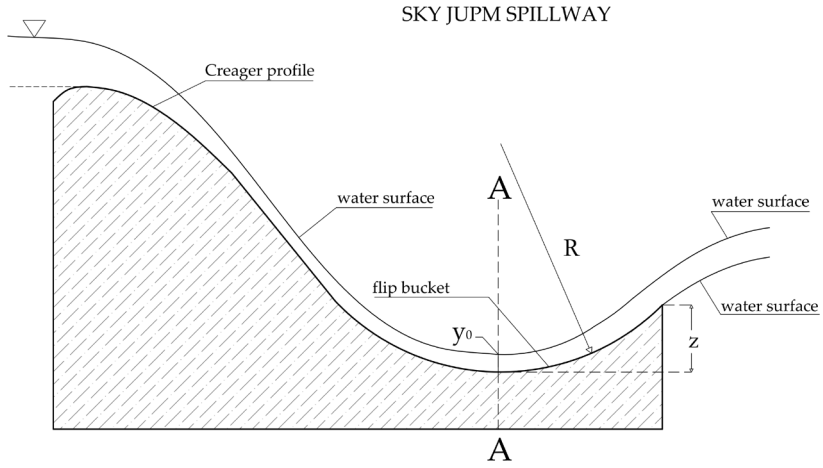

Figure 4. Section of a spillway with a flip bucket with a radius of curvature R and with a depth z, and flow depth y_0 at the lowest point of the flip bucket.

The *characteristic curve of the flip bucket* can be obtained by applying the momentum Equation at the instant of initiation of the jet flow, using the new proposed formula (Equation (13)). It establishes a relationship between the parameter z/y_0, where z is the depth of the flip bucket, and the Froude number F_0 at the lowest point of the bucket. This Equation can also be expressed as a function of the unit flow rate q and the flow depth at the lowest point of the flip bucket y_0, taking into consideration Equations (10)–(12):

$$y_0^3 - y_0^2 z + y_0 \left(\frac{q^2}{gR} - 3\frac{q^{\frac{4}{3}}}{g^{\frac{2}{3}}} - z\frac{q^{\frac{2}{3}}}{g^{\frac{1}{3}}} \right) + 2\frac{q^2}{g} - \frac{zq^2}{gR} = 0. \quad (14)$$

The function $y_0 = s(q)$ can be built point by point using Equation (14), under the hypothesis of cylindrical flip bucket and neglecting the effect of the flow aeration. This is the curve we call *flip bucket characteristic curve.*

The *chute characteristic curve* $y_0 = f(q)$ can be built using a CFD numerical model with greater accuracy than using Bernoulli theorem. We determined the value of y_0 for different unit flow rates q using the commercial CFD code Flow3D.

Jet flow initiates when the operation conditions of the chute and the flip bucket are physically compatible, at the intersection of both characteristic curves: The operating point. It provides the flow rate for the initiation of the jet flow and the flow depth at the lowest point of the bucket deflector at that instant.

5. Experimental Work with Physical Models

The testing channel (Figure 5 and Figure 6) has a width of 2.46 m, is 1.3 m high, and 13.7 m long. It is divided into three functional areas. The first zone is for water supply and dissipation of its energy. The second is the testing area: 2.46 m wide and 6.37 m long. The testing area is filled with sand up to a height of 0.5 m, and is limited upstream by a wall. The sky-jump spillway is positioned in the middle of that wall. In the third and final zone of the testing channel there is a decant pond to prevent any dragged material to reach the tank, which is under the laboratory floor. On the left side of the channel, in the direction of the flow, there is a glass window 4.6 m long and 1.1 m high, which allows the visual inspection of the test and also to take photographs and video recording.

The water inlet to the model is regulated by a motorized valve. The flow rate was measured at two locations: Upstream, by means of an ultrasonic flow meter positioned in the supply pipe, and downstream,

using a thin-plate rectangular weir located in the return channel that takes water to the tank. Two ultrasonic level probes based on the pulse-eco method, positioned upstream and downstream of the sky-jump spillway, were used for the recording of the water levels. The hardware specifications of the ultrasonic flow meter and the ultrasonic level probe are shown in the (Table 1).

Table 1. Hardware specifications used in the experiments.

Instrumentation	Measuring Range	Accuracy
FLUXUS-ADM7407	0.01–25 m/s	± 1.6 % of reading ±0.1 m/s
Ultrasonic distance measuring system UAS	0.3 m–2 m	>=1 mm

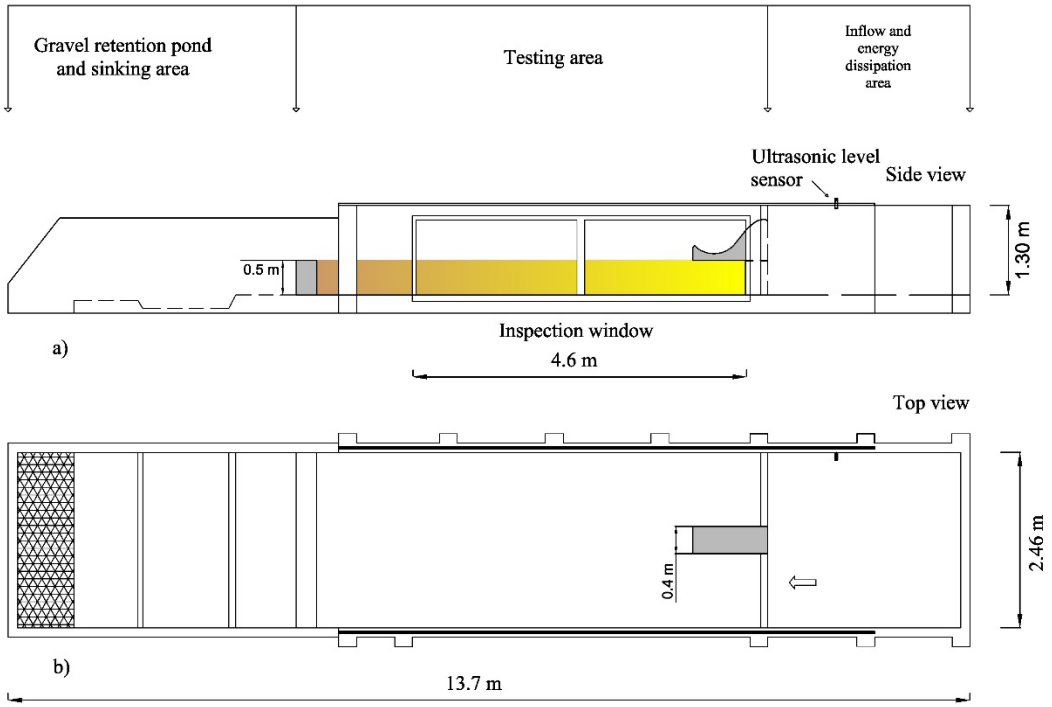

Figure 5. Testing set-up. (**a**) Side view; (**b**) Plan view.

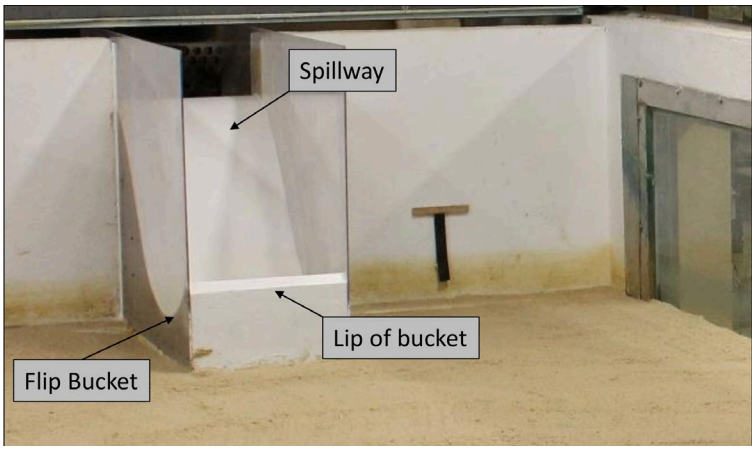

Figure 6. Sky-jump spillway in the testing channel. Case: radius of curvature 0.4 m; flip angle 45°.

Six cement-made sky-jump spillways were built (Figure 7). The design followed the criteria specified by the United States Bureau of Reclamation [22]. The spillway has a Creager profile. The slopes of the physical model are vertical upstream and 0.8H:1.0V downstream; the height H is 0.6 m; and the distance between the bottom of the flip bucket and elevation spillway is 0.5 m; it is 0.4 m wide. Three different values of radius of curvature R were modeled: 0.2 m, 0.3 m, and 0.4 m; and also three different values of exit angle of flip bucket α: 15°, 30°, and 45°. The radius of curvature and the flip angle allow to determine z, depth of the flip bucket, using the geometric relation $z = R\ (1 - \cos \alpha)$. In order to inspect and measure the water depth, the sides of the physical models were built with methacrylate.

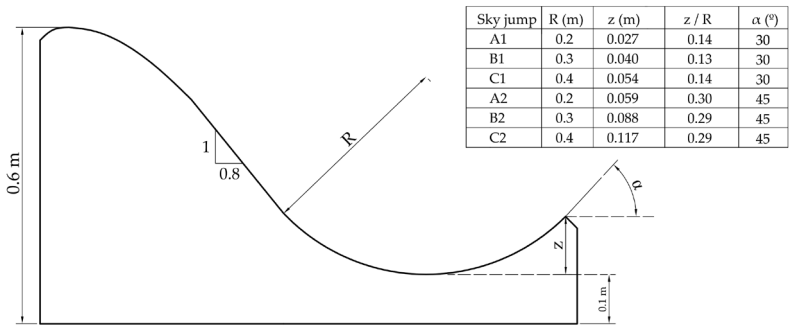

Sky jump	R (m)	z (m)	z / R	α (º)
A1	0.2	0.027	0.14	30
B1	0.3	0.040	0.13	30
C1	0.4	0.054	0.14	30
A2	0.2	0.059	0.30	45
B2	0.3	0.088	0.29	45
C2	0.4	0.117	0.29	45

Figure 7. Geometrical configuration of the physical models: radius of curvature R, depth of the flip-bucket z, flip angle α, and parameter z/R are variable parameters.

A protocol was followed for the experimental determination of the flow rate for the initiation of the jet flow. The level of the reservoir was maintained 0.04 m below the ogee crest threshold to allow the flow to stabilize before allowing the specified flow rate to enter the spillway. Every flow rate was maintained during 10 min flowing along the spillway. After that, if the jet flow did not occur, the procedure was repeated with the next higher flow rate discharge, and so on until the jet flow occurred. The flow rate for the initiation of the jet flow was measured for every geometrical configuration. The flow depth at the lowest point of the flip bucket could only be measured with sufficient accuracy for the sky-jump spillway with radius of curvature of 0.4 m and flip angle of 45° (C2). For the rest of the physical models the depth of water was too small. It was possible to differentiate for the case C2 an intensely aerated area, in the upper part of the flow, from a predominantly liquid area in the lower part (Figure 8).

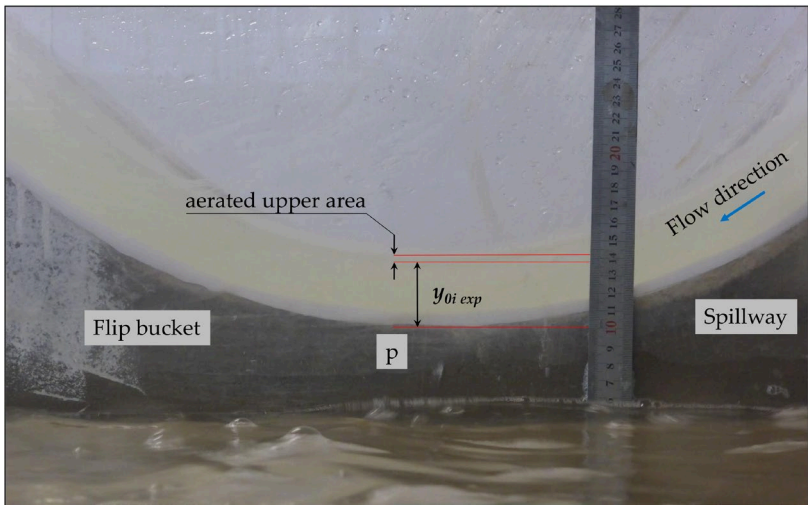

Figure 8. Flow at the lower part of the flip-bucket for case C2, with a discharge of 43.56 L/s. The upper part of the flow is intensely aerated. The lowest point of the flip bucket is "p" and the flow depth without intensely aerated upper area is $y_{0i\ exp}$.

The experimental results (Table 2) are later in this paper compared with the results obtained applying the proposed *method of the characteristic curves*, using the new formula for the characteristic curve of the flip bucket, and with the results obtained from the CFD numerical model (Flow3D), described in the following section. The CFD numerical model was calibrated and validated with the experimental data of the physical model C2.

Table 2. Experimental results: Flow rate for the initiation of the jet flow Qi_{exp} (L/s) for each physical model and total flow depth $y'_{0i\,exp}$ (mm) and flow depth without intensely aerated upper area $y_{0i\,exp}$ (mm).

Physical Model	[1]A1	[2]B1	[3]C1	[4]A2	[5]B2	[6]C2
Qi_{exp} **(L/s)**	1.65	2.75	3.70	4.80	7.65	11.95
$y'_{0i\,exp}$ **(mm)**	-	-	-	-	-	*14.50
$y_{0i\,exp}$ **(mm)**	-	-	-	-	-	**13.00

[1] (R = 0.2 m, α = 30°); [2] (R = 0.3 m and α=30°); [3] (R = 0.4 m α = 30); [4] (R = 0.2 m α = 45°); [5] (R = 0.3 m α = 45°); [6] (R = 0.4 m α = 45° (C2) The total flow depth $y'_{0i\,exp}$ (mm) with aerated upper area is * 14.50 mm and the flow depth without intensely aerated upper area $y_{0i\,exp}$ (mm) is ** 13.00 mm, corresponding to the measured flow rates for the flip bucket (C2), at the lowest point of the flip bucket.

6. Numerical Models: Chute Characteristic Curve and Flow Rate for The Initiation of the Jet Flow.

Every physical model was also modelled numerically. As above mentioned, the *chute characteristic curve* was obtained point by point by means of the CFD numerical modeling code Flow3D. This software solves Reynolds–Navier–Stokes averaged Equations (RANS) in three dimensions along with the FAVOR and VOF algorithms for solid contouring and free surface tracking respectively [23]. Due to a finite difference approach, Flow3D requires the resolution of structured meshes. The software uses the Fractional Area/Volume Obstacle Representation (FAVOR) method, developed by Hirt and Sicilian [24]. This preprocessor is a tool that allows to represent a solid obstacle in a control volume. Control volumes with dead spaces are assumed empty, and value 1 is assigned, and volumes with geometry are assumed solid volumes and a value of 0 is assigned. The Volume of Fluid (VOF) method is described by Nichols and Hirt [25], Nichols et al. [26], and Hirt and Nichols [27]. This method is similar to FAVOR; it defines whether a cell is empty, full, or partially filled with water. Cells without fluid have a value equal to 0. The filled cells have value equal to 1, and between 0 and 1 those partially filled.

The software Flow3D solves in three directions the mass continuity Equation (Equation (15)) and the momentum Equations (Equations (16)–(18)) besides the volume of fluid (VOF) Equation, that ensures that proper boundary conditions are applied at the free surface (Equation (19)). For Cartesian coordinates (x_i, x_j, x_z) and for incompressible fluid (fluid density constant), these Equations are:

$$\frac{\partial}{\partial x_i}(u_i A_i) + \frac{\partial}{\partial x_j}\left(u_j A_j\right) + \frac{\partial}{\partial x_k}(u_k A_k) = \frac{R_{SOR}}{\rho} \tag{15}$$

$$\frac{\partial u_i}{\partial t} + \frac{1}{V_F}\left\{u_i A_i \frac{\partial u_i}{\partial x_i} + u_j A_j \frac{\partial u_i}{\partial x_j} + u_k A_k \frac{\partial u_i}{\partial x_k}\right\} = -\frac{1}{\rho}\frac{\partial p}{\partial x_i} + G_{x_i} + f_{x_i} \tag{16}$$

$$\frac{\partial u_j}{\partial t} + \frac{1}{V_F}\left\{u_i A_i \frac{\partial u_j}{\partial x_i} + u_j A_j \frac{\partial u_j}{\partial x_j} + u_k A_k \frac{\partial u_j}{\partial x_k}\right\} = -\frac{1}{\rho}\frac{\partial p}{\partial x_j} + G_{x_j} + f_{x_j} \tag{17}$$

$$\frac{\partial u_k}{\partial t} + \frac{1}{V_F}\left\{u_i A_i \frac{\partial u_k}{\partial x_i} + u_j A_j \frac{\partial u_k}{\partial x_j} + u_k A_k \frac{\partial u_k}{\partial x_k}\right\} = -\frac{1}{\rho}\frac{\partial p}{\partial x_k} + G_{x_k} + f_{x_k} \quad (18)$$

$$V_F \frac{\partial F}{\partial t} + \nabla (AUF) = 0 \quad (19)$$

where t is time, ρ is fluid density, p is pressure, (u_i, u_j, u_k) are velocity component in Cartesian coordinates (x_i, x_j, x_k), A_i is fractional area in the i-direction, A_j and A_k are similar area fractions in the j and k direction, respectively, (Gx_i, Gx_j, Gx_k) are body acceleration and (fx_i, fx_j, fx_k) are viscous acceleration. In Equation (19) A is the average flow area, U is the average velocity and F is the volume flow function. When the cell is filled with fluid, the value of F is 1, and when it is empty, F is 0.

The fluid-dynamic variables at a point in space are made up of a series of fluctuations of different scales, for this reason, the analysis of the turbulence is carried out from a statistical point of view, that is, with average velocity and intensity of "Reynolds averaged" fluctuations. This consideration helps solve the closure problem. For the numerical solution of turbulent flows, the Reynolds-Averaged Navier–Stokes Equations are applied, which supplies the turbulence kinetic energy k and the rate of turbulent energy dissipation $\mathcal{E}$ to achieve Reynolds stresses and the turbulent kinematic viscosity.

A quantitative verification, as defined in Jakeman et al. [28] and in Blocken et al. [29], was made for this numerical study, using the available data from Paul Guy Chanel [30].

The turbulence model used in this study is the RNG k-ε [31], which usually provides better performance for swirling flows than standard k-ε model [32,33]. Its formulation is represented in Equations (20) and (21):

$$\frac{\partial}{\partial t}(\rho k) + \frac{\partial}{\partial x_i}(\rho k u_i) = \frac{\partial}{\partial x_j}\left[\left(\mu + \frac{\mu_t}{\sigma_k}\right)\frac{\partial k}{\partial x_j}\right] + P_k - \rho\varepsilon \quad (20)$$

$$\frac{\partial}{\partial t}(\rho \varepsilon) + \frac{\partial}{\partial x_i}(\rho \varepsilon u_i) = \frac{\partial}{\partial x_j}\left[\left(\mu + \frac{\mu_t}{\sigma_\varepsilon}\right)\frac{\partial \varepsilon}{\partial x_j}\right] + C_{1\varepsilon}\frac{\varepsilon}{k}P_k - C_{2\varepsilon}\rho\frac{\varepsilon^2}{k} \quad (21)$$

where μ is dynamic viscosity, μ_t is turbulent dynamic viscosity and P_k is production of turbulence kinetic energy. The remaining terms $C_{1\varepsilon}$, $C_{2\varepsilon}$, σ_k and σ_ε are model parameters whose values can be found in Yakhot et al. [31]. Finally, the turbulence viscosity can be computed using the parameter $C\mu = 0.085$ in the Equation (22):

$$\mu_t = \rho\, C_\mu \frac{k^2}{\varepsilon} \quad (22)$$

The numerical model is implemented by importing the geometry of the entire physical model. A domain of 2.3 m long and 1 m high was defined. Although Flow3D is inherently a 3D software, it was considered a small thickness in the Y direction, transverse to the model section, in such a way that the behavior of the flow could be studied in 2D (Figure 9), since the analyzed phenomenon is essentially two-dimensional.

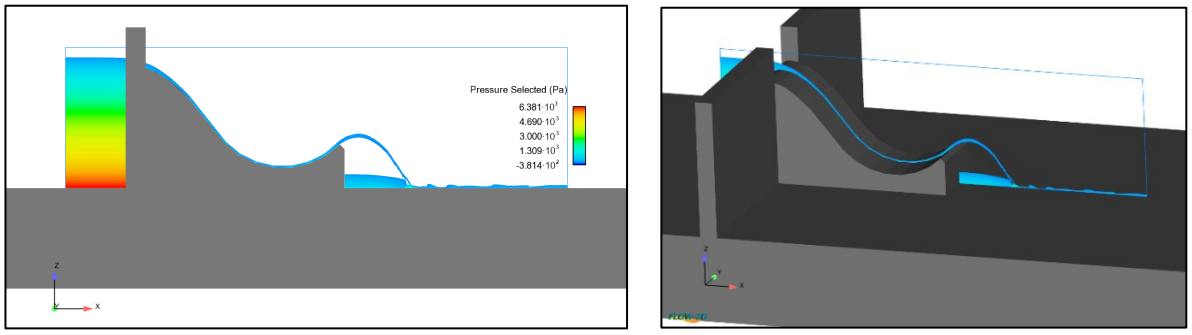

(**a**) (**b**)

Figure 9. Geometric model implemented in Flow3D: (**a**) 2D view; (**b**) 3D view.

The flow depths corresponding to the flow rate for the initiation of the jet flow for every modelled case are in the order of millimeters for most of the cases.

The boundary conditions must accurately represent those of the physical phenomenon: Two boundary conditions are fixed for each Cartesian plane: For the plane (XY) the atmospheric pressure and the wall condition are considered, for the plane (YZ) the hydrostatic pressure distribution and the output are defined, for the plane (XZ) the symmetrical smooth walls (free-slip/symmetry) are defined.

The numerical model was calibrated and validated using the experimental data corresponding to the 0.4 m radius of curvature and flip angle of 45°(C2). The test with the smallest flow rate was used to calibrate the roughness of the chute, and the test with the larger flow rate was used to validate the value obtained in the calibration. The flow depth with and without the intensely aerated upper area of the flow were separately considered.

The numerical simulation was started with the Mesh-sensitivity analysis and calibration of the Flow3D model. The measured value of the flow depth without the intensely aerated area ($y_{0\ exp}$) was used, since the proposed analytical formula does not consider the effect of aeration, and the purpose is to compare both results.

The absolute roughness of the chute was used as the calibration parameter. The roughness of the smooth cement is between 0.03 mm and 0.50 mm [21]. We developed numerical models with 0.03 mm, 0.10 mm, 0.25 mm, and 0.50 mm.

The available experimental data refer to the 0.4 m flip bucket's radius and lip angle of 45° (C2), for which we have two flow depth data at the lowest point of the flip bucket and the two related flow rates.

Mesh-sensitivity analysis, categorized as part of the quantitative verification, was performed diminishing the cell size, until changes were not reported in the results (Table 3). However, the results with a 1 mm mesh were computationally unfeasible and a trade-off between computational time and accuracy was made.

The cell with the size of 1.25 mm was adopted because it restores the same water depth value observed experimentally and it also was computationally feasible. Then, different absolute roughness values were considered, as indicated in the (Table 3), checking if the jet flow occurred.

Table 3. Calibration results (roughness variation) and mesh-sensitivity analysis (cell side variation).

Roughness (mm)	Q_{sim} (L/s)	$y_{0\ sim\ cell\ 1\ mm}$ (mm)	$y_{0\ sim\ cell\ 1.25\ mm}$ (mm)	$y_{0\ sim\ cell\ 2.5\ mm}$ (mm)
0.03	11.34	12.98	13.01	14.78
0.10	12.21	14.00	14.10	15.35
0.25	12.64	14.25	14.36	15.48
0.50	doesn't jump	doesn't jump	doesn't jump	doesn't jump

Roughness was set to 0.03 mm and a cell size of 1.25 mm was adopted, because they restore the same water depth value experimentally observed (Table 4).

Table 4. Comparison between experimental and numerical flow rate and flow depth for calibration.

Q_{exp} (L/s)	Q_{sim} (L/s)	*AE$_Q$ (L/s)	**RE$_Q$ (%)	$y'_{0\ exp}$ (mm)	$y_{0\ exp}$ (mm)	$y_{0\ sim\ cell\ 1.25}$ (mm)	***AE$y'_{0\ exp-\ sim}$ (mm)	****RE$y'_{0\ exp-sim}$ (%)
11.95	11.34	0.61	5.07	14.50	13.00	13.01	1.49	10

* AE$_Q$ (Absolute Error) and ** RE$_Q$ (Relative Error) between experimental flow rate and numerical flow rate. *** AEy_0 (Absolute Error) and **** REy'_0 (Relative Error) between experimental flow depth considering the intensely aerated area and numerical flow depth.

This absolute roughness is compatible with the surface of sanded concrete of the physical models. The calibration results were then validated. For that, the flow rates obtained experimentally and numerically that produce the same flow depth at the lowest point of the flip bucket were compared, without considering the intensely aerated area. Validation was performed for an experimental flow rate of 43.56 L/s (Table 5).

Table 5. Comparison between experimental and numerical flow rate and flow depth for validation.

Q_{exp} (L/s)	Q_{sim} (L/s)	*AE$_Q$ (L/s)	**RE$_Q$ (%)	$y'_{0\ exp}$ (mm)	$y_{0\ exp}$ (mm)	$y_{0\ sim}$ (mm)	***AE$y'_{0\ exp-sim}$ (mm)	****RE$y'_{0\ exp-sim}$ (%)
43.56	42.86	0.70	1.61	42.00	38.00	38.22	3.78	9

*AE$_Q$ (Absolute Error) and **RE$_Q$ (Relative Error) between experimental flow rate and numerical flow rate. ***AEy_0 (Absolute Error) and ****REy'_0 (Relative Error) between experimental flow depth considering the intensely aerated area and numerical flow depth.

The relative error between flow rates observed and obtained from the numerical models is in the order of 5% in calibration and lower in validation. It is in accordance with the expected error in the numerical model [23] and in the laboratory test.

Once the numerical model was calibrated and validated, it was used for two purposes: (a) To build the *chute characteristic curve*; (b) to determine the flow rate for the initiation of the jet flow; both for the different laboratory-tested geometric configurations. For the first purpose, three spillways, corresponding to each considered radius, were numerically modeled (Figure 10). As expected, the differences between the curves of the three cases were minimal, since they only differ slightly on the initial curved part (Table 6). The *chute characteristic curve* was obtained by interpolation from the points defined by numerical modeling, (Figure 11), where the fixed parameters are: total height *H* of 0.6 m and distance *P* from the bottom of the flip bucket to the ground of 0.1 m; variable parameters are: radius of curvature *R*, horizontal distance *La* from the upstream vertical wall to the point where the straight part of the chute ends, horizontal distance *Lc* from the upstream vertical wall and measurement point "p", and horizontal distance *Lt* between the measurement point "p" and the flip bucket's lip. The part of the flip bucket downstream point "p" has no influence on the chute flow, due to the supercritical regime.

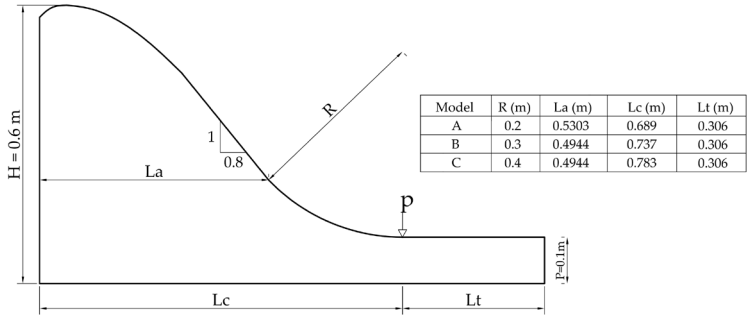

Figure 10. Outline of the geometric configuration used to obtain the *chute characteristic curves* using numerical modeling.

Table 6. Modeled points (Q_{sim}, $y_{0\,sim}$), to draw the *chute characteristic curves* with radius 0.2 m (A), 0.3 m (B), 0.4 m (C).

Q_{sim}_A (L/s)	$y_{0\,sim}\_A$ (mm)	Q_{sim}_B (L/s)	$y_{0\,sim}\_B$ (mm)	Q_{sim}_C (L/s)	$y_{0\,sim}\_C$ (mm)
0.000	0.000	0.000	0.000	0.000	0.000
0.701	2.041	0.701	2.043	0.701	2.044
1.188	2.791	1.188	2.798	1.188	2.873
1.581	3.409	1.581	3.492	1.581	3.474
1.994	3.899	1.994	3.799	1.994	3.892
2.952	4.806	2.952	4.858	2.952	4.861
3.276	5.126	3.276	5.155	3.276	5.211
3.839	5.666	3.839	5.666	3.839	5.712
4.844	6.358	4.844	6.358	4.844	6.557
5.075	6.465	5.075	6.525	5.075	6.707
7.239	8.054	7.239	8.094	7.239	8.094
8.505	8.890	8.505	8.890	8.502	8.977
9.877	9.877	9.877	9.877	9.877	9.917
11.247	10.973	11.247	10.991	11.247	11.027
14.335	13.500	14.335	13.500	14.335	13.433

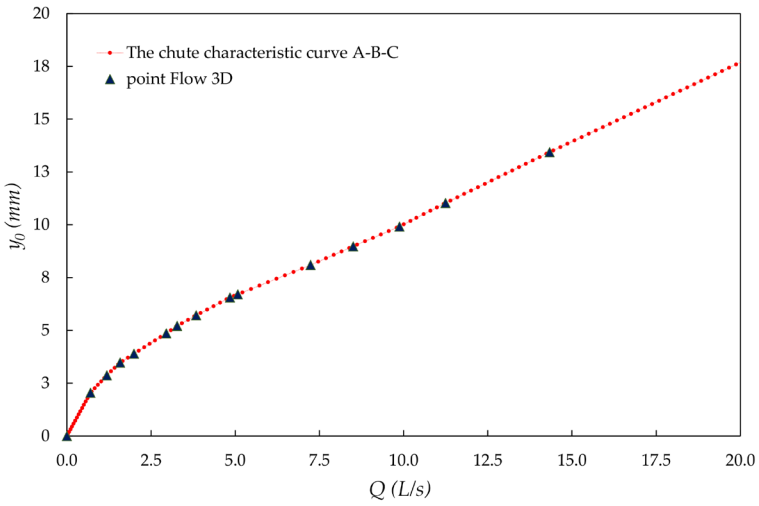

Figure 11. Three *chute characteristic curves*, with radius of 0.2 m (**A**), 0.3 m (**B**) and 0.4 m (**C**), are visually overlapped because they only differ slightly on the initial curved part.

The flow rate for the initiation of the jet flow was determined for each of the six laboratory-tested geometric configurations, using the numerical model, by trial and error, increasing the flow discharge in small steps until the jet flow occurred (Figure 12; Table 7).

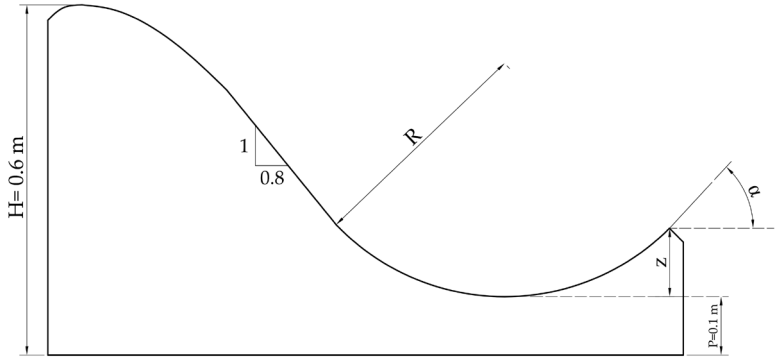

Figure 12. General geometry of the trampoline-type spillway.

Table 7. Results of flow rate for the initiation of the jet flow Qi_{sim} and flow depth $y_{0i\ sim}$ at the lowest point, obtained with numerical simulation for each geometrical configuration.

Tested Geometry	R (m)	α (°)	z (m)	Qi_{sim} (L/s)	$y_{0i\ sim}$ (mm)
A1	0.2	30	0.027	1.12	2.61
B1	0.3	30	0.040	2.03	4.01
C1	0.4	30	0.054	2.86	4.61
A2	0.2	45	0.059	3.79	5.38
B2	0.3	45	0.088	5.76	7.06
C2	0.4	45	0.117	8.49	9.08

7. Results and Discussion

The main purpose of this research is to define and validate a methodology that allows to determine the flow rate for the initiation of the jet flow of a sky-jump spillway, taking into account the effect of the radius of curvature R of the flip bucket.

According to the proposed methodology, the flow rate for the initiation of the jet flow is the abscissa of the *operating point* at the intersection of two curves, *the flip bucket characteristic curve* and *the chute characteristic curve.*

The *flip bucket characteristic curve* was built point by point using the proposed analytical formula (Equation (13)), that includes the effect of the flip bucket curvature. The *chute characteristic curve* was built also point by point using the results of the numerical simulations performed with Flow3D. The operating point was identified for each geometrical configuration considered for the spillway. This way the flow rate Qi_p and flow depth y_{0ip} were determined, and compared to the results of the numerical simulation (Qi_{sim}, $y_{0i\ sim}$) and to the values experimentally observed (Qi_{exp}, $y_{0i\ exp}$). The main results of the different phases of the research are summarized in (Table 8).

Table 8. The flow rate for the initiation of the jet flow and the flow depth at the lowest point of the flip bucket are showed.

Tested Geometry	R (m)	α (°)	z (m)	Qi_p (L/s)	Qi_{sim} (L/s)	Qi_{exp} (L/s)	y_{0ip} (mm)	$y_{0i\ sim}$ (mm)	$y'_{0i\ exp}$ (mm)	$y_{0i\ exp}$ (mm)
A1	0.2	30	0.027	1.20	1.12	1.65	2.81	2.61	-	-
B1	0.3	30	0.040	2.18	2.03	2.75	4.20	4.01	-	-
C1	0.4	30	0.054	2.93	2.86	3.70	4.84	4.61	-	-
A2	0.2	45	0.059	3.86	3.79	4.80	5.67	5.38	-	-
B2	0.3	45	0.088	5.97	5.76	7.65	7.17	7.06	-	-
C2	0.4	45	0.117	8.84	8.49	11.95	9.21	9.08	14.50	13.00

Note: (Qi_p, y_{0ip}) is obtained using the proposed methodology and formula, (Qi_{sim}, $y_{0i\ sim}$) is obtained by numerical simulation and (Qi_{exp}, $y_{0i\ exp}$) experimentally in laboratory. Experimental flow depth was measured with enough accuracy only for the C2 flip bucket, being $y_{0i\ exp}$ the flow depth excluding the intensely aerated upper area.

The flow rates for the initiation of the jet flow obtained by means of the proposed methodology and analytical formula and those obtained by numerical simulation are quite similar, while the values experimentally obtained are somewhat higher. The oscillation of ±0.75 L/s in the flow rates supplied to the physical model does not allow to explain the observed differences. It should be emphasized that both the proposed formula and the Flow3D numerical model do not include the effect of flow aeration, which is present on the physical model tests. This fact might explain the differences observed. If this was the reason, the effect of aeration would be to increase the flow rate for the initiation of the jet flow. In the tests performed the increase was around 26% (Table 9). A greater increase might be expected at prototype size, due to the higher degree of aeration of the flow as compared to the laboratory size.

Let us now consider the differences between the flow depths at the lower point of the flip bucket obtained using the proposed methodology and formula and those obtained by numerical modeling. It is observed that by increasing the flow rate, the relative error decreases. For the flow rate, the MAE value is 0.15 L/s, the MRE is 4.20%, and the relative error reaches 6.88%. Similarly, for the flow depth it is observed that the MAE is 0.19 mm, and the absolute error does not exceed 0.29 mm; moreover, the MRE is 4.12% and relative error slightly exceeds 7%. For the proposed methodology and formula, it can be said in short, that the mean errors are less than 5%, related to the values obtained by numerical modeling.

Table 9. AE: Absolute Error and RE: Relative Error.

Tested geometry	Mean Value	$AE_{Qi\ (p\text{-}sim)}$ (L/s)	$RE_{Qi\ (p\text{-}sim)}$ (%)	$AE_{y0i\ (p\text{-}sim)}$ (mm)	$RE_{y0i\ (p\text{-}sim)}$ (%)	$AE_{Qi\ (exp\text{-}sim)}$ (L/s)	$RE_{Qi\ (exp\text{-}sim)}$ (%)
A1		0.08	6.66	0.20	7.11	0.53	32.12
B1		0.15	6.88	0.19	4.52	0.72	26.18
C1		0.07	2.39	0.24	4.95	0.84	22.70
A2		0.07	1.81	0.29	5.11	1.01	21.04
B2		0.21	3.52	0.12	1.67	1.89	24.70
C2		0.35	3.96	0.13	1.41	3.46	28.95
	*MAE-MRE	0.15	4.20	0.19	4.12	1.41	22.84

*MAE: Mean Absolute Error and MRE: Mean Relative Error between the flow rate obtained by the proposed formulation Qi_p and the Qi_{sim} flow rate determined with Flow3D; between the flow rate obtained experimentally Qi_{exp} and the numerical flow rate Qi_{sim}; and between the flow depth obtained by the proposed formulation y_{0ip} and the flow depth $y_{0i\ sim}$ determined with Flow3D.

Error is generally greater for small values of the flow rate for the initiation of the jet flow. Some uncertainty should be expected due to the markedly sharp angle of the characteristic curves of chute and flip bucket at the intersection point (Figure 13). A small change in any of the two parameters involved may cause a significant variation in the other one, and so in the *chute-flip bucket system*. The high sensitivity of

the system to small alterations might explain the difficulty to accurately measure the flow rate for the initiation of the jet flow and the corresponding water depth at the lower point of the flip bucket.

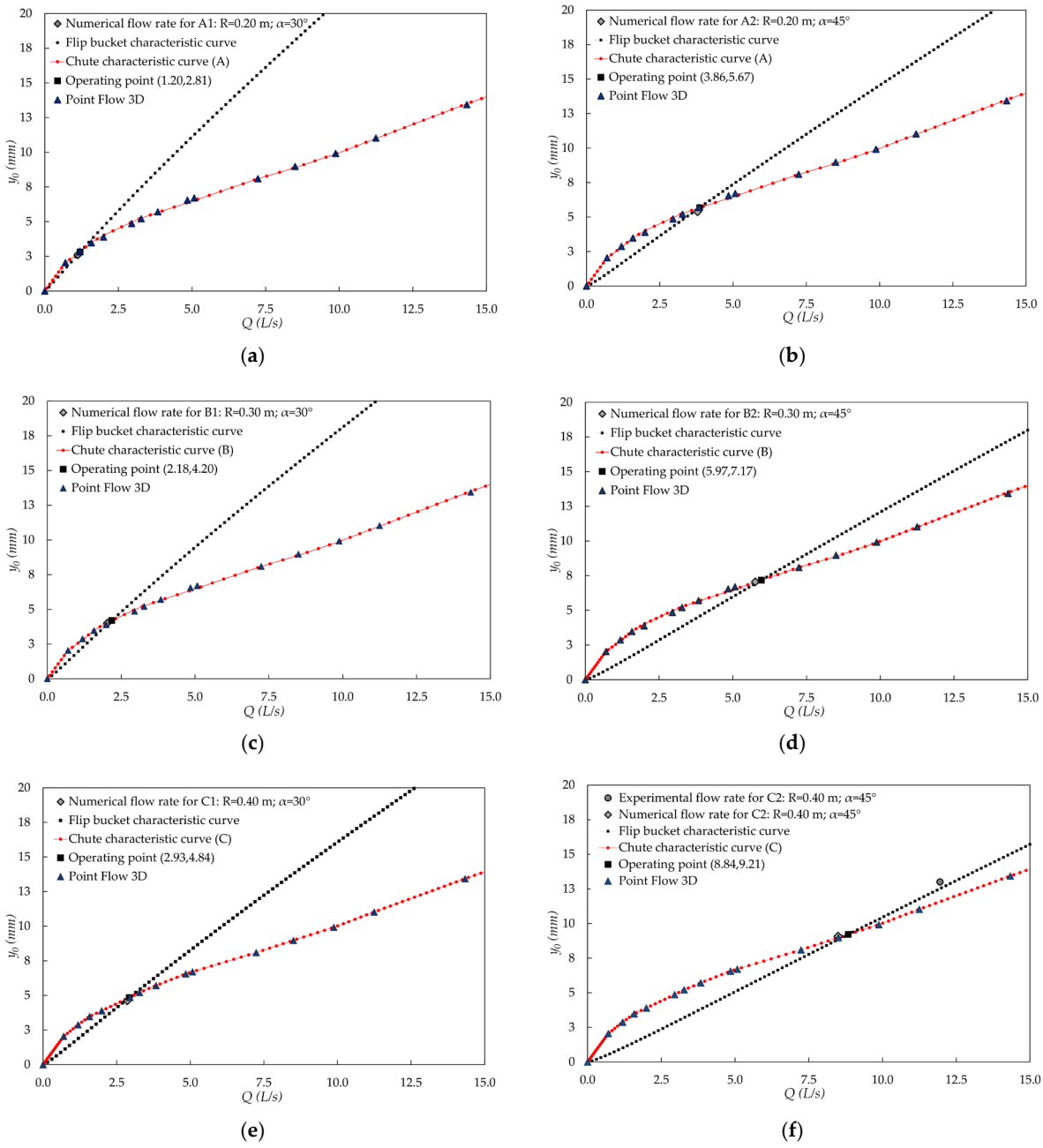

Figure 13. Characteristic curves and operating point of the chute-flip bucket system: (**a**) A1 (R = 0.2 m; α = 30°); (**b**) A2 (R = 0.2 m; α = 45°); (**c**) B1 (R = 0.3 m; α = 30°); (**d**) B2 (R = 0.3 m; α = 45°); (**e**) C1 (R = 0. 4 m; α = 30°); (**f**) C2 (R = 0.4 m; α = 45°).

It is observed that the flow rate for the initiation of the jet flow increases with the depth z of the flip bucket. It should be expected z to be the parameter with greater influence in the jet flow triggering. The supercritical flow stream, coming from the chute, must have enough energy to push the water mass out of the flip bucket. The water in the flip bucket has a depth z plus the height of water necessary to discharge over the lip, which acts as a weir before the jet flow occurs. On the other hand, it should be noticed that when the obstacle is not a simple wall, but a flip bucket with a certain radius of curvature, the geometric configuration of the flip bucket would be expected to influence the overspill conditions, and therefore to

affect the flow rate for the initiation of the jet flow. The influence of the flip bucket curvature is included into the formula through the parameter *R*, radius of curvature of the flip bucket.

The effect of the radius of curvature of the flip bucket on the flow rate for the initiation of the jet flow can be easily analyzed by comparing the flow rate for the initiation of the jet flow obtained using the proposed formula with the actual *R* radius of each flip bucket and that obtained with the same formula considering an infinite radius, equivalent to the absence of curvature. The goodness of the result is assessed by comparison with the results of the numerical simulations performed with Flow3D, since the influence of aeration is present in physical models (Figure 14).

It was determined the difference between the flow rate for the initiation of the jet flow obtained by numerical simulation, and the values obtained by applying the proposed analytical formula with real radius and infinite radius, at the limit (without curvature). For infinite radius the term of the formula containing the radius becomes zero in Equation (13). Considering the results of the numerical models as the reference, the Mean Absolute Error and the Mean Relative Error were determined (Table 10). It is noted that the Relative Error that is committed considering the complete proposed formula, with the term that includes the radius, does not exceed 8%, while if the proposed formula is considered by removing that term, the Relative Error reaches 24%. Consequently, the inclusion of radius in the formulation is relevant.

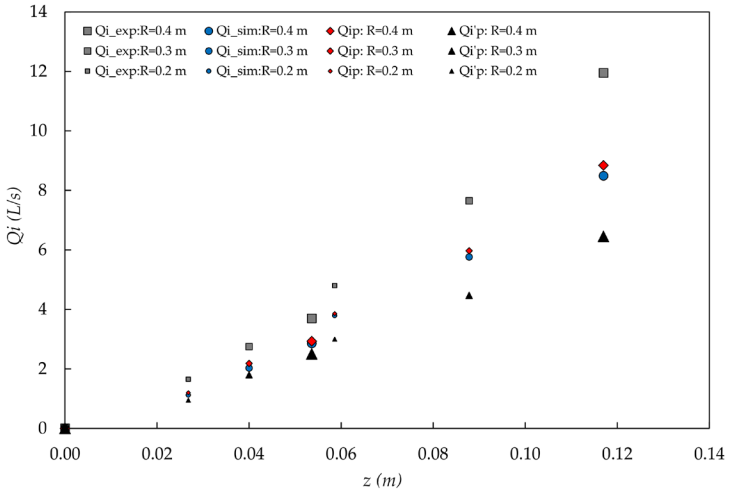

Figure 14. Flow rate for the initiation of the jet flow based on *z* and *R*. Qi_p theoretical flow rate considering *R*; Qi'_p theoretical flow rate not considering *R*; Qi_{exp} experimental flow rate; Qi_{sim} numerical flow rate.

Table 10. Comparison using the Absolute Error and the Relative Error of the numerical flow rate and theoretical flow rate for the initiation of the jet flow considering or not *R*.

Tested Geometry	Qi_p (L/s)	Qi'_p (L/s)	Qi_{sim} (L/s)		$AE_{Qi\ (sim-p)}$ (L/s)	$RE_{Qi\ (sim-p)}$ (%)	$AE_{Qi'(sim-p)}$ (L/s)	$RE_{Qi'\ (sim-p)}$ (%)
A1	1.20	0.95	1.12		0.08	7.14	0.17	15.18
B1	2.18	1.80	2.03		0.15	7.39	0.23	11.33
C1	2.93	2.50	2.86		0.07	2.45	0.36	12.59
A2	3.86	3.00	3.79		0.07	1.85	0.79	20.84
B2	5.97	4.47	5.76		0.21	3.65	1.29	22.40
C2	8.84	6.45	8.49		0.35	4.12	2.04	24.30
				*MAE-MRE	0.15	4.43	2.44	17.80

* MAE: Mean Absolute Error and MRE: Mean Relative Error between the flow rate for the initiation of the jet flow, for the different physical models, obtained by the proposed formulation Qi_p and Qi'_p, respectively, considering or not the term that depends on the radius, and the flow rate for the initiation of the jet flow obtained by numerical simulation Qi_{sim}.

For the purpose of quantifying the influence of the radius on the flow rate for the initiation of the jet flow, the proposed methodology and formula were applied to three flip buckets with radius 0.2 m, 0.3 m, and 0.4 m, keeping the z parameter fixed with value of 0.054 m (Table 11). It was observed that, for the same z value, the flow rate for the initiation of the jet flow increased as the radius was reduced, or, equivalently, as the flip angle was increased (Figure 15). The increase in flow rate was 17.4% when the radius is halved, from 0.4 to 0.2 m. In accordance, the error due to neglecting the effect of the curvature of the flip bucket increases by decreasing the radius, in fact, the Relative Error increased from 12.97% to 25.87% when the radius was reduced by half, from 0.4 m to 0.2 m.

Table 11. Comparison using the Absolute Error and the Relative Error of the flow rate for the initiation of the jet flow, obtained by the proposed methodology and formula and considering whether or not the radius-dependent term, respectively Qi_p and Qi'_p, for z=0.054 m.

R (m)	z (m)	α (°)	Qi_p (L/s)	Qi'_p (L/s)	$AE_{Q\text{-}Q'}$ (L/s)	$RE_{Q\text{-}Q'}$ (%)
0.4	0.054	30	2.93	2.55	0.38	12.97
0.3	0.054	34.78	3.09	2.55	0.54	17.50
0.2	0.054	42.95	3.44	2.55	0.89	25.87

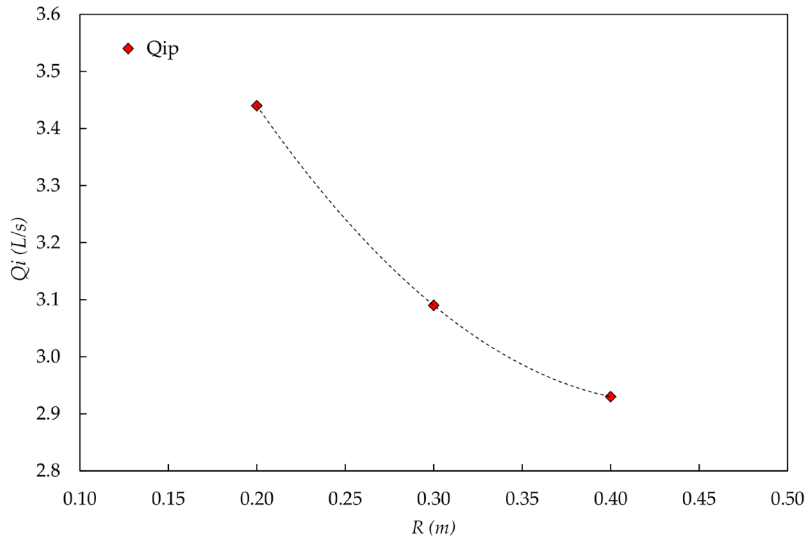

Figure 15. Flow rate for the initiation of the jet flow, obtained by the proposed methodology and formula for different values of R, Qi_p, for a constant value of z = 0.054 m.

It is interesting to compare the flow rate for the initiation of the jet flow obtained through the proposed methodology and formula, which includes the effect of the curvature of the flip bucket, with those obtained using the formulas previously proposed by various authors. The *flip bucket characteristic curve* is usually expressed as a relationship between parameter z/y_0 and the Froude number F_0, both at the lowest point of the flip bucket (Equations (1)–(6)). It can also be expressed as a relationship between y_0 and the unit flow rate for the initiation of the jet flow q (Table 12). This is useful for quantifying the flow rate for the initiation of the jet flow using the proposed *method of the characteristic curves*.

Table 12. Relationship between z/y_0 and the Froude number F_0 at the lowest point of the flip bucket, expressed as a function of the flow depth y_0 and the unit flow rate q.

Authors	Initiation Condition	End Condition
Abecasis-Quintela (Equations (1) and (2))	$y_0^3 - y_0\left(3\frac{q^{4/3}}{g^{2/3}} + 2z\frac{q^{2/3}}{g^{1/3}}\right) + 2\frac{q^2}{g} = 0$	$y_0^3 - z\,y_0^2 - y_0\left(3\frac{q^{4/3}}{g^{2/3}} + z\frac{q^{2/3}}{g^{1/3}}\right) + 2\frac{q^2}{g} = 0$
Muskatirovic-Batinic (Equations (3) and (4))	$\frac{y_0}{2}\left(\sqrt{1+\frac{8q^2}{y_0^3 g}} - 1\right) + \frac{q^2}{g y_0^2\left(1+\frac{4q^2}{g y_0^3} - \sqrt{1+\frac{8q^2}{g y_0^3}}\right)} - \frac{3q^{2/3}}{g^{1/3}} + z = 0$	$y_0^3 - y_0\left(3\frac{q^{4/3}}{g^{2/3}} + 2z\frac{q^{2/3}}{g^{1/3}} + z^2\right) + 2\frac{q^2}{g} = 0$
Heller-Hager-Minor (Equations (5) and (6))	$y_0^3 g - 2g y_0\left[\left(\frac{3}{2}\frac{q^{4/3}}{g^{2/3}}\right) + \left(z\frac{q^{2/3}}{g^{1/3}}\right) + \left(\frac{z^2}{2}\right)\right] + 2q^2 = 0$	$y_0^3 g - 2g y_0\left[\left(\frac{q^2}{g\left(\frac{q^{2/3}}{g^{1/3}} + z\right)}\right) + \left(\frac{q^{4/3}}{2g^{2/3}}\right) + \left(\frac{z^2}{2}\right) + \left(\frac{zq^{2/3}}{g^{1/3}}\right)\right] + 2q^2 = 0$

The *flip bucket characteristic curve* was built point by point, and the previously determined *chute characteristic curve* was used, and both were drawn for each geometrical configuration of the flip bucket, using the formula of different authors (Figure 16). The operating points were obtained at the intersection of the characteristic curves, and therefore the flow rate for the initiation of the jet flow and the flow depth at the lowest point of the flip bucket for that flow rate (Table 13; Figure 17). It is noted that the proposed formula provides the best prediction for the flow rate for the initiation of the jet flow in all cases, taking as reference the one obtained by numerical modeling, followed by the formula of Abecasis and Quintela [16,17]. The obtained results using the formulas of the rest of the authors differ significantly, showing great dispersion.

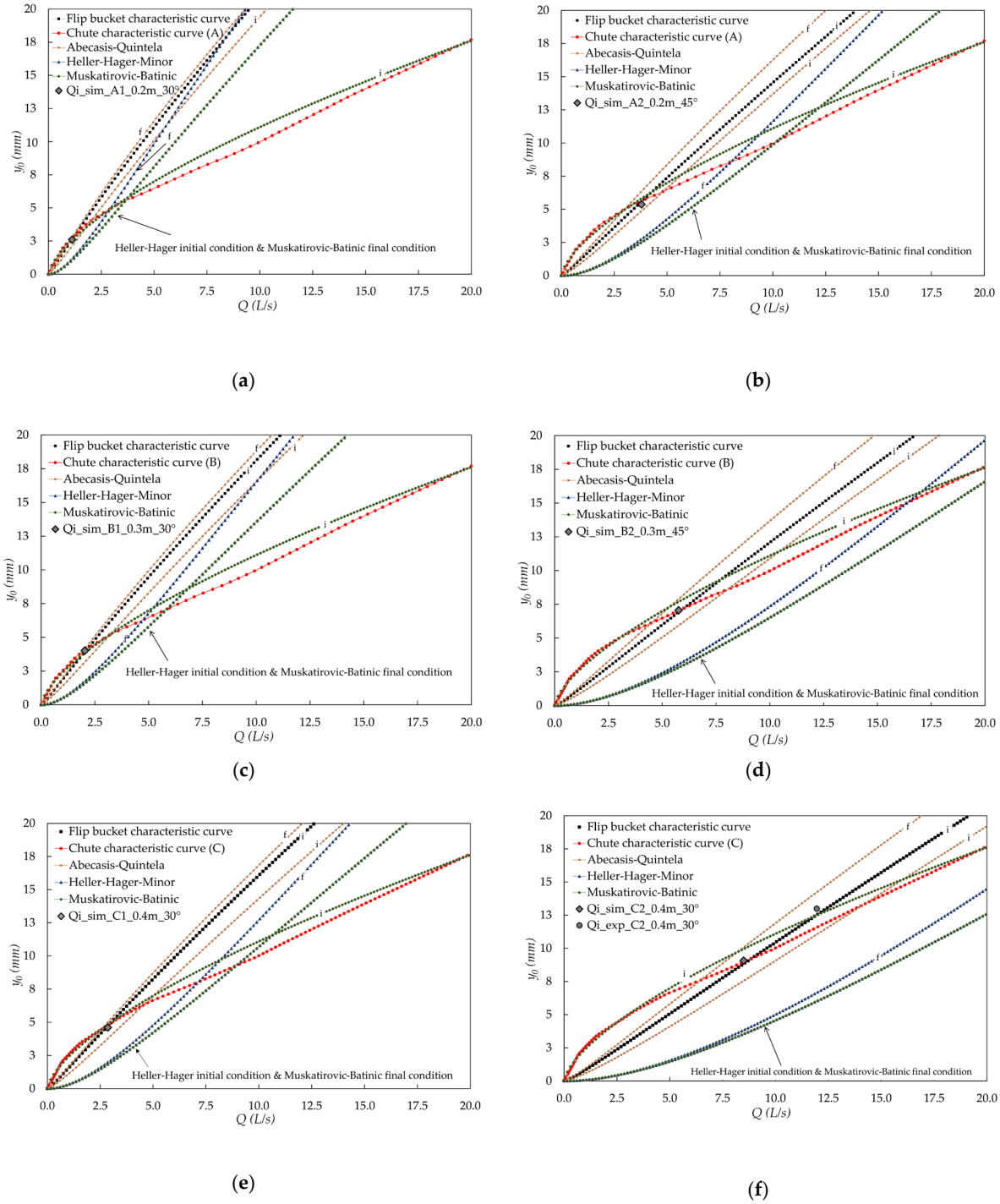

Figure 16. Comparison of the results obtained using the formulas of various authors. The *flip bucket characteristic curve* is represented according to the formula of different authors. For the previous formulas, it is indicated with "i" the initiation condition of the jet flow, and with "f" the end condition of the jet flow: (**a**) A1; (**b**) A2; (**c**) B1; (**d**) B2; (**e**) C1; (**f**) C2.

Table 13. Flow rate for the initiation of the jet flow Qi and flow depth at the lowest point of the flip bucket y_{0i} obtained using the formula of different authors, by means of the proposed formula and by numerical simulation Absolute Error and Relative Error, taking as the reference the flow rate obtained with the numerical simulation Qi_{sim}.

Tested Geometry	Author	Initial Condition	Qi (L/s)	y_{0i} (mm)	$AE_{Qi\ (p\text{-}sim)}$ (L/s)	$RE_{Qi\ (p\text{-}sim)}$ (%)
A1	Abecasis-Quintela	final	0.95	2.35	0.17	15.18
A1	Abecasis-Quintela	initial	1.89	3.86	0.77	40.74
A1	Muskaritovic-Batinic	final	3.69	5.56	2.57	69.65
A1	Muskaritovic-Batinic	initial	3.24	5.92	2.12	65.43
A1	Heller-Hager-Minor	final	2.93	4.88	1.81	61.77
A1	Heller-Hager-Minor	initial	3.69	5.56	2.57	69.65
A1	Proposed Model	initial	1.20	2.81	0.08	6.66
A1	Numerical Model	initial	1.12	2.61	-	-
A1	Experimental	initial	1.65	-	0.53	32.12
B1	Abecasis-Quintela	final	1.80	3.66	0.23	12.78
B1	Abecasis-Quintela	initial	3.18	5.17	1.15	36.16
B1	Muskaritovic-Batinic	final	6.02	7.21	3.99	66.28
B1	Muskaritovic-Batinic	initial	6.90	8.67	4.87	70.58
B1	Heller-Hager-Minor	final	4.74	6.29	2.71	57.17
B1	Heller-Hager-Minor	initial	6.02	7.21	3.99	66.28
B1	Proposed Model	initial	2.18	4.20	0.15	6.88
B1	Numeric Model	initial	2.03	4.01	-	-
B1	Experimental	initial	2.75	-	0.72	26.18
C1	Abecasis-Quintela	final	2.5	4.45	0.36	14.40
C1	Abecasis-Quintela	initial	4.73	6.46	1.87	39.53
C1	Muskaritovic-Batinic	final	9.11	9.38	6.25	68.61
C1	Muskaritovic-Batinic	initial	19.76	17.50	16.90	85.53
C1	Heller-Hager-Minor	final	7.36	8.18	4.50	61.14
C1	Heller-Hager-Minor	initial	9.11	9.38	6.25	68.61
C1	Proposed Model	initial	2.93	4.84	0.07	2.39
C1	Numeric Model	initial	2.86	4.61	-	-
C1	Experimental	initial	3.70	-	0.84	22.70
A2	Abecasis-Quintela	final	3.0	5.01	0.79	26.33
A2	Abecasis-Quintela	initial	4.91	6.50	1.12	22.81
A2	Muskaritovic-Batinic	final	10.20	10.14	6.41	62.84
A2	Muskaritovic-Batinic	initial	19.51	17.33	15.72	80.57
A2	Heller-Hager-Minor	final	8.09	8.61	4.30	53.15
A2	Heller-Hager-Minor	initial	10.20	10.14	6.41	62.84
A2	Proposed Model	initial	3.86	5.67	0.07	1.81
A2	Numeric Model	initial	3.79	5.38	-	-
A2	Experimental	initial	4.80	-	1.01	21.04
B2	Abecasis-Quintela	final	4.47	6.07	1.29	28.86
B2	Abecasis-Quintela	initial	8.18	6.68	2.42	29.58
B2	Muskaritovic-Batinic	final	23.68	20.42	17.92	75.58
B2	Muskaritovic-Batinic	initial	19.68	17.40	13.92	70.73
B2	Heller-Hager-Minor	final	16.35	14.99	10.59	64.77
B2	Heller-Hager-Minor	initial	23.68	20.42	17.92	75.68
B2	Proposed Model	initial	5.97	7.17	0.21	3.52
B2	Numeric Model	initial	5.76	7.06	-	-
B2	Experimental	initial	7.65	-	1.89	24.70
C2	Abecasis-Quintela	final	6.45	7.59	2.04	31.63
C2	Abecasis-Quintela	initial	13.95	13.08	5.46	39.14
C2	Muskaritovic-Batinic	final	50.10	39.73	41.61	83.05
C2	Muskaritovic-Batinic	initial	19.95	17.59	11.46	57.44
C2	Heller-Hager-Minor	final	29.25	24.57	20.76	70.97
C2	Heller-Hager-Minor	initial	50.10	39.73	41.61	83.05

C2	Proposed Model	initial	8.84	9.21	0.35	3.96
C2	Numeric Model	initial	8.49	9.08	-	-
C2	Experimental	initial	11.95	13.00	3.46	28.95

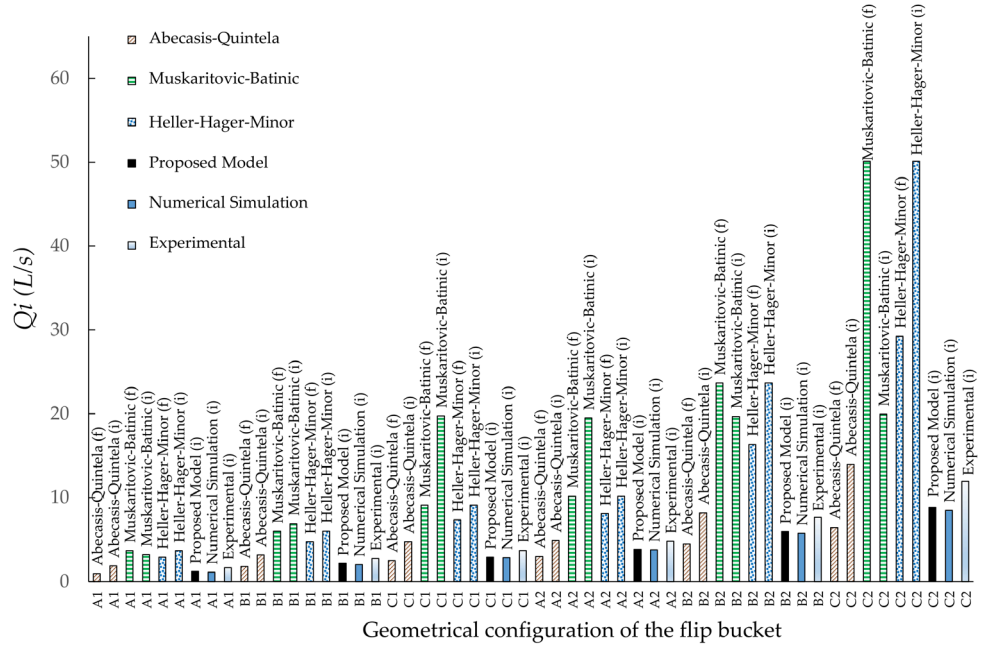

Figure 17. Flow rate for the initiation of the jet flow *Qi* obtained using the formula of various authors, the proposed formula, numerical modeling and physical models in the laboratory.

8. Conclusions

The flip bucket might be used as a stilling basin in the range of low discharges. In some cases, it might be advisable to delay the initiation of the jet flow. This way, the dissipation of most of the energy would occur inside the flip bucket, by means of the hydraulic jump, for low discharges, which are the most frequent working condition.

For the jet flow, the energy is fully dissipated through the impact with the riverbed, which implies lower erosion control for the lower range of discharges. If a pre-excavated stilling basin is considered, it should be larger, and therefore more expensive, if jet flow occurs for low discharges.

In order to minimize the scour basin, and increase the distance between the bucket toe and the impact point, the flow rate for initiation of the jet flow should be as high as possible. It implies a longer impact distance, something beneficial for the spillway, and for the dam if it is in the vicinity of the flip bucket.

Determining the position of the erosion basin downstream of a sky-jump spillway allows to control the impact area. Its shape and size depend on both the geometrical configuration of the flip bucket and the operating flow rates. Knowing the flow rate for the initiation of the jet flow is of interest, since it allows to establish the position of the impact area closest to the spillway, and usually to the dam itself.

This study proposes a methodology that allows to determine the flow rate for the initiation of the jet flows by the intersection of two curves, by analogy with a pumping system: The *chute characteristic curve* and the *flip bucket characteristic curve*. For the latter a new formula is proposed that incorporates the effect of the curvature of the flip bucket. The flow rate for the initiation of the jet flow obtained with the proposed methodology and formula are similar to the value obtained by numerical modeling, with differences less than 5%. Experimentally obtained flow rates are somewhat higher, possibly due to the influence of the aeration of the water stream.

Accurate determination of this flow rate is difficult, as small variations of any of the parameters involved might imply a relatively significant change in the flow rate for the initiation of the jet flow. This

is explained graphically by the chute and *flip bucket characteristic curves*, which form very sharp angles at the intersection.

The curvature of the flip bucket was found to affect significantly the flow rate for the initiation of the jet flow, although it is not the most influential parameter. In the cases that were studied, the RE that is committed considering the complete proposed formula, with the term that includes the radius, does not exceed 8%, while if the proposed formula is considered by removing that term, the RE reaches 24%. Consequently, the inclusion of radius in the formulation is relevant, which justifies the interest of using the proposed new formula. It was observed that, being constant the depth of the flip bucket (z), the flow rate for the initiation of the jet flow increases as the radius is reduced or, equivalently, by increasing the throwing angle. The increase is 17.4% when the radius is halved, from 0.4 to 0.2 m. In line with this, the error made, without considering the effect of the curvature of the flip bucket, increases, by decreasing the radius, from a RE of 12.97% to 25.87% when the radius is reduced by half, from 0.4 m to 0.2 m.

The flow rate for initiation of the jet flow is determined during the design of the flip bucket, and we have shown that it depends not only on the depth of the flip bucket (z), but also on the bucket radius. If the designer desires a high flow rate for the initiation of the jet flow, a high lip angle and the minimum radius compatible with flow conditions should be specified at the design stage. The here proposed formula should be used for considering the effect of the bucket radius. The proposed method of the characteristic curves might be used for determining the flow rate for the initiation of the jet flow. It is a decision of the designer to choose where to dissipate the low and frequent discharge flows: in the riverbed or inside the flip bucket. The decision should me made taking into consideration the geological characterization of the riverbed and the flow depth in the impact area, and also the need and cost of implementing a pre-excavated basin.

It is necessary to carry out additional research on the influence of flow aeration on the value of the flow rate for the initiation of the jet flow.

Author Contributions: Conceptualization, M.Á.T.; methodology, M.Á.T., R.P., V.A.; validation, R.P.; formal analysis, R.P., V.A.; investigation, R.P., V.A.; resources, M.Á.T.; data curation, R.P.; writing—original draft preparation, R.P.; writing—review and editing, M.Á.T., V.A.; visualization, R.P.; supervision, M.Á.T.; project administration, M.Á.T. All authors have read and agreed to the published version of the manuscript.

Funding: This research received no external funding.

Acknowledgments: We are grateful to the members of the research group SERPA-Dam Safety Research for the support provided.

Conflicts of Interest: "The authors declare no conflict of interest."

Abbreviations

The following abbreviations are used in this paper:

A	average flow area;
AR	absolute error;
α	flip angle;
$C_{1\varepsilon}$, $C_{2\varepsilon}$	k-ε turbulence model parameters;
σ_k, σ_ε	k-ε turbulence model parameters;
F	is the volume flow function;
f_{xi}, f_{xj}, f_{xk}	viscous acceleration;
F_0	Froude number;
g	gravity acceleration;
G_{xi}, G_{xj}, G_{xk}	body acceleration;
H	spillway total height;
La	horizontal distance from the upstream spillway vertical wall to the point where the straight part of the chute ends;

Lc	horizontal distance from the upstream spillway vertical wall and measurement point "p";
Lt	horizontal distance between the measurement point "p" and the flip bucket's lip;
MAE	mean absolute error;
MRE	mean relative error;
R	radius of curvature of flip bucket;
RE	relative error;
P	distance from the bottom of the flip bucket to the ground;
p	pressure;
P_k	production of turbulence kinetic energy;
Q	flow rate;
q	unit flow rate;
Qi	flow rate for the initiation of the jet flow;
Qi_{exp}	experimental flow rate for the initiation of the jet flow;
Qi_p	theoretical flow rate for the initiation of the jet flow;
Qi'_p	theoretical flow for the initiation of the jet flow not considering R;
Qi_{sim}	numerical flow rate for the initiation of the jet flow;
Qf	flow rate for the finishing of the jet flow;
y_c	critical flow depth;
y_0	flow depth;
y_{0i}	flow depth for the initiation of the jet flow;
y'_{0iexp}	experimental flow depth for the initiation of the jet flow with aerated upper area;
y_{0iexp}	experimental flow depth for the initiation of the jet flow without aerated upper area;
y_{0ip}	theoretical flow depth for the initiation of the jet flow;
$y_{0i\ sim}$	numerical flow depth for the initiation of the jet flow;
U	average velocity;
u_i, u_j, u_k	velocity component;
v_0	velocity;
v_c	critical velocity;
z	vertical height of the obstacle or depth of the flip bucket
x_i, x_j, x_k	Cartesian coordinates;
k	turbulence kinetic energy;
ε	rate of turbulence energy dissipation;
μ	dynamic viscosity;
μ_t	turbulent dynamic viscosity;
t	time;
ϱ	fluid density.

References

1. Godon, R. Le barrage et l'usine hydro-électrique de Marèges sur la Dordogne. *Techniques des Travaux* **1936**, *12*, 101–110.
2. Rhone, T.J.; Peterka, A.J. Improved tunnel spillway flip buckets. *J. Hydraul. Div.* **1959**, *85*, 53–76.
3. Vischer, D.L.; Hager, W.H. *Dam Hydraulics*; Wiley: Chichester, UK; New York, NY, USA, 1998.
4. Rajan, B.H.; Shivashankara Rao, K.N. Design of trajectory buckets. *Water Energy Int.* **1980**, *37*, 63–76.

5. Bollaert, E.F.R.; Duarte, R.; Pfister, M.; Schleiss, A.J.; Mazvidza, D. Physical and numerical model study investigating plunge pool scour at Kariba Dam. In Proceedings of the 24th ICOLD Congress, Kyoto, Japan, 2–8 June 2012; pp. 241–248.
6. Peterka, A.J. *Hydraulic Design of Stilling Basins and Energy Dissipators*; U.S. Dept. of the Interior, Bureau of Reclamation, Technical Service Center: Denver, CO, USA, 1964; pp. 199–205.
7. Schleiss, A.J. Scour evaluation in space and time—The challenge of dam designers. In *Rock Scour due to Falling High-Velocity Jets*; A A Balkema Publishers: Rotterdam, The Netherlands 2002; pp. 3–22.
8. Pfister, M.; Schleiss, A.J. Ski jumps, jet and plunge pools. In *Energy Dissipation in Hydraulic Structures*; Hubert Chanson; Taylor & Francis Group: London, UK, 2015; pp. 105–140.
9. Rouve, G. Some observation on flow over spillway flip buckets. In Proceedings of the 6th Symposium of Civil and Hydraulic Engineering Department, High Velocity Flows, Indian Institute of Science, Bangalore, India, 18–20 January 1967.
10. Baines, P.G. A unified description of two-layer flow over topography. *J. Fluid Mech.* **1984**, *146*, 127–167.
11. Lawrence, G.A. Steady flow over an obstacle. *J. Hydraul. Eng. ACE* **1987**, *8*, 981–991.
12. Pratt, L.J. A note on nonlinear flow over obstacles. *Geophys. Astrophys. Fluid Dyn.* **1983**, *24*, 63–68.
13. Baines, P.G.; Whitehead, J.A. On multiple states in single-layer flows. *Phys. Fluids* **2003**, *15*, 298–307.
14. Mehrotra, S.C. Hysteresis effect in one-and two fluid system. In Proceedings of the V Australian Conference on Hydraulics and Fluid Mechanics, University of Canterbury, Christchurch, New Zeland, 9–13 December 1974; Volume 2, pp. 452–461.
15. Austria, P.M. Catastrophe model for the forced hydraulic jump. *J. Hydraul. Res.* **1987**, *25*, 269–280.
16. Abecasis, F.M.; Quintela, A.C. *Hysteresis in the Transition from Supercritical to Subcritical Flow*; memoria n.523; Laboratorio National de Engeharia Civil: Lisbon, Portugal, 1979.
17. Abecasis, F.M.; Quintela, A.C. Hysteresis in steady free-surface flow. *Water Power* **1964**, *4*, 147–151.
18. Muskatirovic, D.; Batinic, D. The influence of abrupt change of channel geometry on hydraulic regime characteristics. In Proceedings of the 17th IAHR Congress, Baden Baden, Germany, 15–19 August 1977; pp. 397–404.
19. Heller, V.; Hager, W.H.; Minor, H.E. Ski jump hydraulics. *J. Hydraul. Eng.* **2005**, *131*, 347–355.
20. Arangoncillo, V. *Análisis del Funcionamiento con Pequeños Caudales, del Deflector de los Aliviaderos Trampolín*; Trabajo de Suficiencia Investigadora; Universidad Politécnica de Madrid: Madrid, Spain, 2011.
21. Falvey, H.T. *Engineering Monograph No.42: Cavitation in Chutes and Spillways*; US Department of the Interior, Bureau of Reclamation: Denver, CO, USA, 1990.
22. U.S. Bureau of Reclamation. *Design of Small Dams*; U. S. Government Printing Office: Washington, DC, USA, 1977.
23. Flow Science, Inc. FLOW-3D *User Manual Release 11.0.3*; Flow Science, Inc.: Santa Fe, NM, USA, 2014.
24. Hirt, C.H.; Sicilian, J.M. A porosity technique for the definition of obstacles in rectangular cell meshes. In *Proceedings 4th International Conference on Numerical Ship Hydrodynamics*; National Academy of Science: Washington, DC, USA, 1985; pp. 1–19.
25. Nichols, B.D.; Hirt, C.W. Methods for calculating multidimensional, transient free surface flows past bodies. In *Proceedings of 1st Int.Conf. Ship Hydrodynamics*; Schot, J.W., Salvesen, N., Eds.; Naval Ship Research and Development Center: Bethesda, MD, USA, 1975; pp. 253–277.
26. Nichols, B.D.; Hirt, C.W.; Hotchkiss, R.S. *Volume of Fluid (VOF) Method for the Dynamics of Free Boundaries*; Rep. LA-8355; Los Alamos Scientific Lab.: Los Alamos, NM, USA, 1980.
27. Hirt, C.W.; Nichols, B.D. Volume of fluid (VOF) method for the dynamics of free boundaries. *J. Comput. Phys.* **1981**, *39*, 201–225.
28. Jakeman, A.J.; Letcher, R.A.; Norton, J.P. Ten iterative steps in development and evaluation of environmental models. *Environ. Modell. Softw.* **2006**, *21*, 602–614.
29. Blocken, B.; Gualtieri, C. Ten iterative steps for model development and evaluation applied to Computational Fluid Dynamics for Environmental Fluid Mechanics. *Environ. Model. Softw.* **2012**, *33*, 1–22.
30. Chanel, P.G. An Evaluation of Computational Fluid Dynamics for Spillway Modeling. Master' Thesis, University of Manitoba, Winnipeg, MB, Canada, 2008.
31. Yakhot, V.; Orszag, S.; Thangam, S.; Gatski, T.; Speziale, C. Development of turbulence models for shear flows by a double expansion technique. *Fluid Dyn.* **1992**, *4*, 1510–1520.

32. Speziale, C.G.; Thangam, S. Analysis of an RNG based turbulence model for separated flows. *Int. J. Eng. Sci*. **1992**, *30*, 1379–1388.
33. Pope, S.B. *Turbulent Flows*; Cambridge University Press: Cornell University, New York, NY, USA, 2000.